Cooling Performance Analysis of Nanofluid Assisted Novel Photovoltaic Thermoelectric Air Conditioner for Energy Efficient Buildings

Balaji Bakthavatchalam [a*], Khairul Habib [a], R. Saidur [b, c] and Bidyut Baran Saha [d]

[a] *Department of Mechanical Engineering, Universiti Teknologi PETRONAS, 32610 Bandar Seri Iskandar, Perak Darul Ridzuan, Malaysia*

[b] *Research Centre for Nano-Materials and Energy Technology (RCNMET), School of Engineering and Technology, Sunway University, Malaysia*

[c] *Department of Engineering, Lancaster University, LA1 4YW, United Kingdom*

[d] *International Institute for Carbon-Neutral Energy Research, Kyushu University, 744 Motooka Nishi-ku Fukuoka-shi, Fukuoka 819-0395, Japan*

Corresponding author, E-mail address: balaji_17004028@utp.edu.my

Tel: +60 11 36218966

ABSTRACT

Carbon emissions and excessive power usage are addressed by applying thermoelectric cooling, which benefits from its ability to be portable, economical, and reliable. However, a conventional thermoelectric air conditioner's coefficient of performance (COP) is much less due to the sustained heat generated on the thermoelectric module's hot side. This work presents a novel idea of utilizing a nanofluid cooled radiator as an external cooling jacket around the thermoelectric module's hot side to enhance the heat transfer rate of thermoelectric air conditioners. In this research, the performance of a newly designed thermoelectric air conditioner (TEAC) powered by photovoltaic systems (PV) installed in a residential building is analyzed using nanofluid as a coolant. Furthermore, by supplying different input currents (2-6A), the cooling characteristics and performance of the newly designed nanofluid assisted thermoelectric air conditioner (NTEAC) system were experimentally studied in a test room of 25.6 m^3 volume in Malaysia's tropical climate. The system's best performance was at 6A, with a maximum temperature drop of 4.9 °C, a cooling capacity of 571W, and a coefficient of performance of 1.27. In addition, the NTEAC system showed an energy saving of 67% and CO_2 emission mitigation of 76% when compared with a conventional split air conditioner. Thus, an alternative to the traditional air conditioning system was developed from this research, which is Freon free. This system is expected to consume less energy and emit less CO_2 for the tropical climatic conditions.

Keywords: Nanofluid assisted thermoelectric air conditioner (NTEAC); photovoltaic; nanofluid; Coefficient of performance; energy saving; CO_2 emission.

1. INTRODUCTION

Conventional air conditioning systems have become more efficient in recent years, but they also account for most electricity use and CO_2 emissions in most residential, commercial, and industrial buildings [1,2]. According to the International Energy Agency, air conditioners (ACs) in buildings will increase from 1.6 to 5.6 billion by 2050 [3]. In 30 years, each second, there will be ten new ACs purchased. Furthermore, the HVAC industry is dominated by vapour-compression systems. However, these systems employ harmful refrigerants that pollute the atmosphere. Thermoelectric cooling is seen as a valuable alternative to vapour compression, possessing several advantages compared to traditional vapour compression technologies, including smaller size and weight, excellent reliability, no moving parts, zero noise, and the possibility of using photovoltaic. Although the fundamental principles of thermoelectricity are widely understood, studies to comprehend the heat transfer process in small and medium-sized prototypes have been carried out throughout the years [4–6]. A thermoelectric module (TEM) or thermoelectric cooler (TEC) is a novel solid-state cooling system of thermocouples that rely on the Peltier effect to transfer heat from one side of a device to another. As shown in Figure 1, a thermocouple has a sequence of p-type and n-type semiconductors connected with top and bottom electrodes in series. The other components are thermally connected in parallel. Additionally, TECs may be directly connected to renewable energy systems to meet the urgent requirement for lowering building energy consumption [7].

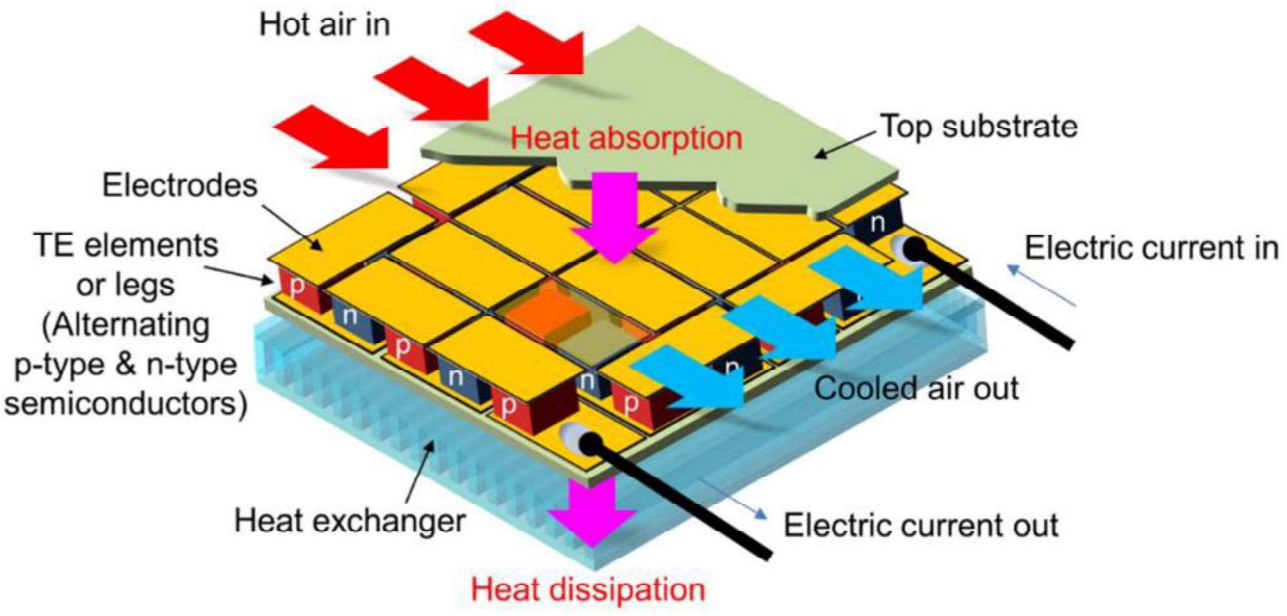

Figure 1: Thermoelectric module with semiconductor elements and heat exchangers [8]

Thermoelectric air conditioners (TEACs) are composed of multiple thermoelectric modules (TEMs) that are selected in accordance with the building's cooling load (for example, a 600W cooling load requires 12 TEMs of 50 W). When an electric current is provided to the TEMs in a TEAC, heat is transferred through the TEMs from the cold side to the hot side, making one junction colder and the other junction warmer. Then the cooled air from the cold junction is subjected to the building while the hot air is released into the atmosphere. The typical working principle of TEAC installed in a house is described in Figure 2. One of the significant problems with TEAC is poor COP (Coefficient of Performance), especially in high-performance applications. A high COP can be attained by improving heat transfer on the TEM's hot side and increasing the number of TEMs. A critical review on maintaining the cold side temperature of a TEM through different heat dissipation mechanisms was conducted by Sajid et al. [9]. Their study demonstrates that the performance of a thermoelectric device depends on effective thermal management of TEM's cold side and a hot side. On the other hand, Dizaji et al. [10] discovered that when the hot side of a thermoelectric module is cooled by a liquid such as water, the cold side may work as an excellent air conditioning system.

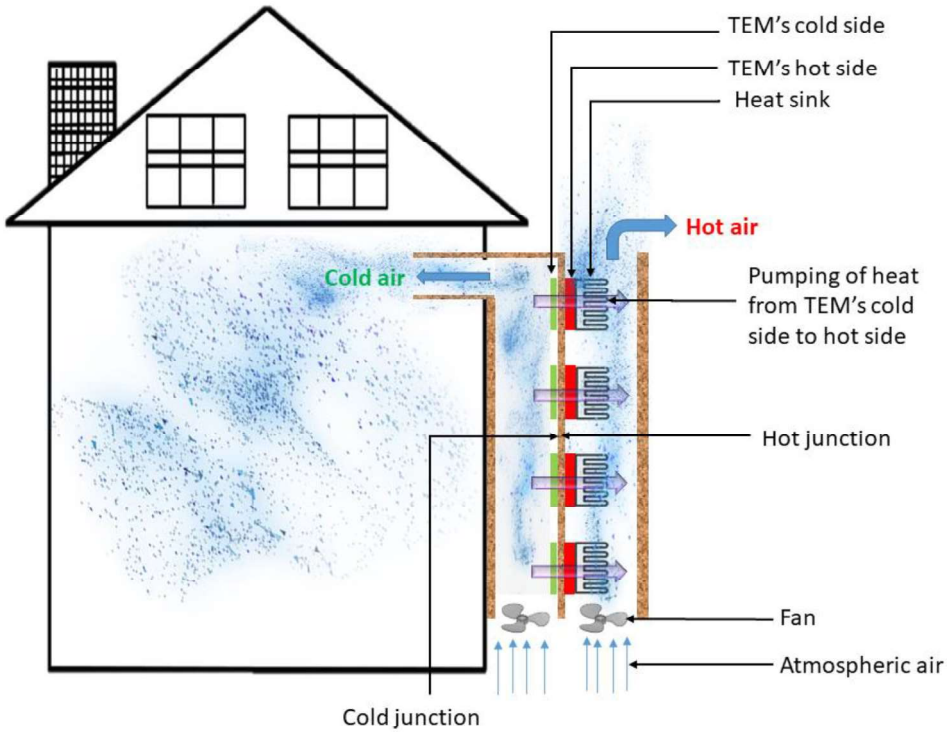

Figure 2: Schematic illustration of a building equipped with TEAC

Atta et al. [11] evaluated the performance of a TEAC system coupled with liquid-to-air heat exchangers. Within 90 minutes, the system could chill an enclosed space at a temperature of 14 °C below ambient and showed a maximum COP of 0.72. In another study, Sun et al. [12] employed a flat heat pipe to dissipate heat and saved ten minutes of the total thermal reaction time. Additionally, Zhao et al. [13] used the heat radiated by the TEM to heat the hot water by combining

it with a radiative sky cooler. This helps to minimize energy usage and save natural resources. Cheng et al. [14] reported that both the absorbed solar energy and the generated heat in the thermoelectric cooler might be evacuated via the cooling water, resulting in higher performance for the cooling module. Liu et al. [15] examined the performance of a solar thermoelectric air conditioner (STACHWS) with water as a heat transfer fluid (HTF). From their results, the water temperature has an enormous impact on the operation of the STACHWS system. The STACHWS system's COP reached a high of 4.51 and 2.74 with water temperatures of 20 °C and 42 °C, respectively. Putra et al. [16] investigated the use of nanofluids in conjunction with thermoelectric cooling to cool a computer's CPU using a heat pipe liquid block system. With the nanofluids, their cooling system can lower the CPU temperature by an immense value than the other typical cooling systems. Thermoelectric coolers are still employed for refrigeration and electrical equipment, despite their intriguing features for buildings.

Recently, new ideas for using TECs in buildings have been explored. For instance, Manikandan et al. [17] improved a thermoelectric cooler's COP and cooling performance using modified pulse operation for building space cooling. Compared with the thermoelectric cooler's regular operating mode, the modified pulse operation increased the cooling power and COP by 23.3% and 2.12%, respectively. Tian et al. [18] developed a novel air cooler composed of thermoelectric modules arranged in a tube-bundle shape. According to the author, a tubular thermoelectric system that includes a tubular component is more efficient and functional because it does not require channels to divide the hot and cold sides. Su et al. [19] proposed a novel building envelope with TEC and a radiative sky cooler (RSC) to avoid heat gains and deliver cooling. The TEC-RSC exhibited a cooling capability of 25.49 W/m^2 under global solar radiation of 1000 W/m^2, with an outdoor temperature of 35°C and relative humidity of 60%. Han et al. [20] studied a unique split-type liquid circulation thermoelectric cooling performance under various parameters. Their findings demonstrate that as the outdoor temperature is reduced from its expected value, the device cooling power and COP increase. Kang et al. [21] conducted trials in active and passive modes to examine the performance of a PCM integrated radiant cooling panel. Their proposed system had an active cooling capacity of about 58 W/m^2 and a passive cooling capacity of about 54 W/m^2 when the mean radiant temperature (MRT) was 26 °C. He et al. [22] developed a solar-driven thermoelectric cooling system for a model room of 0.125 m^3. The authors reported a maximum COP of 0.45 and a minimum temperature of 17 °C. In a recent study, Khalvati et al. [23] analyzed the effects of air temperature attenuation, working interval time, and the number of modules on the performance of a thermoelectric cooling system. Operating the thermoelectric air-cooling system during a short period reduces energy consumption while using it for a longer time might raise it. Also, TEAC with

more than twenty TEMs will increase the energy consumption, attributed to less COP. In 2021, Garayo et al. [24] optimized the COP of a thermoelectric cooling system with double flux mechanical ventilation in a house of 80 m^2 area. The authors emphasized the significance of airflows, voltage supply, and temperature gaps attributed to a maximum cooling capacity and COP of 375W and 2.5. Gillott et al. [25] used eight TEMs in a small-scale building to generate a cooling capacity and COP of 220W and 0.46. Their results reveal that TEMs' cooling capacity relies on the temperature (hot and cold side) and quantity of the TEMs. Therefore, minimizing the temperature difference between the hot and cold sides is critical for optimal heat transfer via the thermoelectric cooling module.

Accordingly, the reviewed literature affirms a direct correlation between the TEAC's COP and hot/cold side temperature difference, which may be enhanced with more effective thermal management techniques. Since the heat flow on the hot side is enormous, the thermoelectric cooling system's hot side thermal management is more complicated than the cold side. Reduced hot/cold side temperature difference generally results in better cooling [26]. Higher-efficient heat sinks or high thermal conductivity heat transfer fluids can reduce the hot side temperature. Nanofluid is considered one of the best heat transfer fluids suitable for low-temperature and high-temperature applications. For instance, nanoparticle-based working fluids were investigated in cooling systems where the authors reported a maximum COP of 4.7 [27]. Furthermore, Akkaya et al. [28] enhanced the performance of a refrigeration system with TiO_2 and polyol ester oil, resulting in a COP improvement of 39%. Likewise, Akkaya and Yurtdaş [29] experimentally investigated the COP of a heat pump using deionized water and CuO/ZnO hybrid nanofluids. The COP of the heat pump ranged from 4.23 to 4.44 for deionized water and CuO/ZnO nanofluid, respectively. Recently, Çiftçi et al. [30,31] used binary hybrid nanofluids to develop an efficient heat pipe for air to air heat exchangers and thermosiphon. Most prior methods have revolved around using nanofluid on heat exchangers [32–36], electronic devices [37–39] and heat sinks [40–42]. None of the previous studies was conducted on a system that integrated a nanofluid, a radiator coupled heat sink, and a thermoelectric air conditioner utilizing solar photovoltaic systems in real-time buildings. The novelty of this paper is that it studies the use of nanofluid cooled radiators as an alternative to conventional methods (air-cooled heat sinks) in thermoelectric air conditioners. The newly proposed nanofluid cooled radiator can cool the hot side junction of the TEAC. This can provide a cheap and straightforward retrofit solution that can contribute to increasing the performance of TEACs in residential buildings. Against this background, this study proposed a novel thermoelectric air conditioner coupled with a radiator integrated with nanofluids (NTEAC) consisting of air and liquid (nanofluid) cooled heat sinks for space conditioning. Heat is removed

from the thermoelectric cooling system's hot side junction via nanofluid. The radiator unit transfers the heat from the nanofluid inside to the outside atmospheric air, cooling the nanofluid turn cools the TEM's hot side. Therefore, this research aims to design, build, and evaluate the performance of a novel NTEAC system for a building located in the tropical climate of Malaysia.

2. EXPERIMENTAL APPARATUS AND METHODOLOGY

This section intends to illustrate the experimental research involved in field measurements in Tronoh, Perak, Malaysia's realistic climatic environments, utilizing a test room fitted with PV and NTEAC. The experimental test room or building configuration is outlined in section 2.1. The preparation of MWCNT/Water nanofluid is explained in section 2.2. The fabrication, description, evaluation of NTEAC components and NTEAC system are discussed in sections 2.3 and 2.4. Furthermore, the design and arrangement of the test room equipped with the NTEAC system are presented in section 2.5. Ultimately, the methodology for data acquisition and uncertainty analysis is depicted in sections 2.6 and 2.7.

2.1. Building description

In a test room at Universiti Teknologi Petronas in Tronoh, Perak, Malaysia (4° 23' 2.292" N and 100° 58' 16.824" E), the studied NTEAC system was installed. The schematic image of the test room or building is depicted in Figure 3(a). The test room is installed with photovoltaic panels and a weather link station. Figure 3(b) illustrates the dimensions of the test room, which are as follows: 3200 mm (length), 3200 mm (width) and 2500 mm (height). The external walls are three-layered, with a 200 mm thick stone centre layer, while all side walls are cemented. The inside layer of cement is 13 mm thick, while the exterior layer is 18 mm thick. Clay roof tiles were used for the roof cover, and the ceiling (1800 × 1200 × 6.3 mm) is made of a Gypsum board. The wall window is 304 mm high, 1200 mm wide, and 22 mm thick plywood. In addition, the test room has a single steel door measuring 2000 mm in height, 850 mm in width, and 450 mm in thickness on the northwest wall. Table 1 summarises the thermophysical parameters of the materials utilized in the test room.

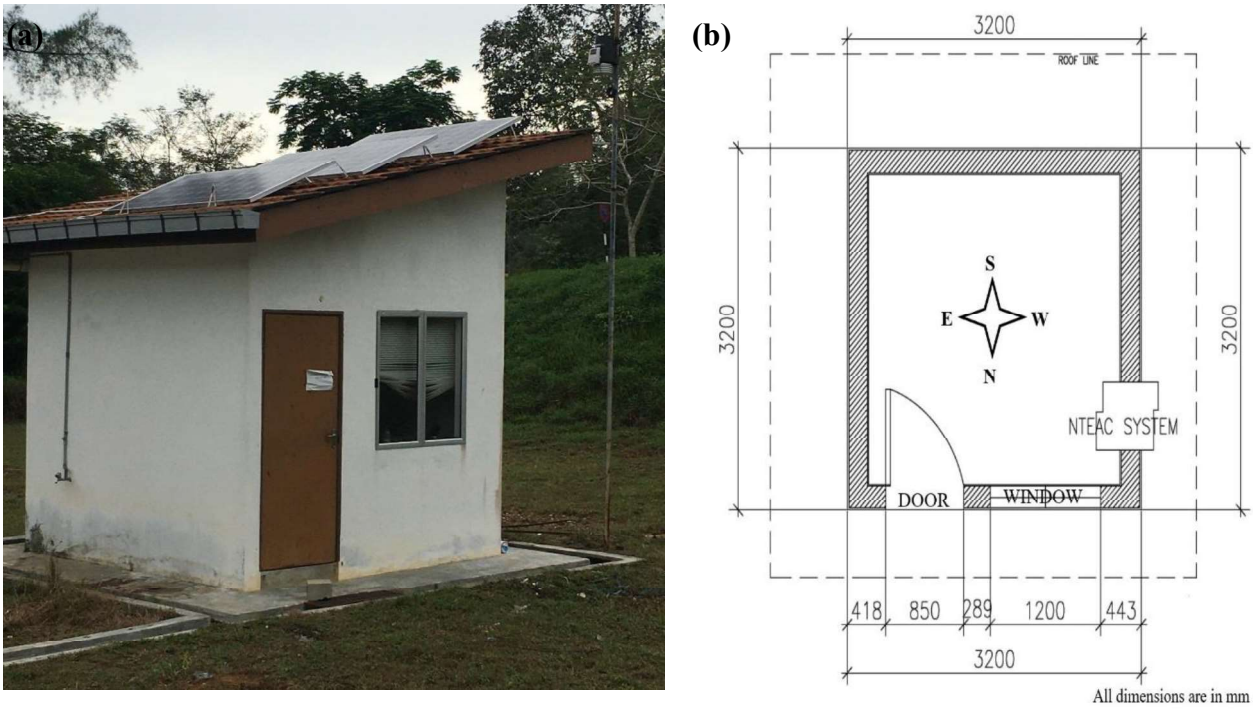

Figure 3: (a) Original image and (b) floor plan of the studied building

Table 1: Significant parameters of the building materials

Materials	**Thermal conductivity (W/m. K)**	**Density (kg/m^3)**	**Specific heat capacity (kJ/kg.K)**
Limestone tile	1.8	2420	0.84
Sand grave	1.740	2240	0.84
Brick tile	0.798	1892	0.88
Mud brick	0.75	1731	0.88
Soil	0.518	1620	0.88
Cement mortar	0.716	1647	0.92
Cement plaster	0.719	1761	0.84
Roof tile	0.632	2531	1.42
GI sheet	61.06	7520	0.50

2.2. Nanofluid preparation

The Multiwalled Carbon Nanotubes (MWCNTs) with 10nm diameter purity 98% was bought from Sigma Aldrich, USA. Distilled water-based MWCNT nanofluid was prepared using the two-step method. MWCNT nanoparticles are dispersed in distilled water with SDBS surfactant to create a highly effective and stable heat transfer fluid. A mixture of MWCNTs and SDBS at 0.5wt% concentration is swirled together using a magnetic stirrer for 30 minutes at 800 RPM without increasing the temperature to ensure uniformity in MWCNT/SDBS mixture distribution. Our

previous literature can provide more detailed information on the studied nanoparticle, base fluid, and nanofluid [43]. The schematic image of the nanofluid preparation is depicted in Figure 4.

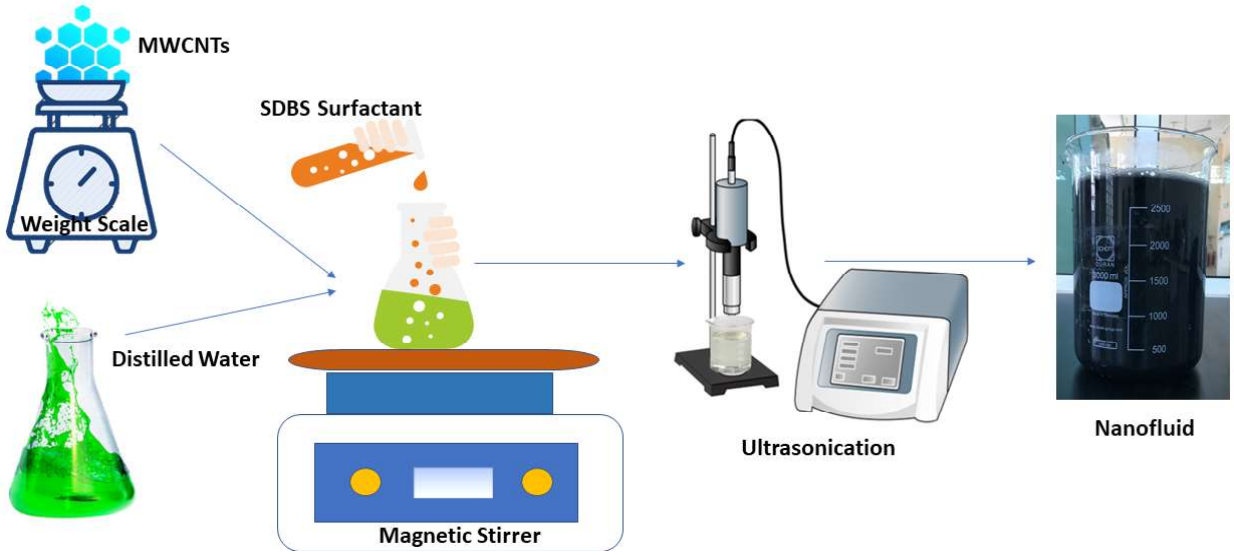

Figure 4: Schematic presentation of nanofluid preparation

2.3. Description of heat sinks, radiators, TEMs and PV panels

2.3.1 Air-cooled heat sinks

A heat sink may effectively absorb or disperse heat from thermal systems to atmospheric air with extended surfaces such as fins and spines. When effective heat dissipation is necessary, heat sinks are utilized in a broad range of applications; notable examples include refrigeration, heat engines, and electronic equipment that need to be cooled. Most heat sinks are made of metal with a cluster of cooling fins, called a fin array. The heat sink's performance can be increased by increasing the surface area, thermal conductivity, or heat transfer coefficient. Longitudinal fins are available in various shapes, including rectangular, triangular, and parabolic fins. The rectangular design is the most fundamental and extensively utilized when it comes to multiple fin arrays. In this study, a multiple-fin array with forced convection is herein preferred for the rectangular profile. The proposed finned heat sink was fabricated based on the conventional heat sink designs [44]. Figure 5 indicates the schematic view of the multi finned heat sink and its dimensions. This heat sink has a channel height of 20 mm, a channel width of 4 mm, a fin width of 2 mm, a total length and breadth of 55 mm, and a base height of 3 mm.

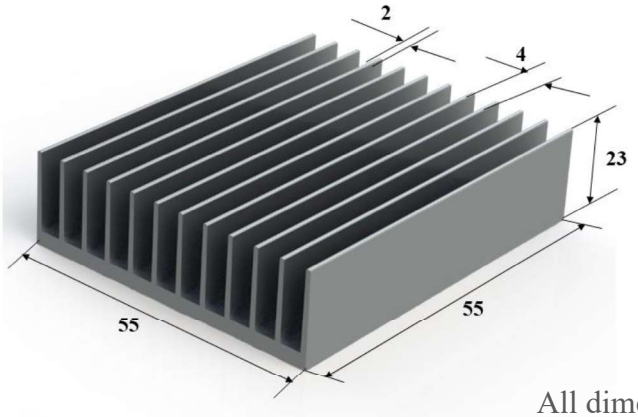

All dimensions are in mm

Figure 5: Schematic diagram of the air-cooled heat sink

2.3.2 Nanofluid cooled heat sinks

Increasing the thermal performance of heat sinks employing traditional heat transfer fluids (HTF) has become ubiquitous in the last decade. The improved thermophysical characteristics of nanofluids compared to conventional HTF allowed them to operate as highly efficient HTF to solve various heat transfer challenges. In this study, MWCNT/Water nanofluid is used as a coolant. A schematic view of the proposed heat sink with a circular channel is presented in Figure 6. The heat sink used for cooling the hot side of the TEMs has a total length of 196 mm, width of 72 mm and height of 23 mm. The diameter of each channel is 2.8 mm, and each channel is surrounded by solid material. The heat generated due to the current flow in TEMs is removed by circulating MWCNT/Water coolant through a channelled heat sink. The heat transfer is carried by conduction in the solid material and the coolant by convection. The nanofluid enters the heat sink in the axial direction with controlled speed and temperature.

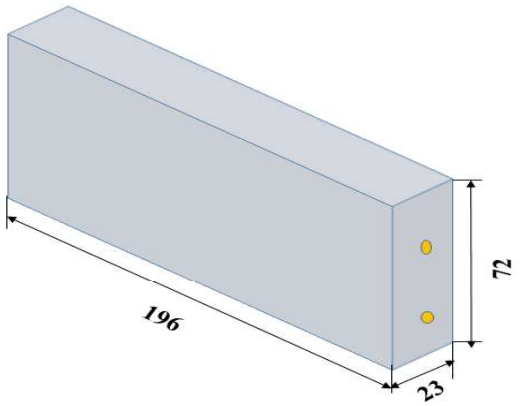

All dimensions are in mm

Figure 6: Schematic diagram of the nanofluid cooled heat sink

2.3.3 Electrical connections of TEMs

The amount of heat absorbed at the cold junction is associated with the Peltier cooling, the half of Joule heating, and the thermal conduction. Figure 7 depicts a basic electrical circuit for the studied thermoelectric cooler. Three rows of twelve thermoelectric modules (55 × 26 × 15 cm) were placed in four columns. The positive wires of each series of TEMs were linked to the negative cables of the following sequence of TEMs. Furthermore, the positive cables are connected to a bus bar (positive side) at the end of each row, and the negative cables are attached to a separate bus bar (negative side) at the end. The positive bar was then attached to the positive power supply terminal, and the negative bar was connected to the negative power supply terminal.

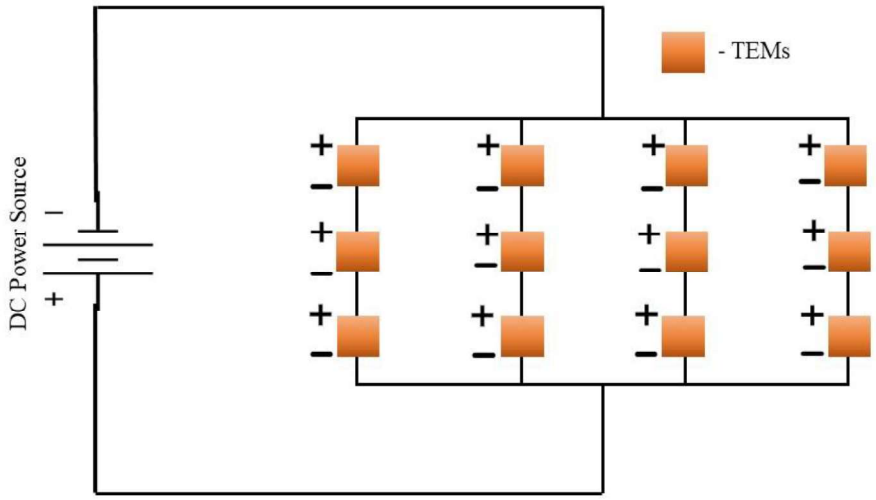

Figure 7: Electrical connection of TEMs

As shown in Figure 7, the internal connection between columns was in series, while connections to other columns were in parallel, and all the columns (with TEMs) were installed in plastic nylon. The configuration of the studied thermoelectric modules is listed in Table 2. The dimension of the plastic nylon layer is 303 × 294 × 25 mm. The nylon layer is extruded to the TEM size, and small ways are paved for wire connections.

Table 2: Specification of the selected TEMs

Company	Model	Current (A)	Max. Voltage (V)	Max. Cooling Power (W)	Max. Temperature Difference (°C)	No. of p-n couples
Ferrotec	9500/391/ 085B	8.5	53.8	248	72	391

2.3.4 Arrangement of heat sinks and thermoelectric modules

On the hot side of the TEMs, waste heat is dissipated into the environment (outdoor space) using nanofluid cooled heat sinks coupled with a radiator. Also, on the cold side of the TEMs, the cooling capacity is enhanced by using air-cooled heat sinks and blower fans, as illustrated in Figure 8. The first aspect of this project is that six nanofluid-cooled heat sinks are connected to the hot side of the twelve TEMs, where each heat sink is connected to two TEMs using thermally conductive grease. Secondly, each TEM's cold side is fixed to separate finned heat sinks, supported by a nylon layer. Consequently, twelve TEMs are connected to twelve heat sinks to stimulate the sustained cooling favoured by the TEMs' cold sides. Furthermore, the cooling obtained by the finned heat sink is fanned out to the test room through the twelve small axial flow fans and a single large fan. The specifications of a single small fan (80 × 80 × 25 mm) are 0.96 W, 2050 RPM, 33.5 CFM, 21.5 Pa, 22 dB and 95 g. Meanwhile, the big fan (200 × 200 × 50 mm) has a configuration of 78 W, 285 CFM, 1800 RPM, 285 CFM, 50 dB, and 400 g. All the layers are tightly enclosed via nuts and bolts to prevent leakage. The NTEAC dimensions were in line with the ASHRAE standard [45].

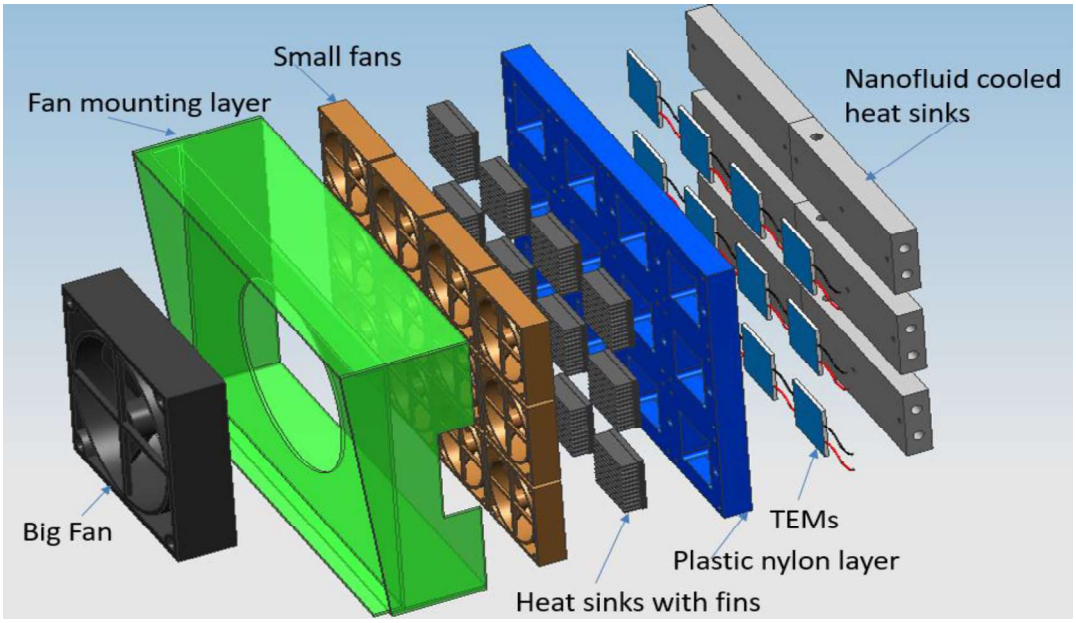

Figure 8: Arrangement of thermoelectric modules and heat sinks (Part B)

2.3.5 Radiator

In the NTEAC system, a Proton automobile radiator made of aluminium material with a louvre fin type is used. On both sides of the tubes, louvred fins are connected. When air enters the radiator's system, it blows in a transverse direction to the arrangement of tubes. Steel is used for both the tube and the louvred fins. Radiators consist of three main parts: heat pipes, an aluminium substrate, and flat fins. Steel is a common material used in radiators since it has a strong anti-corrosion property. It is built to handle heat flow from the hot nanofluid coolant, which passes through it and transfer to

the outside air. Figure 9 depicts the schematic design of the radiator. There are 46 aluminium fins with a dimension of 430 mm × 350 mm × 38 mm. The heat transfer performance of the nanofluid coolant directly affects the running state of the NTEAC system. The MWCNT/water coolant carries the waste heat generated by the TEM incorporated heat sinks (Part B) to the radiator for cooling.

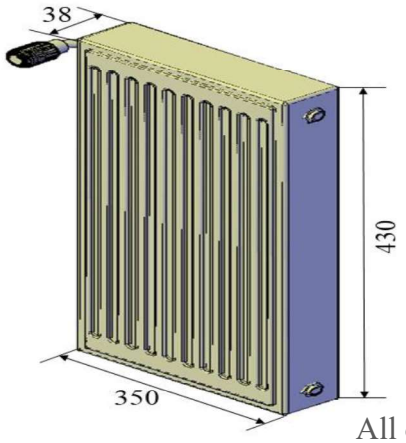

All dimensions are in mm

Figure 9: Schematic diagram of the studied radiator

2.3.6 Photovoltaic panels

Malaysia's energy sector strongly depends on non-renewable fuels as a source of energy, such as natural gas or fossil fuels. The government of Malaysia has made various efforts to promote investment in solar photovoltaic projects. Solar energy has fewer potential environmental consequences than other energy sources, such as fossil fuels, often generated with adverse side effects. A solar PV system comprises several PV modules, also known as solar panels. A module consists of tiny solar cells, each generating 1 to 2 watts of electricity. A PV module with a surface area of one square metre will produce 150 W of electricity. At an angle of 15°, the PV panels are installed on the test room's east-facing roof. Figure 3(a) in the earlier section shows the installed PV on the test room roof. In the current research, three pieces of polycrystalline photovoltaic panels of 325 Wp each generate the PV-NTEAC system's electricity. Table 3 lists the configurations of the PV panels.

Table 3: Specifications of the PV panel

Parameters	**Specifications**
Mechanical properties:	
Type of element used	Polycrystalline silicon
Size (Length × Breadth × Height)	1.99 × 1× 0.035 m
Weight	24 kg
Cells used	72

Type of output node	Amphenol H4
Gauge of output cable wire	12 AWG
Length of the output cable	1.2 m
Electrical properties:	
Maximum efficiency	16.3%
Tolerance limit of power	±3%
Maximum current	8.8A
Maximum voltage	36V
Current of the short circuit (I_{sc})	9.4A
Voltage of the open circuit (V_{oc})	46.4V
Nominal operating cell temperature	45°C
Coefficient of temperature for I_{sc}	0.05 %/K
Coefficient of temperature for V_{oc}	-0.134V/K
Coefficient of temperature of the power	-0.4%/K
Fuse rating of series connection	15A
Maximum voltage of the system	1000V

2.4. Novel proposed NTEAC system description

Evaporative air conditioners and refrigerative air conditioners are the two types of air conditioners typically used in houses. These systems, which use compressors to disperse heat, are called "air-cooled systems" and operate similarly to a car radiator. Since this cooling system absorbs moisture as it cools, it dehumidifies the air. The system absorbs water from the air within the cooled region and distributes it as hot air to the outside air. The proposed NTEAC system also follows the same principle, and it is illustrated in Figure 10, combining a nanofluid tank (Part A), TEMs incorporated heat sinks (Part B), and a radiator (Part C). The basic principle of the NTEAC system is the transfer of heat from the indoor air to the atmospheric air using forced convection. The components used in this system are a submersible pump, a small tank, an adjustable valve, a liquid-cooled heat sink, TEMs, air-cooled heat sinks, nylon layer, connecting pipes, and a radiator. The major part of the NTEAC system is Part B, where the thermoelectric modules are installed. It consists of six layers: a big fan; a fan mounting layer; small fans; air-cooled heat sinks; nylon layer; TEMs; and nanofluid-cooled heat sinks. Hot and humid weather conditions in Malaysia's Perak state were considered while designing the manufactured system.

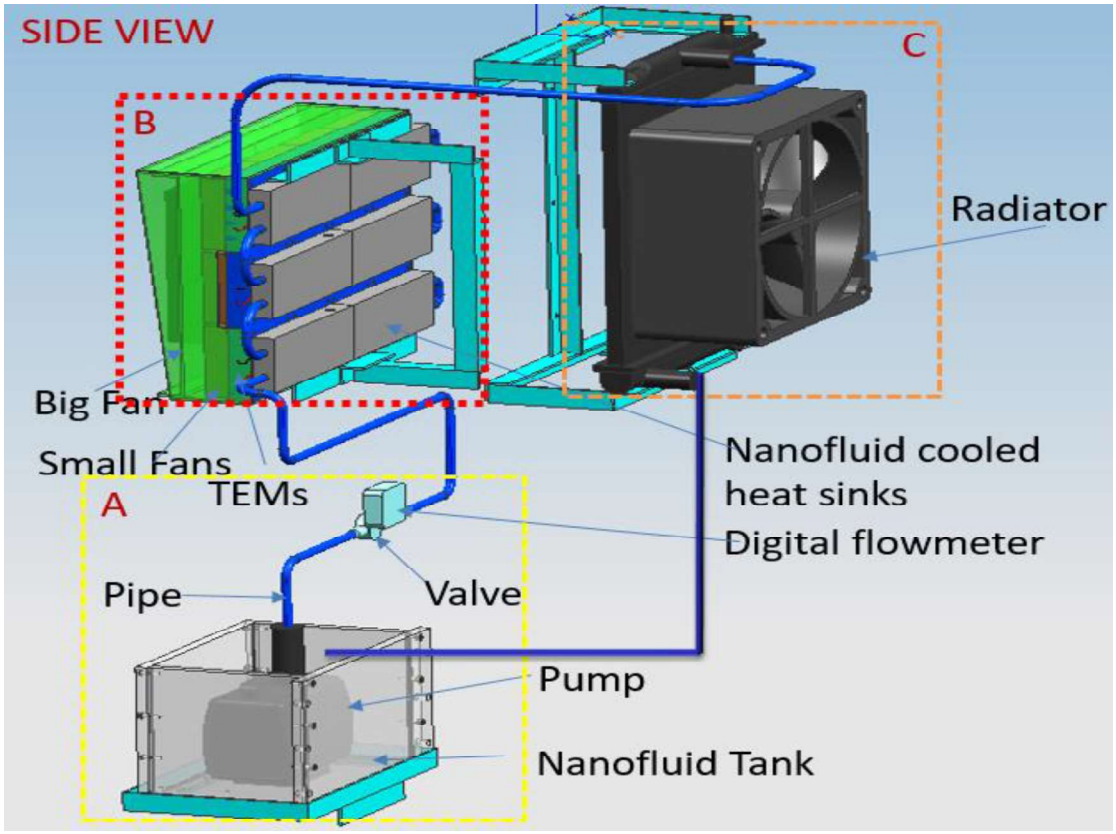

Figure 10: Schematics of the Nanofluid Assisted Thermoelectric Air Conditioner

The proposed NTEAC system has two main units: an indoor unit (pump and TEM combined heat sinks) and an outdoor unit (radiator). An adjustable valve and a digital flowmeter control the nanofluid flow and measure the flow rate. The sequential operations in the NTEAC system are demonstrated as follows. (i) MWCNT/Water nanofluid is pumped to the TEM combined heat sinks with a 13.50 LPM flow rate and 1012.6 kPa pressure. (ii) Heat from the hot side of the thermoelectric module is absorbed by the circulated nanofluid, while the cooling side of the TEM is subjected to indoor air via air-cooled heat sinks and fans resulting in a reduction in test room temperature. (iii) Then, the heated nanofluid flows to the radiator, where the heat is transferred to the atmosphere and enters the pump (with tank) to repeat the cycle. The schematic diagram of the processes in the NTEAC system is illustrated in Figure 11. The design details of the NTEAC components are listed in Table 4.

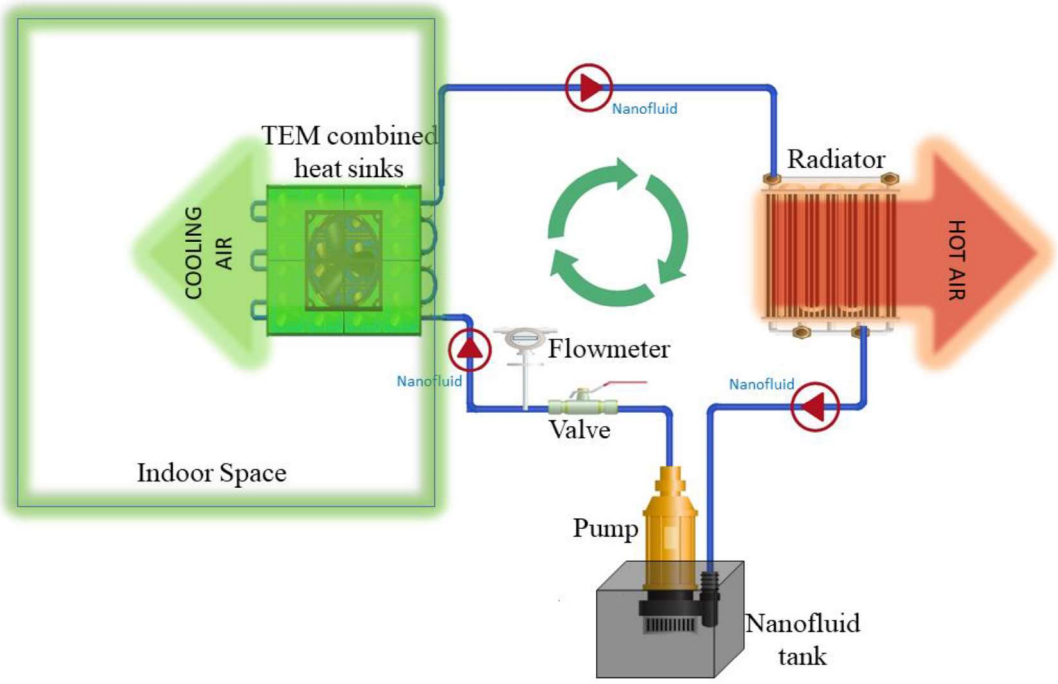

Figure 11: Schematic diagram of the processes in the NTEAC system

Table 4: Technical details of the NTEAC components

Sl. No.	Components	Parameters	Unit	Quantity
1.	Submersible Pump	220 V, 50 Hz, 85 W, 4000 L/H, 4m	-	1 No.
2.	Nanofluid tank	250 × 155 × 155	mm	1 No.
3.	TEM	I_{max} = 8.5 A V_{max} = 53.8 V	-	12 Nos.
4.	Air-cooled heat sinks	55 × 55 × 23 (20 fins)	mm	12 Nos.
5.	Small fan	24 V, 0.04 A, 33.5 CFM	-	12 Nos.
6.	Big fan	12 V, 6.5 A 200 × 200 × 50	mm	1 No.
7.	Nanofluid cooled heat sink	196 × 72 × 25	mm	6 No.
8.	Brass valve	½	inch	1 No.
9.	MWCNT/Water nanofluid	k = 0.71	W/m.K	5 Litres

10.	Radiator	430×350×38, 0.09 (fin thickness), 0.3 (Radiator tube)	mm	1 No.
11.	Digital flowmeter	0.3 – 15	LPM	1 No.

2.5. Building equipped with NTEAC system

The actual NTEAC system installed in a building consists of three main parts, namely a tank filled with nanofluids (Part A), TEMs incorporated with heat sinks (Part B), and a radiator (Part C). Figure 12 illustrates the studied PV-NTEAC device installed in the test room. From 1st September to 30th September 2020, the experiment was conducted in a test room situated at the Universiti Teknologi PETRONAS, Malaysia. Before the installation of the NTEAC system, the test room's estimated peak cooling demand was 590 W. Each TEM produced a cooling power of 50 W at an applied voltage of 10 V and 5 A. Since the required cooling load for the test room is 590W, the NTEAC system uses twelve 50W (600 W) thermoelectric modules, which are slightly more (10 W) than the required cooling load. Once the DC power supply was turned on, the current flowed through the TEMs, creating a temperature difference between the module's cold and hot sides. With an exhaust fan (78 W), the ambient air was scattered inside the test room through the NTEAC device (Part B) mounted on the test room's inside wall. There were twenty-four fins in each heat sink linked to the cold side of the TEMs, which absorbed the heat sustained in the test room's ambient air. The heat sinks were also cooled using 0.96 W (12 Nos) power exhaust fans by forced convection.

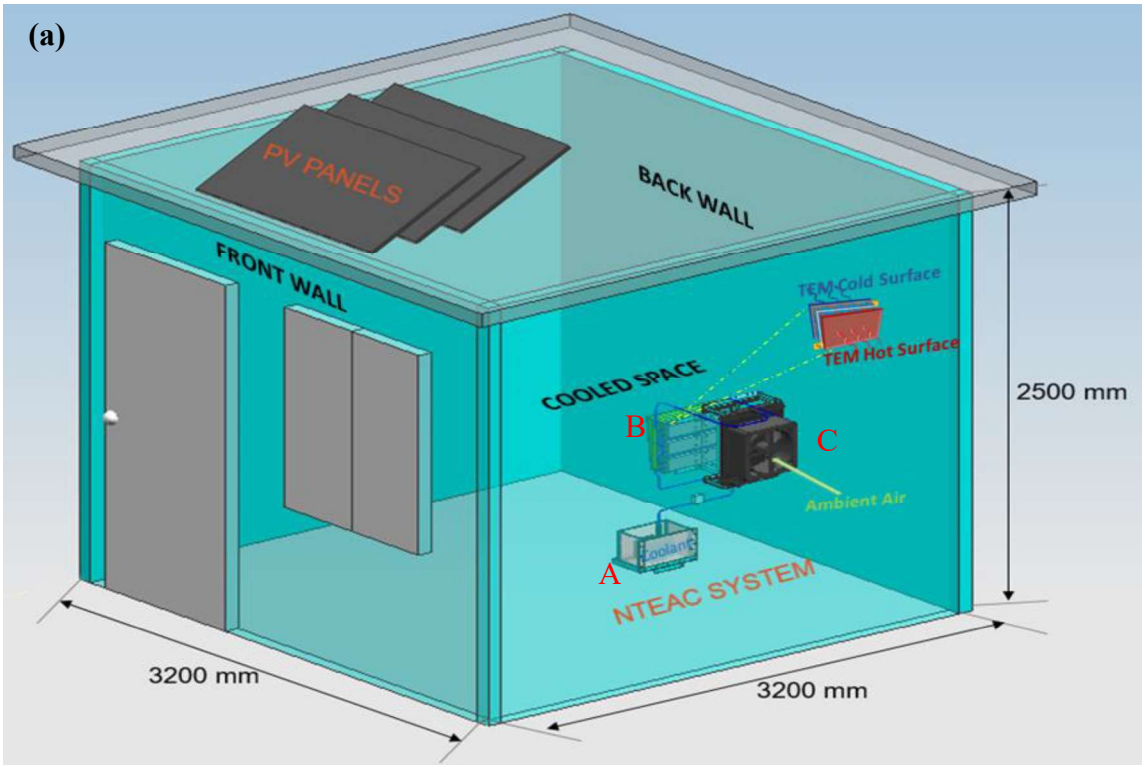

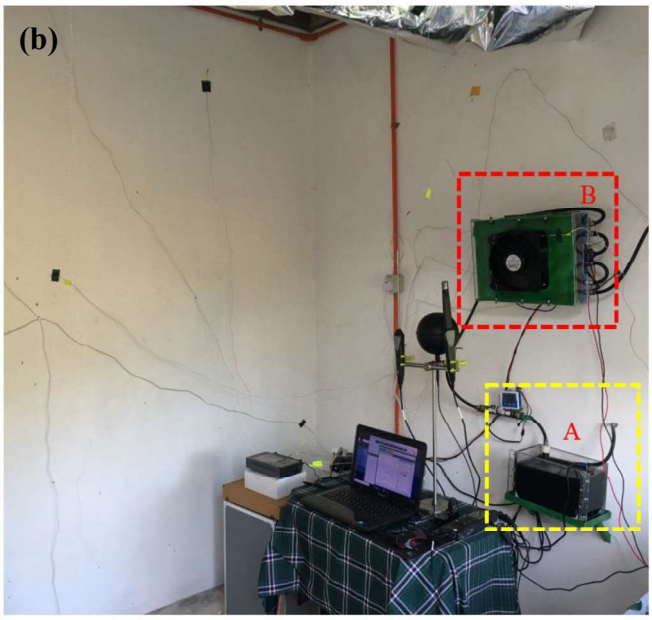

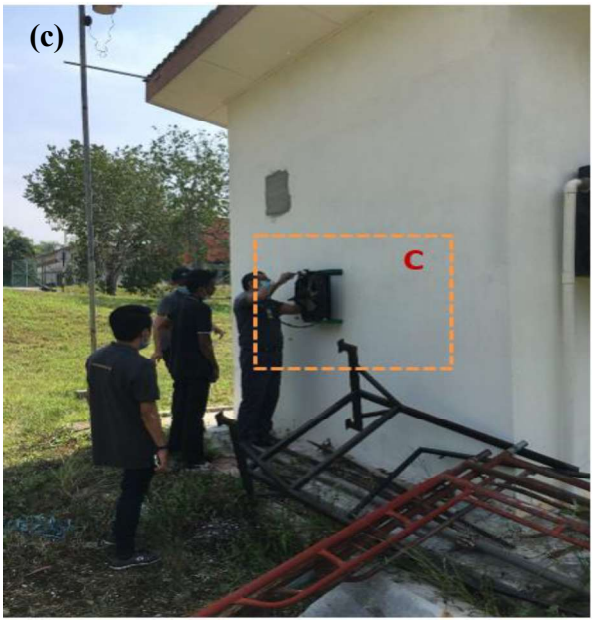

Figure 12: Building equipped with PV-NTEAC(a) Schematic diagram (b) Indoor unit with Part A and Part B (c) Outdoor unit with Part C

2.6. Experimental procedure

As mentioned earlier, the experiment was conducted in September 2020. The CLTD (Cooling Load Temperature Difference) calculation showed that the test room needed 590 watts of cooling capacity to compensate for the thermal acceptability criteria without considering the influx of heat through the floor. As shown in Figure 13, the electricity generated from photovoltaic panels was

stored in batteries (RA-12-40 Batteries) through a solar charge controller (Beta 2.0). This research explores the PV-NTEAC system's performance at current levels, ranging from 2 A to 6 A.

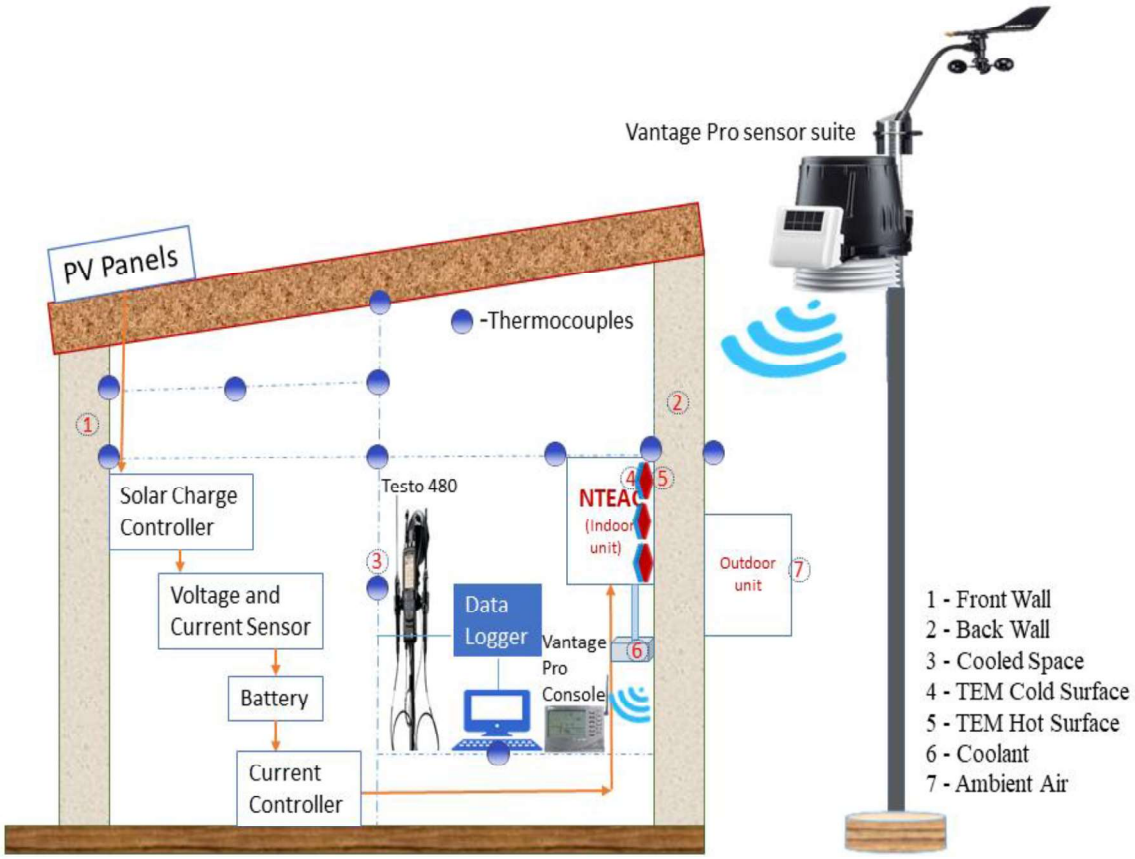

Figure 13: Schematic diagram of the experimental setup

It also uses an adjustable current controller (DPS 5015) to control the current supply into the PV-NTEAC system. Moreover, different temperatures, such as inlet temperature (T_{in}), hot junction temperature ($T_{hot,out}$), cold junction temperature (T_c) and cold outlet temperature ($T_{c,out}$), were measured at various positions in the test room using 10 K-type thermocouples. Based on the ASHRAE standard 55 [46], the methodology for measuring the test room's indoor thermal condition was chosen. The Class II field research protocol [47] was followed to render the data collection method. To obtain the indoor air quality (IAQ) such as room temperature (T_{room}), room humidity (RH), air pressure (P_{room})and air velocity (Vroom), TESTO 480 was placed at 1000 mm above the ground and near the occupant region. Data were gathered during the solar hours of 8 AM to 8 PM with an interval of 5 minutes for 30 days. Figure 14 shows the original image of the experimental setup used in the study. The details of various electrical instruments used in the NTEAC system are listed in Table 5.

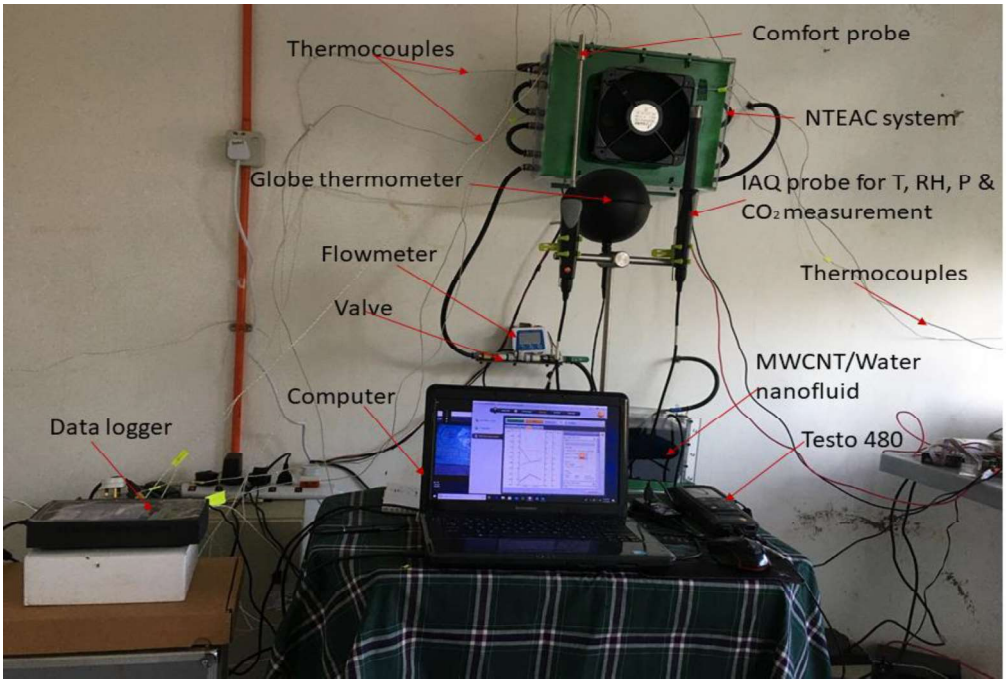

Figure 14: Original image of the experimental setup

Table 5: Specification of electrical devices

Descriptions	**Values**
Current Controller (Model: DPS 5015)	
Voltage output accuracy	0.01V (0.5%)
Voltage input accuracy	6-60V
Maximum Voltage output	50V
Maximum power output	1000W
Maximum output current	20A
Current output accuracy	0.5%
Charge Controller (Model: Solar Beta 2)	
Length × Breadth × Height	0.159 × 0.81 × 0.47 m
Operating voltage of the system	12-24V
Input PV voltage (Max.)	50V
Maximum Charge Current	15A
Terminal voltage of the battery (Max.)	34V
Maximum current supply (Battery)	20A
Voltage drop of the circuit (Charge)	≤0.28V
Voltage drop of the circuit (Discharge)	≤0.20V
Battery Bank (Model: MSB RA 12-40)	

Length × Breadth × Height	0.19 × 0.16 × 0.17 m
Unit voltage	12V
Battery Capacity	40Ah@10hr-rate
Discharge current (Max.)	400 (5) A/sec
Internal resistance	8 mΩ
Temperature range for discharge	-20 to 60
Temperature range for charge	0 - 50°C
Operating temperature during current storage	-20 to 60°C
Operating temperature during normal condition	25±5°C
Maximum charging current	12A
Submersible Pump (Venus Aqua V4800)	
Voltage	220 – 240V
Frequency	50/60 Hz
Power	85 W
Maximum flow rate	4000 L/hr
Maximum flow height	4m

Besides, the Davis Vantage Pro 2 weather station is fixed outside the test room at the height of 3000 mm. All the measured data is displayed on a console placed inside the test room through a low power radio (wireless). The Davis vantage pro 2 can determine the inside temperature, outside temperature, inside humidity, outside humidity, pressure, heat index, wind speed, solar radiation, dew point, UV index, etc. This study measured ambient temperature, humidity, and wind speed at a 5-minute interval via the Davis vantage pro 2 weather station. Table 6 presents the technical specifications of the Davis vantage Pro 2 sensors.

Table 6: Specification of sensors in Davis Vantage Pro 2

Variable	Descriptions	Values
Humidity	Range	1 – 100%
	Resolution	1%
	Accuracy	±2%
Pressure	Range	410 – 820 mmHg
	Resolution	0.1 mmHg
	Accuracy	±0.8 mmHg
Temperature	Range	0 – 60 °C
	Resolution	0.1 °C

	Accuracy	±0.3 °C
Solar radiation	Range	0 – 1800 W/m^2
	Resolution	1 W/m^2
	Accuracy	±5%
Dew point	Range	-76 °C to +54 °C
	Resolution	1 °C
	Accuracy	±1 °C

2.7. Data reduction and uncertainty analysis of the PV-NTEAC system

2.7.1 Data reduction

The cooling capacity (*Qc*) of the NTEAC system is calculated using Eq. 1. [26]

$$Q_C = SIT_c - 0.5I^2R - K\Delta T \quad (1)$$

Where *S*, *I*, *R*, *K* and ΔT represent the Seebeck coefficient, input current, electrical resistance, thermal conductivity, and temperature gradient of the thermoelectric module. T_c and T_h denote the temperature of the hot and cold sides of the TEM, respectively.

The Coefficient of Performance (COP) of the studied PV-NTEAC is estimated using Eq. 2. [20]

$$COP = \frac{Q_c}{P_{TEM} + W} \quad (2)$$

$$P_{TEM} = I^2R + SI\Delta T \quad (3)$$

$$W = P_{small\ fan} + P_{big\ fan} + P_{pump} + P_{radiator} \quad (4)$$

Where P_{TEM} reflects the input power provided by TEM, *W* illustrates the input power given to other components (fan, pump, radiator) of the NTEAC system.

The thermoelectric cooling module's input power is determined using Eq. 5.

$$P = VI \quad (5)$$

I is the input current, and *V* is the input voltage supplied to the TEM.

2.7.2 Uncertainty analysis

Due to calibration and data recording, systematic errors can emerge during the experiment. Therefore, measuring probes such as thermocouples are adjusted to increase the precision of data collection. Therefore, measurement probes such as thermocouples are calibrated with a bi-metallic thermometer immersed in water under different temperatures to enhance their data collection precision. As shown in Table 7, systematic errors are also considered in the uncertainty analysis to get a complete picture of the measurement's accuracy. The root-sum-squares (RSS) technique has been used to do the total uncertainty analysis. Moffat [47] pioneered this method, which defines the uncertainty of a function, δF, as follows:

$$\delta F = \left[\sum_{i=1}^{n} \left(\frac{\partial F}{\partial X_i}\delta X_i\right)^2\right]^{\frac{1}{2}} \quad (6)$$

Where X_i indicates the uncertainty sensitivity coefficient, fore, using the above equation (Eq. 6), the estimated uncertainty of COP (δCOP) is determined with a 98% certainty, and the computed value was less than 0.1%, as far as significant components are concerned.

Table 7: Uncertainty analysis of the obtained experimental data

Variable	**Typical Value (X)**	**Uncertainty (∂X)**	**Relative Uncertainty** $(\frac{\partial X}{X})\%$
T_{in} (°C)	30-35	0.51	1.7
$T_{c,out}$ (°C)	22-25	0.54	2.4
$T_{h,out}$ (°C)	21-23	0.21	1
T_{amb} (°C)	25-28	0.24	0.9
T_{room} (°C)	27-30	0.3	1.1
RH_{in} (%)	85-100	0.6	0.7
RH_{out} (%)	90-94	0.64	0.71
Current (A)	1-6	0.01	0.16
Voltage (V)	5	0.05	1.66
Nanofluid flow rate (LPM)	13 - 15	0.12	1
Solar radiation (W/m^2)	100 - 1000	1.5	1.5

3. RESULTS AND DISCUSSION

In this section, the results of the performed experiments are discussed to observe the PV-NTEAC system's performance with MWCNT/water nanofluids. First, the detailed experimental results of the test room acquitted with the PV-NTEAC system are reported. Then, the effect of changing input current supply on the COP and cooling power of the PV-NTEAC system is discussed in detail. Following that, the test room's indoor thermal conditions during optimal operating conditions are measured and compared to the initial test room to determine the system's suitability for building cooling in Malaysia's climate.

3.1. Thermal environments

3.1.1 Air temperature and Relative humidity

Tronoh, located at latitude 4° 23' 2.292" N and longitude 100° 58' 16.824" E, is a tropical city in Malaysia's hot and humid area. Since the performance of the PV-assisted NTEAC system is dependent on the outside climatic conditions, such as outside temperature, relative humidity (RH), and solar radiation intensity, it is no surprise that the PV-assisted NTEAC system's performance varies widely based on the climate at the installation site. In this study, the ambient air temperature, relative humidity, and UV index were evaluated by Davis Vantage Pro for 30 days (720 hours) in September 2020, as shown in Figure 15. The annual mean temperature ranges between 25 and 27°C, and the monthly mean temperature and humidity in September are 26.5°C and 82%. Moreover, the minimum and maximum temperatures recorded during the September month were 23.6 and 30.1 °C, with an average UV index of 6. The lowest RH ranged between 46 and 55.73% during daylight, while the highest RH ranged from 79.3 to 99% at night.

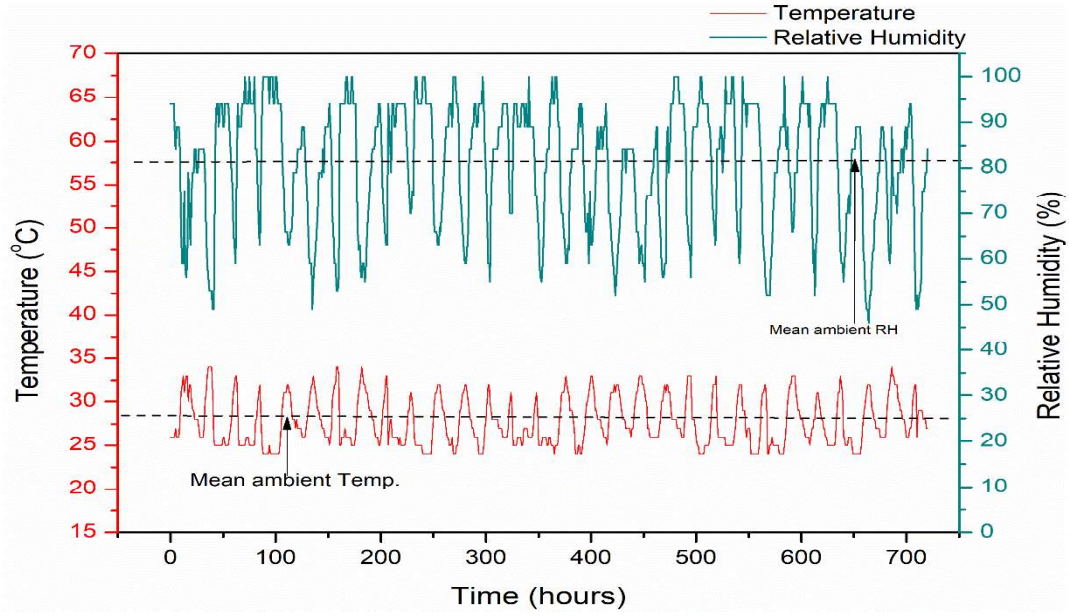

Figure 15: Hourly changes of ambient air temperature and relative humidity for September 2020

3.1.2 Solar irradiance and PV power

Assessment of the solar irradiance of a region is just as critical as evaluating the humidity and temperature data collection for a given time in deciding the viability of a solar-powered project. The variation of solar irradiance and the PV panel power output from 1st to 30th September 2020 is displayed in Figure 16. Underlying darkness and cloudiness lead to reduced electrical power production. An average solar irradiance of 661.42 W/m^2 was observed during the experiment. The maximum solar irradiance was 1045.81 W/m^2 on 18th September 2020, and a minimum solar irradiance of 126.03 W/m^2 was detected on 19th September 2020. The photovoltaic (PV) panel delivered a maximum of 595.81 W and 1.12 kWh of daily power output. Also, three PV panels were used to provide sufficient power to the PV-NTEAC device via batteries. Two solar charge controllers controlled the power supplied by three PV panels and stored directly in the batteries. The impact of input current on the PV-NTEAC device's output was investigated using this as a source of input control.

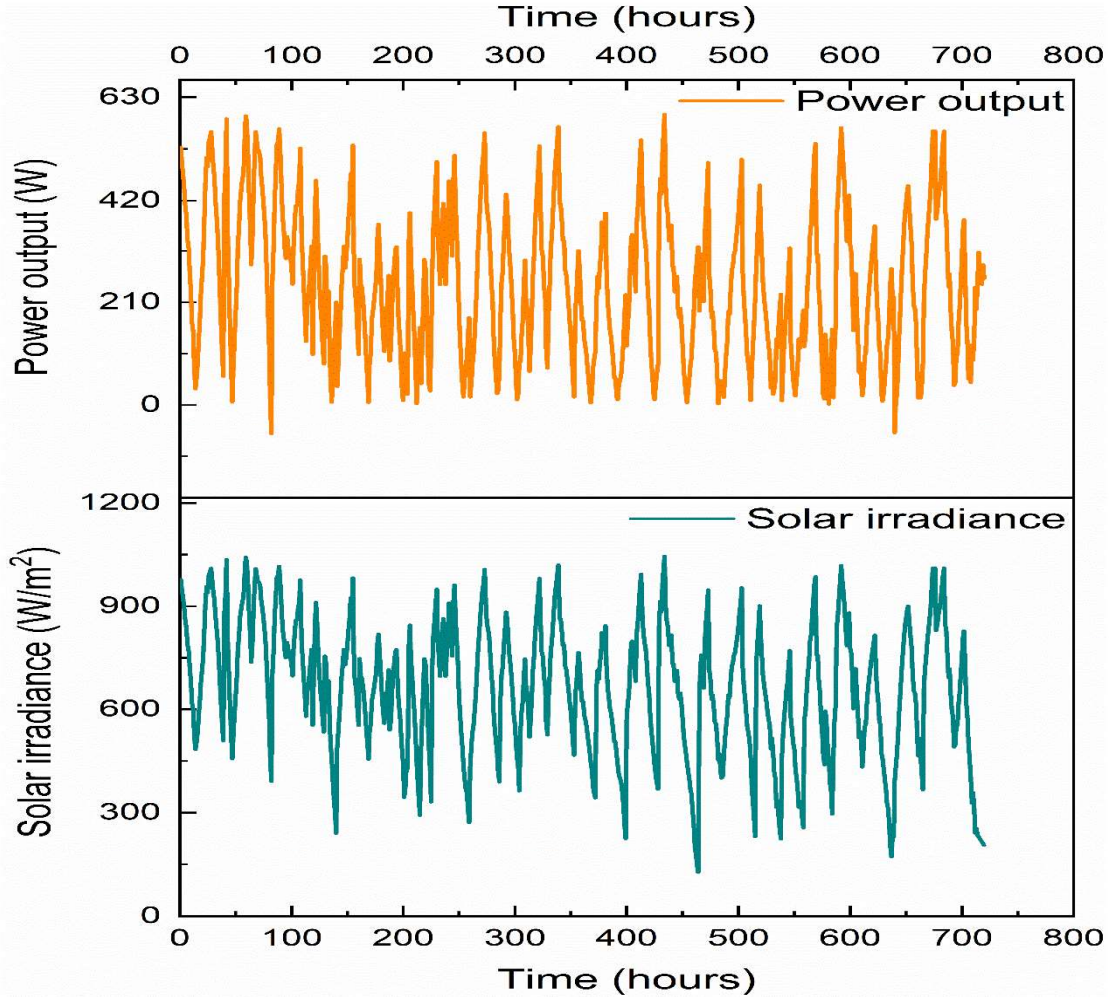

Figure 16: Hourly changes in solar irradiance and PV power output for September 2020

3.1.3 Mean radiant temperature and air velocity

The daily changes of mean radiant temperature (MRT) and air velocity from 1st to 30th September 2020 are depicted in Figure 17. Air temperature, velocity, and globe temperature were used to determine mean radiant temperature (MRT) according to ISO 7726 standards [48]. The average ambient air velocity was 1.16 m/s, with a minimum and maximum air velocity of 0.67 m/s and 2.02 m/s observed on September 16th and 20th. Therefore, the daily change of MRT is similar to that of the air temperature. Many of the MRT values recorded in the analysed building were much higher than the air temperature (about 1°C), indicating a significant radiant impact that needed to be accounted for.

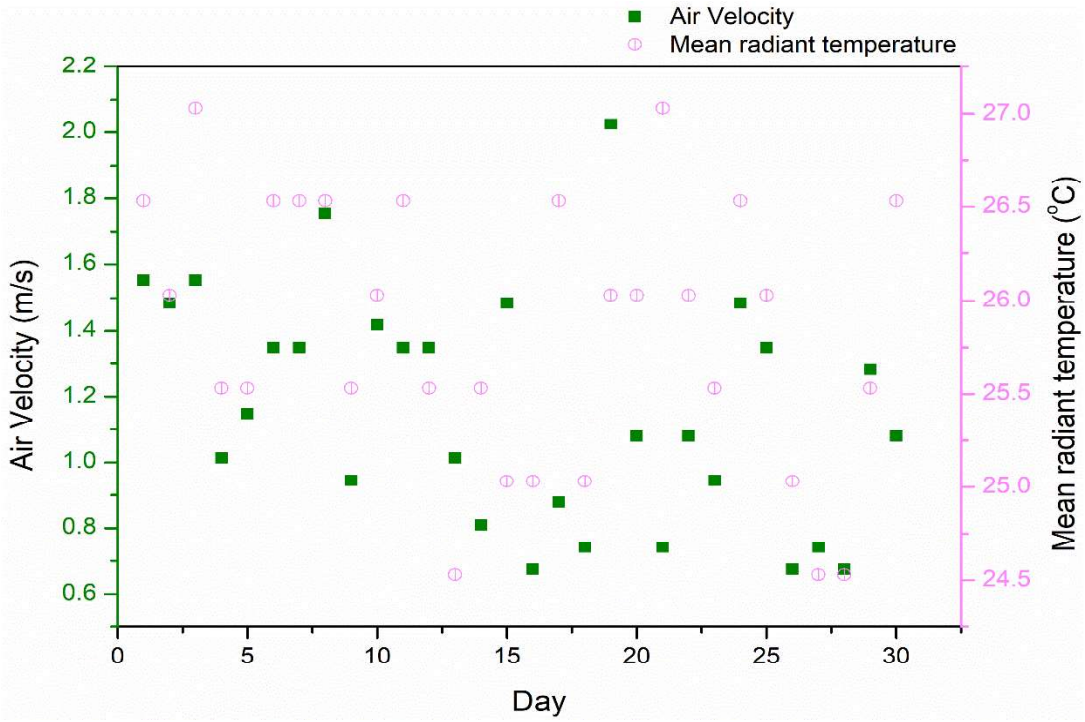

Figure 17: Daily changes of mean radiant temperature and air velocity for September 2020

The ambient data from 7th to 11th September (8 hours to 20 hours each day) is considered the most identical to ensure the results are comparable under natural weather conditions. The ambient weather conditions are presented in Table 8.

Table 8: Summary of ambient weather conditions of the test room

Parameters	Description	7/9/2020	8/9/2020	9/9/2020	10/9/2020	11/9/2020
Outdoor Temperature (°C)	Minimum	24.9	26.02	25.11	26.3	25.4
	Maximum	34.23	31.4	33.2	32.1	33.6
	Mean	27.7	27.41	28.33	29.2	30.1

	Standard Deviation	2.70	2.60	4.10	3.50	3.80
Indoor Temperature (°C)	Minimum	24.01	25.8	25.25	24.92	25.02
	Maximum	33.12	31.78	32.67	32.30	32.9
	Mean	27.26	25.49	27.66	27.31	26.40
	Standard Deviation	2.45	2.80	2.020	2.50	2.90
Radiant Temperature (°C)	Minimum	25	24.90	22.80	23.71	24.50
	Maximum	27.42	27.03	26.89	26.84	26.50
	Mean	27.51	27.26	25.64	26.57	26.8
	Standard Deviation	2.70	2.40	2.90	2.60	2.30
Outdoor Relative Humidity (%)	Maximum	97	96	89	91	93
	Minimum	57	55	49	53	57
	Mean	79	75	82	84	81
	Standard Deviation	5.40	4.80	4.20	6.20	5.10
Indoor Relative Humidity (%)	Maximum	80	83	91	85	79
	Minimum	61	72	59	64	55
	Mean	77	79	84	75	78
	Standard Deviation	3.40	4.20	5.50	5.30	3.80
Velocity of air (m/s)	Maximum	3.20	2.50	2.10	1.80	2.20
	Minimum	0.8	1.20	0.70	1.20	1.00
	Mean	1.60	1.80	1.40	1.30	1.50
	Standard Deviation	0.68	0.30	0.20	0.70	0.50

3.2. Thermal performance of the NTEAC system

Figure 18 presents the time-dependent temperature measurements conducted on a hot, humid day in September 2020 for the internal front wall, internal rear wall, the hot surface of TEM, cold surface of TEM, cooled space, ambient air, and coolant (MWCNT/water nanofluid) of the NTEAC system installed in the test room. While the cold side temperature of the TEM ranged between 29.3 and

69.4°C, this value ranged between 47.1 and 147.7 °C for the TEM's hot side. An improvement of 17% was obtained in the cooling system using 0.5wt% MWCNT/Water nanofluid with respect to pure distilled water when the initial and final state temperature differences were compared. As the temperature of the surrounding environment rises, the temperature difference (ΔT) of the test room is cooled using the studied nanofluid-based TEAC. The obtained data also shows that MWCNT/water nanofluids give the most impressive improvements in heat transfer performance. Furthermore, it is observed that the rate of enhancement depends on various factors, including thermal conductivity, agglomeration, viscosity, density, and the specific heat capacity of the heat transfer fluid. These aspects were briefly explored in our previous literature [43]. In principle, the thermal conductivity of nanofluids has the most significant effect on heat transfer characteristics, which is also supported by the results of ΔT, which shows a similar trend to that seen in the prior research [49]. As a whole, it can be said that the thermal performance of the PV-NTEAC system is highly dependent on solar irradiation and ambient temperature. The PV-NTEAC system, on the other hand, may function differently depending on the climate.

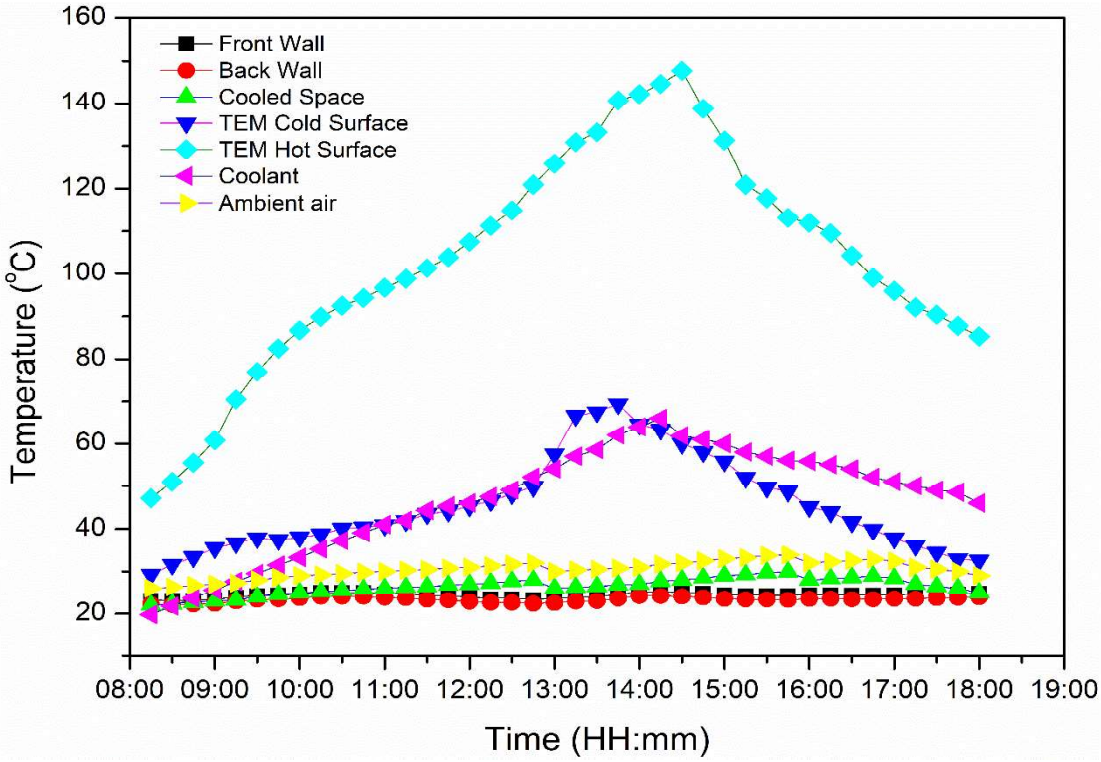

Figure 18: Thermal performance of NTEAC device for 0.5wt% MWCNT/Water nanofluid

3.3. Coefficient of performance and Cooling Capacity of the NTEAC system

The coefficient of performance (COP) was assessed by calculating the cooling energy dissipated inside the test room and the thermoelectric modules' electrical energy input. As aforementioned, the COP of the photovoltaic powered nanofluid assisted thermoelectric air conditioner (PV-NTEAC)

can be improved by reducing the hot side temperature of the thermoelectric modules. This can be done by removing heat more efficiently from the hot side of the TEMs through the nanofluid cooled heat sink unified to a radiator. Nanofluids are ideal coolants for radiators because of their excellent thermal properties, contributing to high heat transfer. To analyze the cooling effect of the enhanced thermophysical properties of working fluid (nanofluid), more tests were performed on the PV-NTEAC system by varying the input current supply (2-6.5A). Figure 19 shows the COP variation of the PV-NTEAC system implemented in the test room. As seen in the above figure, the COP of the PV-NTEAC system increased to its maximum at first and then decreased gradually when the current supply increased to 6.5A. The maximum obtained COP is 1.27 when the applied current is 6A, and the cold side temperature is 22.7 °C. The results show that the PV-NTEAC system requires less electrical energy and works more efficiently with an optimum input current supply of 6A. On the other hand, the COP decreased from 1.27 to 1.19 when the current supply increased from 6A to 6.5A. When the system was operating at current levels greater than 6.5A, it was discovered that a significant quantity of heat was being transmitted to the cold side of the TEMs, thus negating the total cooling capacity of the system.

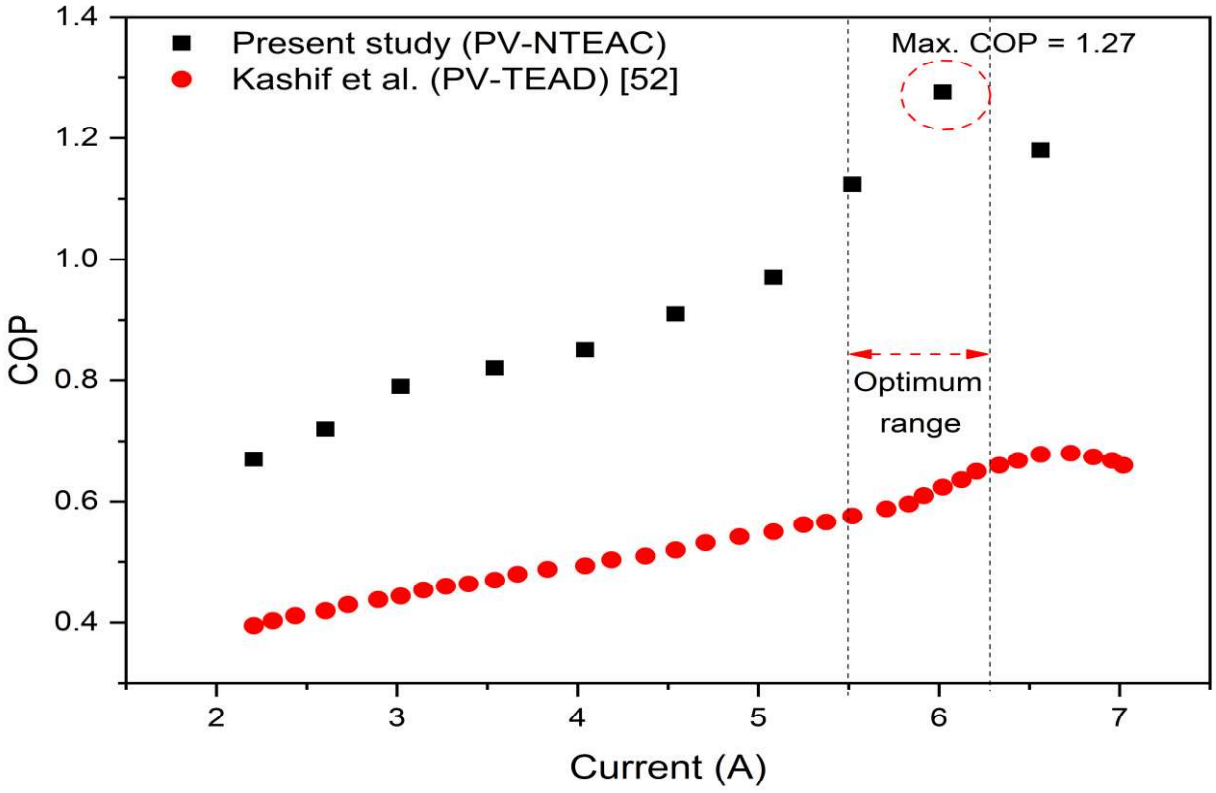

Figure 19: Effect of current on the COP of the PV-NTEAC system

By circulating nanofluids on the heat sink (hot side of TEMs), the temperature difference between the hot and cold sides of the TEMs can be maintained, allowing for constant cooling of the heat

sink (hot side of TEMs). As MWCNT/water nanofluid possesses fascinating heat transfer characteristics, this method effectively calms buildings with a minimum number of TEMs in TEACs. Furthermore, the obtained results are compared with earlier thermoelectric cooling studies, shown in Table 9.

Table 9: Comparison with previous studies on thermoelectric cooling

References	**Number of TEMs & Model No.**	**Operation current(A)/ Voltage(V)**	**Maximum COP**	**Maximum Cooling capacity (W)**	**Application**
Shen et al. 2013, [50]	1 TEM (TEC1-12706)	1.2A	1.77	6.38	Small office space
Tan et al. 2015, [51]	42 TEMs (RC12-8)	5A	0.78	1534	Office room (33.6 m^3)
Kashif et al. 2015, [52]	24 TEMs (TEC1-12730)	2 – 7A	0.679	499	Test room (18.9 m^3)
Puy et al. 2017, [53]	16 TEMs (RC12-8)	12 V	0.78	600	Residential building (0.27 m^3)
Rincon et al. 2018, [54]	12 TEMs (RC12-6L)	120 V	0.77	480	Climatic chamber
Cheon et al. 2019, [55]	9 TEMs (HMN 6040)	1 – 3.2A	0.73	504	Office building (3000 m^3)
Chen et al. 2020, [56]	9 TEMs	1.5 – 9.9A	1.24	324	Simulation box (0.42 m^3)
Looi et al. 2020, [57]	9 TEMs (Ferrotec 9500/391/085B)	5A	1.67	181	Test chamber (3.6 m^3)
Present work	12 TEMs (Ferrotec 9500/391/085B)	2 – 6A	1.27	571	Test room (25.6 m^3)

In order to ensure continuous operation and appropriate performance, the hot sides must efficiently disperse heat into the ambient air. Cooling performance is affected by both the convection heat transfer coefficient and the heat dissipation regions on the hot side TEM. The high heat transfer coefficient of MWCNT/water nanofluid is attributed to the high heat dissipation rate, resulting in cooling capacity enhancement. Figure 20 shows the PV-NTEAC system's cooling capacity (Q_c) with various current supplies. Increasing the input current first allows the cooling capacity to achieve its maximum value. Following that, the Q_c falls in accordance with the rise in electrical current flow. Using a current supply of 6A, the maximum possible Q_c of 571W was obtained. As long as the input current is sufficient, the Peltier cooling rises in proportion to an increase in electrical current, eventually taking over and reducing Q_c ultimately. This is attributed to the rise of Q_c with the rise of electrical current. Apart from that, Q_c declines after reaching its maximum value since Joule heat rises faster than Peltier cooling does. These results are in good agreement with Irshad et al. [52], in which the COP and Q_c increased (3-5A) first and decreased (> 5A) at greater current supply. Furthermore, the COP and Q_c increase when the hot side temperature of the TEMs are lowered. In a nutshell, the maximum COP is 1.27, and the corresponding Q_c is 571W.

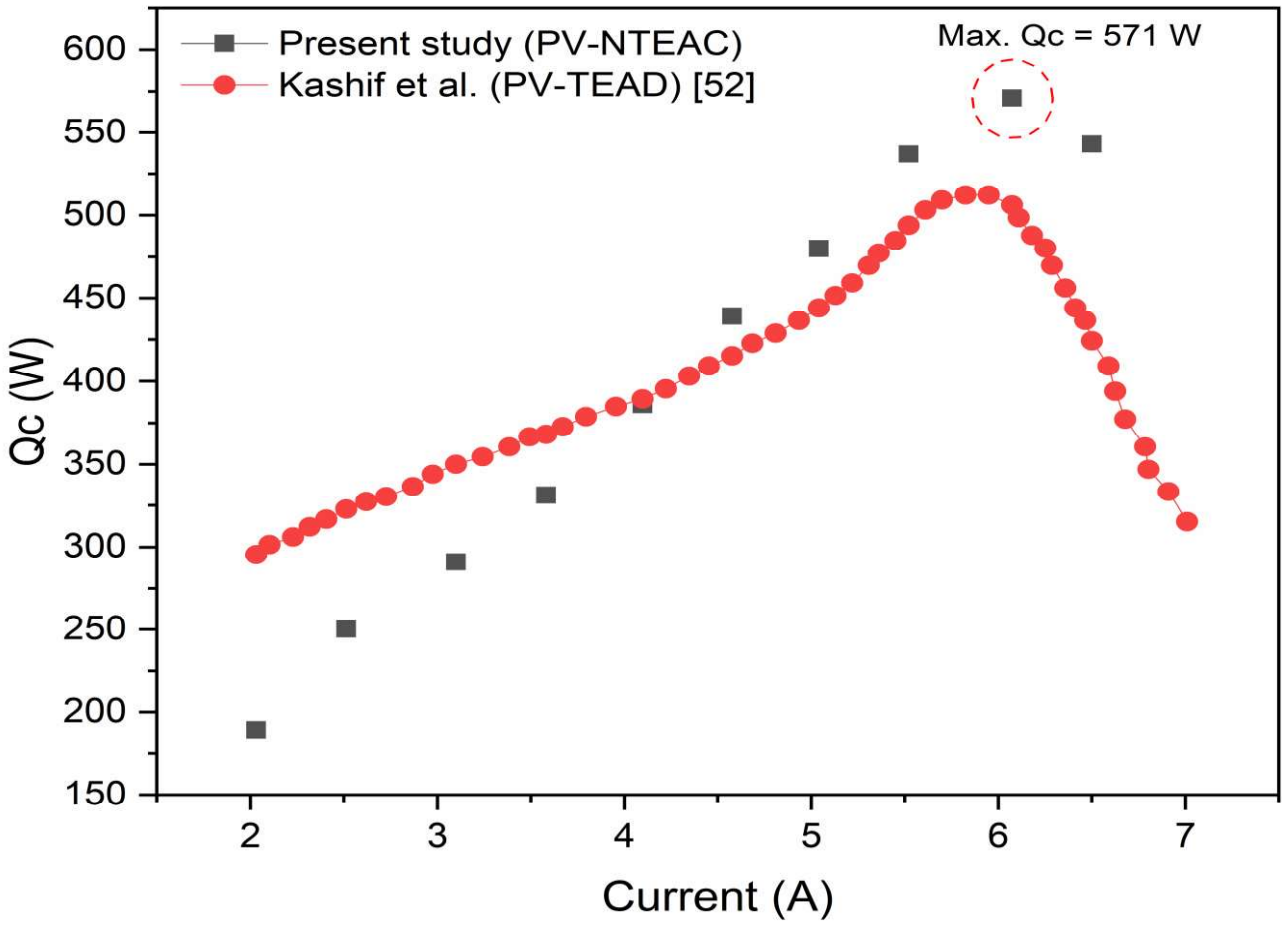

Figure 20: Effect of current on the cooling capacity of the PV-NTEAC system

3.4. Performance of the test room equipped with NTEAC system

This section will present and discuss TEM's cold side and hot side temperatures, indoor temperature, and relative humidity under different input currents to analyze the PV-NTEAC system's performance. The temperature variations seen at the outlet areas of the hot and cold junctions occur due to the Peltier effect when the PV-NTEAC system is turned on at 8 AM. The decrease in the incoming air temperature was due to heat absorption on the cold side of the TEMs, and the absorbed heat was discharged via forced convection, which transferred the heat to the hot side of the system. The airflow rates to the cold junction and the hot junction are monitored to ensure no change for all current supplies. Regarding the experimental findings shown in Figure 21, different outcomes were found for the hot and cold sides' temperatures, depending on the nanofluids' temperature. The results show that both the nanofluid temperature and the hot side temperature rise in tandem, whereas the cold side temperature rises slower. This increases the difference between the hot and cold sides' temperatures, thus making the temperature gradient wider.

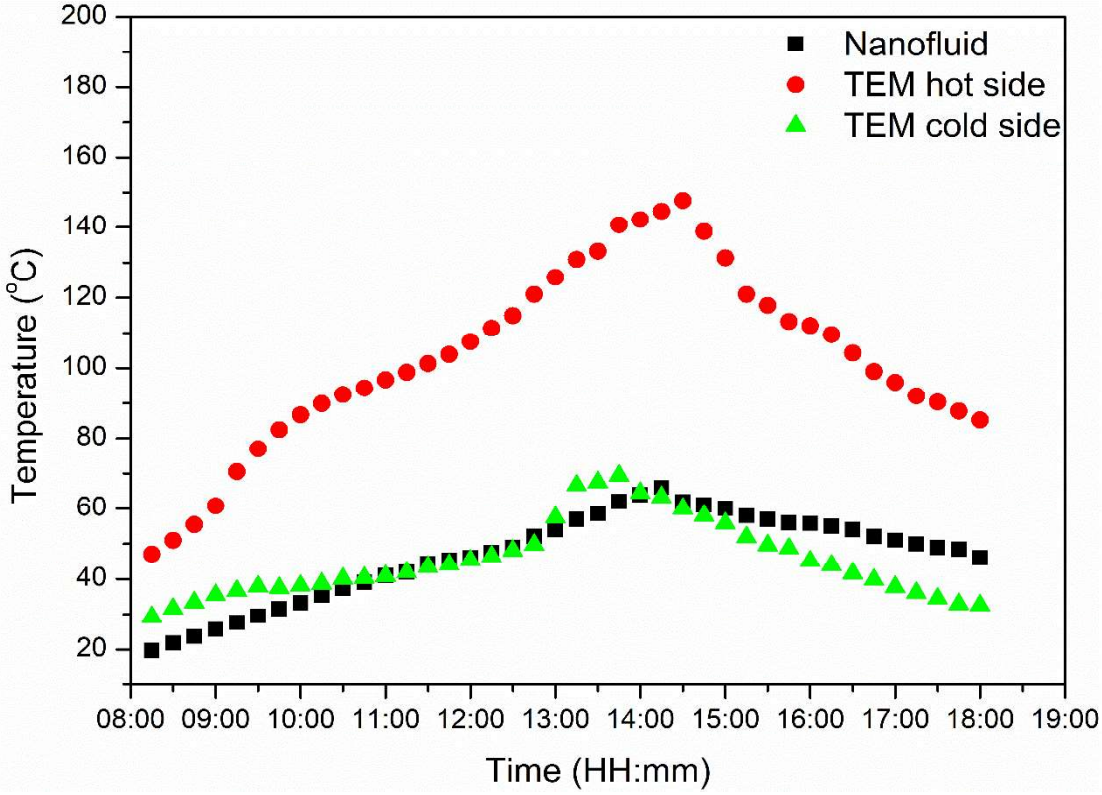

Figure 21: Temperature of TEM and nanofluid at different timings

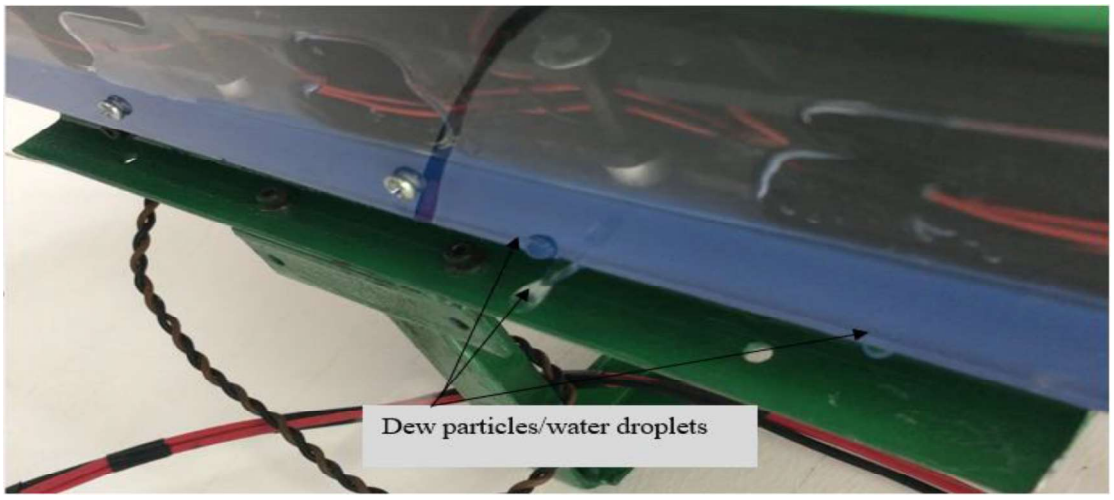

Figure 22: Deposits of dew particles and water drops in the PV-NTEAC

As the temperature of an object drops below the dew point, water vapour condenses on the comparatively cool surface of the object to create water droplets and dew particles. The formation of water droplets and dew particles is shown in Figure 22. At constant pressure and continuous water vapour, moisture in moist air is cooled to achieve the dew point temperature. Due to the fact that the dew point temperature is a measure of humidity, it functions as a comfort index. Usually, the dew point temperature should be lower than the wet-bulb temperature to attain optimum human comfort. Figure 23 illustrates the dry bulb and dew point temperature fluctuation of the processed air at 6A current. Results showed that the dew point and the dry bulb temperature differed slightly, which expedited moisture removal. The maximum dew point and dry bulb temperature were 24.77 °C and 26.14 °C, respectively, which occurred around 13.30 hours.

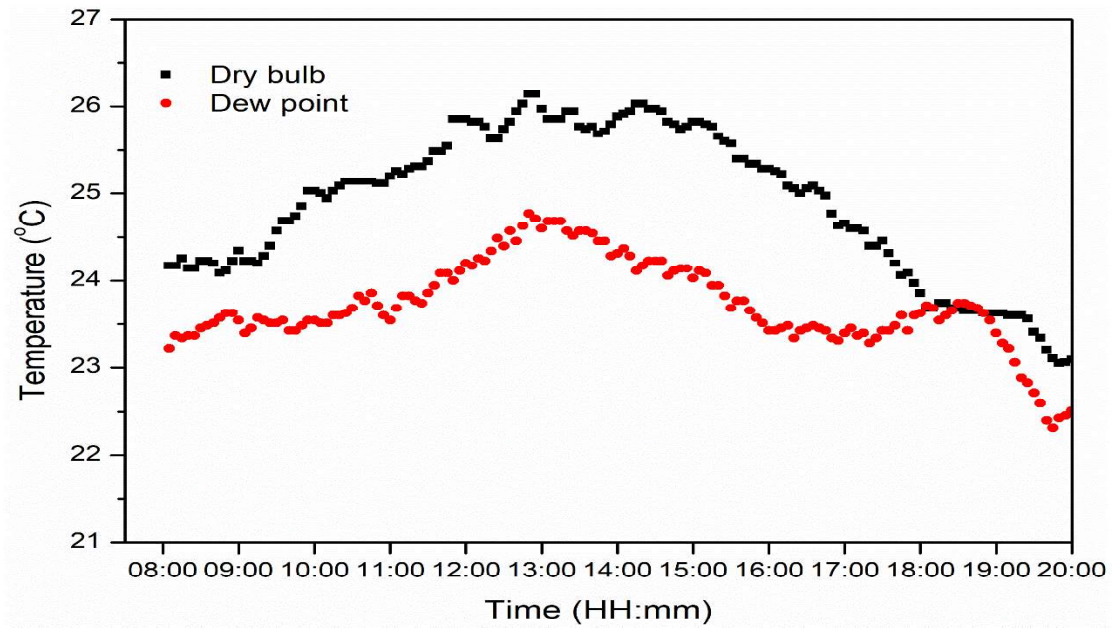

Figure 23: Variation of dry bulb and dew point temperature with time at 6A

The impact of the PV-NTEAC system on the test room's indoor temperature by supplying different input currents from 2-6A to TEMs is shown in Figure 24. The data for five cloudless days (7^{th} – 11^{th} Sept 2020) is presented in Table 8. The results obtained for the operation period between 8 and 20 hours were compared with normal test room conditions (See Table 8). With 2A of input current from the PV and DC power systems to the NTEAC system, the average indoor temperature was 25.26°C, 2°C lower than the normal test room temperature. It was apparent from the figure that the interior temperature of the test room was lower during the morning session (from 8 to 11 hours). Then, during the peak hour session (from 11 to 17 hours), the interior temperature increases and then decreases during the last session of the trial (from 17 to 20 hours). When PV and DC power system current is increased to 3 A, the NTEAC's cooling capacity increases, and the test room temperature is reduced by 2.4 °C, resulting in a final temperature of 23.09 °C. When the current input of the NTEAC system was increased to 4A, the temperature decrease in the test room was 3.2°C less than the typical test room temperature. Additional improvements were made to the test room by increasing the supply current of the NTEAC system from a PV and DC power source that delivered 5A. The temperature within the building was reduced to a maximum of 23.31°C, resulting in a 4°C drop below the room temperature. With an increase in the input current supply of NTEAC to 6A, the system now provided a 4.9°C decrease in indoor room temperature, attributable to an optimum temperature of 21.5°C. So, with 6A of input current, the optimal performance of the PV-NTEAC system was achieved.

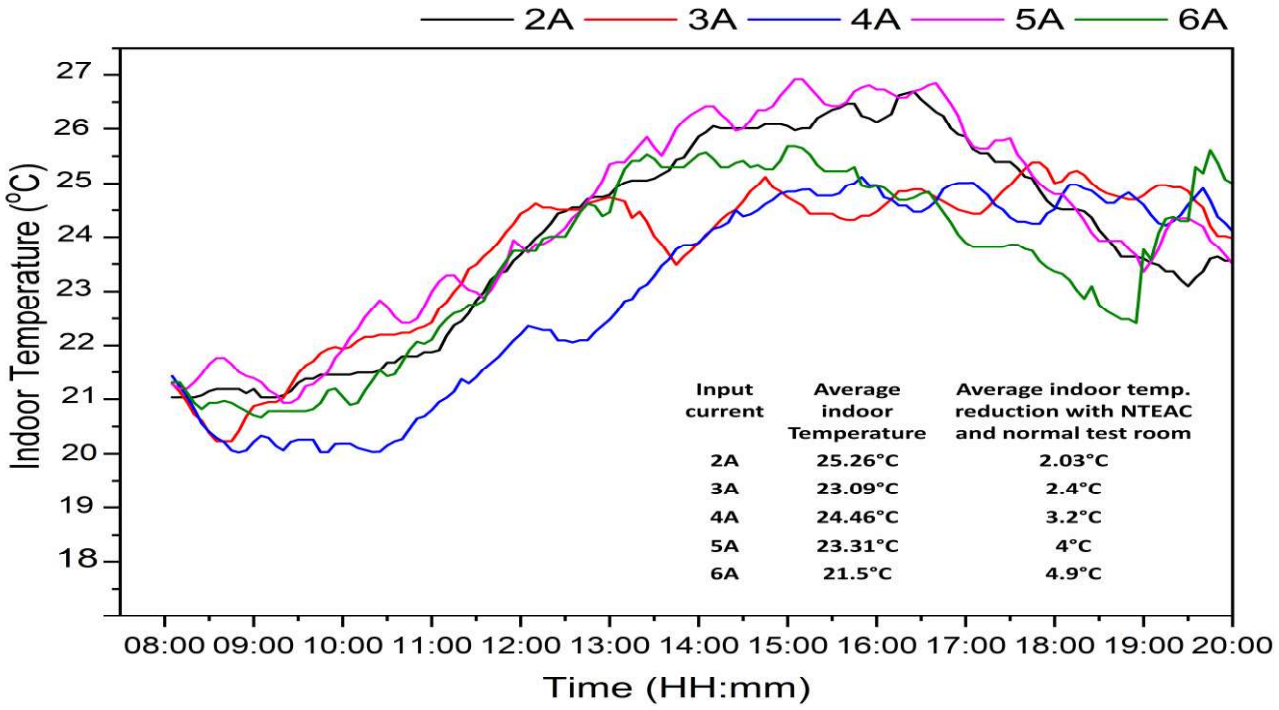

Figure 24: Variation of the indoor temperature of the test room equipped with PV-NTEAC system operated at 2-6A (7^{th} – 11^{th} September 2020)

An acceptable range for specific physical properties of relative humidity is 50 to 60%, according to the Malaysian Industry Code of Practice on Indoor Air Quality (IAQ). Figure 25 illustrates the variation of the relative humidity of the PV-NTEAC system at different input current levels (2-6A) in the test room. The mean ambient outdoor relative humidity ranged from 75 to 84% during September 2020. At the 2A current level, the average relative humidity reduction was 9-15%. Furthermore, when the current supply was increased to 3A, the average relative humidity reduction ranged from 17-23%. Consequently, the current supply to the NTEAC system was raised to 4A and 5A, where the average relative humidity reduction ranged between 23-27% and 30-35%, respectively. To further enhance the indoor relative humidity in the test room, the input current supply of the NTEAC system was increased to 6A using the PV and DC power systems. It showed a maximum average indoor relative humidity decrease of 35 to 41% at this current supply.

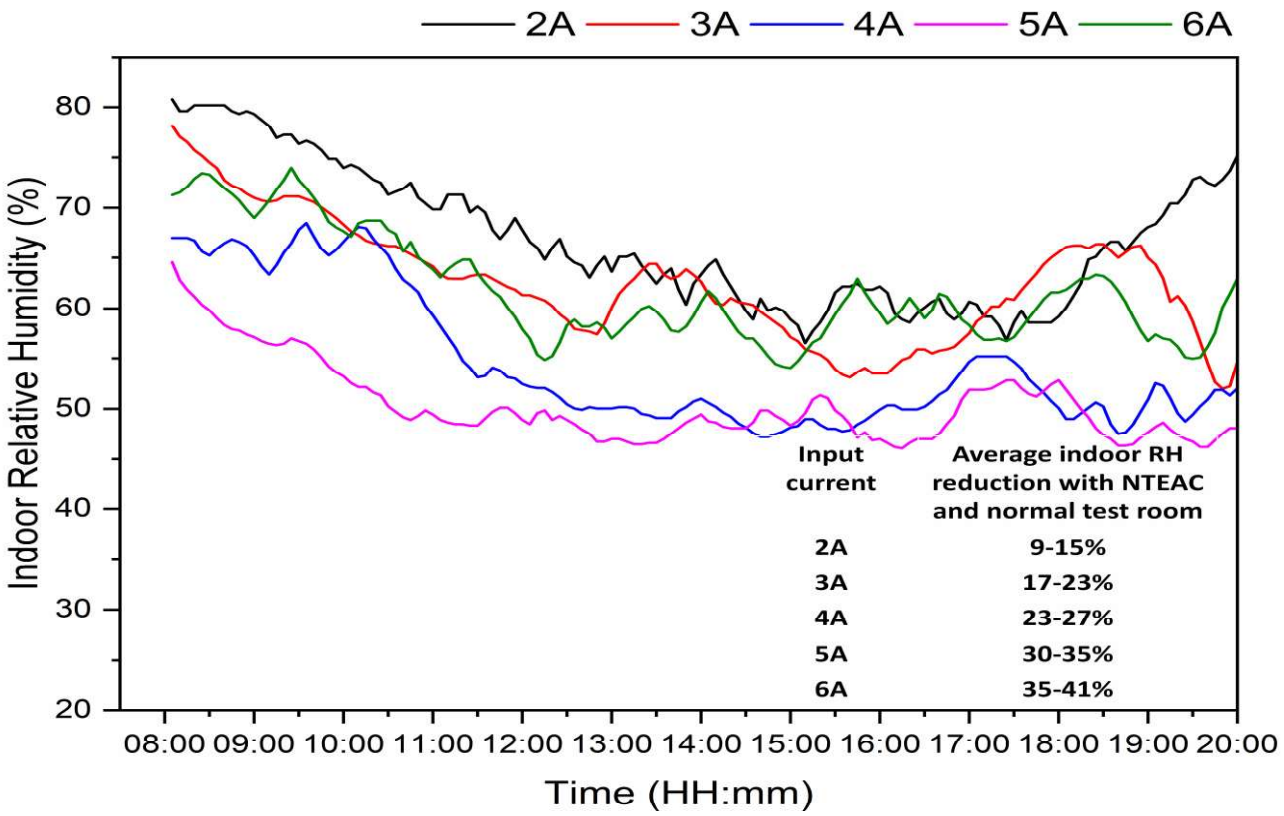

Figure 25: Variation of the indoor relative humidity of the test room equipped with PV-NTEAC system operated at 2-6A (7^{th} – 11^{th} September 2020)

3.5. Carbon credit potential and CO_2 mitigation

Energy is critical for the survival and development of contemporary civilization since it is the main factor that stimulates economic growth and development. A significant amount of energy has been used over the last several decades due to the continuous development of the global economy.

Carbon dioxide emissions have resulted in global climate change, which has now emerged as one of the most significant factors influencing sustainable socio-economic growth throughout the globe. Climate change is becoming an unassailable reality as global CO_2 emissions continue to grow alarming, increasing the unabated global average temperature. Thus, fossil fuel energy use is the most significant contributor to carbon dioxide emissions. Therefore, limiting fossil fuel CO_2 emissions is critical to mitigating global warming. Carbon mitigation should be a significant component of strategies to reduce greenhouse gas emissions. One approach to introduce relevant energy policies is to manage market behaviour, introduce regulation of producers and consumers, and so steer the economy toward a low-carbon country. According to estimates, Malaysia's six major CO_2-emitting industries are power production, transportation, industrial, residential, commercial, and agriculture. Essentially, air conditioners in residential sectors consume many fossil fuels to provide thermal comfort, resulting in a large quantity of CO_2 emissions. In Malaysia, gross CO_2 emissions rose considerably by the end of the 1990s and were more than 160 million metric tons (MMt) by 2003, increasing to 328 MMT by 2020 [58]. The PV-NTEAC device is a highly efficient and environmentally sustainable clean energy solution to minimize CO_2 emissions. The total CO_2 pollution mitigated by the investigated PV-NTEAC system was quantified numerically compared to conventional air conditioning systems. Eq. 7 was used to calculate the cumulative emission of CO_2 pollution from current PV-NTEAC devices and traditional air conditioning systems over 25 years. In general, CO_2 pollution emitted from power plants totalled 2.02 kg/kWh per unit of electricity produced annually [59].

$$Emission\ of\ CO_2\left(\frac{kg}{life}\right) = 2.02\left(\frac{kg}{kWh}\right) \times E\left(\frac{kWh}{year}\right) \times n(years) \tag{7}$$

Where E denotes the annual electrical energy units consumed by the device over a 12-hour cycle and is calculated using Eq. 8:

$$E\left(\frac{kWh}{year}\right) = Daily\ electrical\ load\ \left(\frac{kWh}{day}\right) \times Operation\ days/year \tag{8}$$

The carbon credit allocation is set at 33 US$ per tonne, which is predicted in the article "Malaysia carbon tax could pave the way for potential clean energy" [60], so the value of the carbon credit earned by the system can be calculated by Eq. 9.

$$Carbon\ credit\ earned, C_c = 33\ US\$/ton \times CO_2(\frac{ton}{life}) \tag{9}$$

Due to solar energy and carbon credit potential, the electricity cost is saved, attributed to the initial cost subjugation of the studied PV-NTEAC system. Furthermore, the payback period is evaluated using a line cash flow diagram with the following assumptions:

- The PV-NTEAC system is projected to have a 25-year life span.
- Based on Bank Negara Malaysia (BNM), the payback period of the PV-NTEAC was estimated at a 3% interest rate [61].
- The operational cost of a conventional air conditioner is 197 US$ per annum [62].

The studied PV-NTEAC systems have an operating temperature range of 22.33 to 29 °C with a 6A current supply. The system uses 3.39 kWh of electricity daily when operating in the testing room for 12 hours. The PV-NTEAC system saves 6.89 kWh of electrical energy compared to a 1-ton split air conditioner. The comparison between the test room's electrical energy savings with the PV-NTEAC system and a split air conditioner with a 1-ton capacity is presented in Table 10. Furthermore, this PV-NTEAC system can mitigate 71.54 tonnes of CO_2 emissions from buildings for 25 years.

Table 10: Comparative analysis of PV-NTEAC system with split air conditioner

Parameters	Split air conditioner (1-ton)	PV-NTEAC system
Electrical energy consumption (kWh/year)	3752.2	1237.35
Electrical energy saving (kWh/year)	0	2514.85
CO_2 emission (ton/life)	93.54	22
CO_2 reduction (ton/life)	0	71.54
Carbon credit earned (US$)	0	2360
Operating temperature (°C)	18-40	22.3-29
Weight (kg)	9 (indoor), 10 (outdoor)	7 (indoor), 2.5 (outdoor)
Life span (years)	~15	~25

4. CONCLUSIONS

The research investigated a novel photovoltaic powered nanofluid assisted thermoelectric air conditioner (PV-NTEAC) system for building cooling applications in Malaysia's tropical climate. Feasible heat sinks were designed to integrate nanofluids with thermoelectric air conditioners to

enhance TEM's hot side heat conduction. System performance was examined by evaluating cooling capacity, COP, energy, cost benefits, and CO_2 emission mitigation. Significant conclusions were discussed as follows:

- The use of nanofluids in conjunction with the radiator and TEAC resulted in a significant increase in thermal performance. This is because nanoparticles can compress the fluid's transverse temperature gradient, mainly caused by the enhanced mobility of liquid atoms in the presence of nanoparticles.
- Analysis of NTEAC's cooling performance indicates that raising the input current from 2A to 6A significantly impacted the cooling performance. However, increasing the input current supply further deteriorated the system's performance.
- With an input current of 6A, the test room's optimum temperature difference (indoor and outdoor) reached 4.9 °C, resulting in a COP of 1.27 and a cooling capacity of 571 W.
- The CO_2 emission mitigation resulted in around 71.54 tonnes when compared with a conventional split air conditioner that contributed to a carbon credit allowance of 2360 US$.

Furthermore, to achieve even greater system performance, consider lowering the thermal resistance on the hot side of the thermoelectric modules. Even though the PV-NTEAC system has a lower COP than the traditional split air conditioner, it may be used for space conditioning in rural areas with abundant solar energy. Integration of nanofluids with the PV-NTEAC system reduces the temperature difference between the cold and hot sides of the TEMs, leading to an enhanced cooling performance in thermoelectric air conditioners. As a result, the innovative PV-NTEAC system, in conjunction with the MWCNT/Water nanofluids, offers a freon-free, fossil fuel independent, energy-efficient, and low CO_2 emission approach for space conditioning.

NOMENCLATURE

A	Area (m^2)	*Greek symbols*	
Cp	Specific heat capacity (kj/kg.K)	α	Seebeck coefficient ($V.K^{-1}$)
G	Solar irradiance (W/m^2)	Δ	Delta/difference
i	interest rate (%)	η	Efficiency
I	Current (A)	ω	Specific humidity
K	Thermal conductivity (W/m. K)	σ	Resistivity (Ω cm)
N	Number of thermoelectric couples	χ	Range of measured value
n	Time in years	*Subscripts*	
P	Power (W)	c	cold

PV	Photovoltaic	h	hot
Q	Rate of heat transfer (W)	in	inlet
RH	Relative humidity (%)	out	outlet
t	Time (s)	max	maximum
T	Temperature (°C)	*Abbreviations*	
ΔT	Temperature difference between the hot side and cold side TEM (°C)	NTEAC	Nanofluid Assisted Thermoelectric Air Conditioner
Wt.	Weight fraction (%)	MWCNT	Multiwalled Carbon Nanotubes
wh	Watt-hour	TEM	Thermoelectric module
ZT	Figure of merit	Water	Distilled water

ACKNOWLEDGEMENTS

The authors are grateful to Universiti Teknologi PETRONAS for their facilities for conducting the research. We want to acknowledge the financial support offered through the YUTP grant (YUTP FRG 015LC0-118).

CONFLICTS OF INTEREST

The authors declare no conflicts of interest.

REFERENCES

[1] D.D. Kim, H.S. Suh, Heating and cooling energy consumption prediction model for high-rise apartment buildings considering design parameters, Energy Sustain. Dev. 61 (2021) 1–14. https://doi.org/https://doi.org/10.1016/j.esd.2021.01.001.

[2] B. Bakthavatchalam, K. Habib, Thermoelectric Air Conditioners for Tropical Countries, in: S.A. Sulaiman (Ed.), Clean Energy Oppor. Trop. Ctries., Springer Singapore, Singapore, 2021: pp. 289–307. https://doi.org/10.1007/978-981-15-9140-2_14.

[3] International Energy Agency, The Future of Cooling, IEA, Paris. (2018). https://www.iea.org/reports/the-future-of-cooling (accessed March 23, 2022).

[4] L. Lou, D. Shou, H. Park, D. Zhao, Y.S. Wu, X. Hui, R. Yang, E.C. Kan, J. Fan, Thermoelectric air conditioning undergarment for personal thermal management and HVAC energy saving, Energy Build. 226 (2020) 110374. https://doi.org/https://doi.org/10.1016/j.enbuild.2020.110374.

[5] Y. Lyu, A.R.M. Siddique, S.A. Gadsden, S. Mahmud, Experimental investigation of thermoelectric cooling for a new battery pack design in a copper holder, Results Eng. 10 (2021) 100214. https://doi.org/https://doi.org/10.1016/j.rineng.2021.100214.

[6] M. Di Capua H, W. Jahn, Performance assessment of thermoelectric self-cooling systems for electronic devices, Appl. Therm. Eng. 193 (2021) 117020.

https://doi.org/https://doi.org/10.1016/j.applthermaleng.2021.117020.
[7] M. Duan, H. Sun, B. Lin, Y. Wu, Evaluation on the applicability of thermoelectric air cooling systems for buildings with thermoelectric material optimization, Energy. 221 (2021) 119723. https://doi.org/https://doi.org/10.1016/j.energy.2020.119723.
[8] A. Saini, S.J. Watzman, J.-H. Bahk, Cost-Performance Trade-off in thermoelectric air conditioning system with graded and constant material properties, Energy Build. 240 (2021) 110931. https://doi.org/https://doi.org/10.1016/j.enbuild.2021.110931.
[9] M. Sajid, I. Hassan, A. Rahman, An overview of cooling of thermoelectric devices, Renew. Sustain. Energy Rev. 78 (2017) 15–22. https://doi.org/https://doi.org/10.1016/j.rser.2017.04.098.
[10] H. Sadighi Dizaji, S. Jafarmadar, S. Khalilarya, A. Moosavi, An exhaustive experimental study of a novel air-water based thermoelectric cooling unit, Appl. Energy. 181 (2016) 357–366. https://doi.org/https://doi.org/10.1016/j.apenergy.2016.08.074.
[11] R.M. Atta, Solar thermoelectric cooling using closed loop heat exchangers with macro channels, Heat Mass Transf. 53 (2017) 2241–2254. https://doi.org/10.1007/s00231-017-1965-z.
[12] H. Sun, B. Lin, Z. Lin, Y. Zhu, H. Li, X. Wu, Research on a radiant heating terminal integrated with a thermoelectric unit and flat heat pipe, Energy Build. 172 (2018) 209–220. https://doi.org/https://doi.org/10.1016/j.enbuild.2018.04.054.
[13] D. Zhao, X. Yin, J. Xu, G. Tan, R. Yang, Radiative sky cooling-assisted thermoelectric cooling system for building applications, Energy. 190 (2020) 116322. https://doi.org/https://doi.org/10.1016/j.energy.2019.116322.
[14] T.-C. Cheng, C.-H. Cheng, Z.-Z. Huang, G.-C. Liao, Development of an energy-saving module via combination of solar cells and thermoelectric coolers for green building applications, Energy. 36 (2011) 133–140. https://doi.org/https://doi.org/10.1016/j.energy.2010.10.061.
[15] Z.B. Liu, L. Zhang, G. Gong, Y. Luo, F. Meng, Experimental study and performance analysis of a solar thermoelectric air conditioner with hot water supply, Energy Build. 86 (2015) 619–625. https://doi.org/https://doi.org/10.1016/j.enbuild.2014.10.053.
[16] N. Putra, Yanuar, F.N. Iskandar, Application of nanofluids to a heat pipe liquid-block and the thermoelectric cooling of electronic equipment, Exp. Therm. Fluid Sci. 35 (2011) 1274–1281. https://doi.org/https://doi.org/10.1016/j.expthermflusci.2011.04.015.
[17] S. Manikandan, S.C. Kaushik, R. Yang, Modified pulse operation of thermoelectric coolers for building cooling applications, Energy Convers. Manag. 140 (2017) 145–156. https://doi.org/https://doi.org/10.1016/j.enconman.2017.03.003.
[18] X.-X. Tian, S. Asaadi, H. Moria, A. Kaood, S. Pourhedayat, K. Jermsittiparsert, Proposing tube-bundle arrangement of tubular thermoelectric module as a novel air cooler, Energy. 208 (2020) 118428. https://doi.org/https://doi.org/10.1016/j.energy.2020.118428.
[19] X. Su, L. Zhang, Z. Liu, Y. Luo, D. Chen, W. Li, Performance evaluation of a novel building envelope integrated with thermoelectric cooler and radiative sky cooler, Renew. Energy. 171 (2021) 1061–1078. https://doi.org/https://doi.org/10.1016/j.renene.2021.02.164.
[20] X. Han, Y. Wang, Experimental investigation of the thermal performance of a novel split-type liquid-circulation thermoelectric cooling device, Appl. Therm. Eng. 194 (2021) 117090. https://doi.org/https://doi.org/10.1016/j.applthermaleng.2021.117090.
[21] Y.-K. Kang, H. Lim, S.-Y. Cheon, J.-W. Jeong, Phase-change material-integrated thermoelectric radiant panel: Experimental performance analysis and system design, Appl. Therm. Eng. 194 (2021) 117082. https://doi.org/https://doi.org/10.1016/j.applthermaleng.2021.117082.
[22] W. He, J. Zhou, J. Hou, C. Chen, J. Ji, Theoretical and experimental investigation on a thermoelectric cooling and heating system driven by solar, Appl. Energy. 107 (2013) 89–97. https://doi.org/https://doi.org/10.1016/j.apenergy.2013.01.055.

[23] F. Khalvati, A. Omidvar, F. Hadianfard, Study on summer thermal performance of a solar ventilated window integrated with thermoelectric air-cooling system, Int. J. Energy Environ. Eng. (2021). https://doi.org/10.1007/s40095-020-00376-8.

[24] S. Diaz de Garayo, A. Martínez, P. Aranguren, D. Astrain, Prototype of an air to air thermoelectric heat pump integrated with a double flux mechanical ventilation system for passive houses, Appl. Therm. Eng. 190 (2021) 116801. https://doi.org/https://doi.org/10.1016/j.applthermaleng.2021.116801.

[25] M. Gillott, L. Jiang, S. Riffat, An investigation of thermoelectric cooling devices for small-scale space conditioning applications in buildings, Int. J. Energy Res. 34 (2010) 776–786. https://doi.org/10.1002/er.1591.

[26] M.-W. Tian, F. Aldawi, A.E. Anqi, H. Moria, H.S. Dizaji, M. Wae-hayee, Cost-effective and performance analysis of thermoelectricity as a building cooling system; experimental case study based on a single TEC-12706 commercial module, Case Stud. Therm. Eng. 27 (2021) 101366. https://doi.org/https://doi.org/10.1016/j.csite.2021.101366.

[27] M. Akkaya, T. Menlik, A. Sözen, M. Gürü, EXPERIMENTAL INVESTIGATION OF NANOLUBRICANT USAGE IN A COOLING SYSTEM AT DIFFERENT NANOPARTICLE CONCENTRATIONS, Heat Transf. Res. 51 (2020) 949–965. https://doi.org/10.1615/HeatTransRes.2020033812.

[28] M. Akkaya, T. Menlik, A. Sözen, M. Gürü, The Effects of Triton X-100 and Tween 80 Surfactants on the Thermal Performance of a Nano-Lubricant: An Experimental Study, Int. J. Precis. Eng. Manuf. Technol. 8 (2021) 955–967. https://doi.org/10.1007/s40684-020-00280-w.

[29] M. Akkaya, S. Yurtdaş, ENERGY EFFICIENCY IMPROVEMENT OF THE HEAT PUMP BY EMPLOYING SYNTHESIZED CuO/ZnO HYBRID NANOFLUID, Heat Transf. Res. 53 (2022) 47–60. https://doi.org/10.1615/HeatTransRes.2021040242.

[30] E. Çiftçi, K. Martin, A. Sözen, ENHANCEMENT OF THERMAL PERFORMANCE OF THE AIR-TO-AIR HEAT PIPE HEAT EXCHANGER (AAHX) WITH ALUMINATE SPINEL-BASED BINARY HYBRID NANOFLUIDS, Heat Transf. Res. 52 (2021) 81–97. https://doi.org/10.1615/HeatTransRes.2021039920.

[31] E. Çiftçi, Distilled Water-Based AlN + ZnO Binary Hybrid Nanofluid Utilization in a Heat Pipe and Investigation of Its Effects on Performance, Int. J. Thermophys. 42 (2021) 38. https://doi.org/10.1007/s10765-021-02792-2.

[32] H.M. Maghrabie, K. Elsaid, E.T. Sayed, M.A. Abdelkareem, T. Wilberforce, M. Ramadan, A.G. Olabi, Intensification of heat exchanger performance utilizing nanofluids, Int. J. Thermofluids. 10 (2021) 100071. https://doi.org/https://doi.org/10.1016/j.ijft.2021.100071.

[33] O. Mahian, A. Kianifar, S.Z. Heris, D. Wen, A.Z. Sahin, S. Wongwises, Nanofluids effects on the evaporation rate in a solar still equipped with a heat exchanger, Nano Energy. 36 (2017) 134–155. https://doi.org/https://doi.org/10.1016/j.nanoen.2017.04.025.

[34] A. Sözen, Ç. Filiz, İ. Aytaç, K. Martin, H.M. Ali, K. Boran, Y. Yetişken, Upgrading of the Performance of an Air-to-Air Heat Exchanger Using Graphene/Water Nanofluid, Int. J. Thermophys. 42 (2021) 35. https://doi.org/10.1007/s10765-020-02790-w.

[35] D.Y. Aydın, E. Çiftçi, M. Gürü, A. Sözen, The Impacts of Nanoparticle Concentration and Surfactant Type on Thermal Performance of A Thermosyphon Heat Pipe Working With Bauxite Nanofluid, Energy Sources, Part A Recover. Util. Environ. Eff. 43 (2021) 1524–1548. https://doi.org/10.1080/15567036.2020.1800141.

[36] R.A.A. Babat, K. Martin, E. Çiftçi, A. Sözen, Experimental study on the utilization of magnetic nanofluids in an air-to-air heat pipe heat exchanger, Chem. Eng. Commun. 0 (2021) 1–11. https://doi.org/10.1080/00986445.2021.1977634.

[37] G. Colangelo, E. Favale, M. Milanese, A. de Risi, D. Laforgia, Cooling of electronic devices: Nanofluids contribution, Appl. Therm. Eng. 127 (2017) 421–435. https://doi.org/https://doi.org/10.1016/j.applthermaleng.2017.08.042.

[38] C. Wang, E. Choi, J. Park, High-voltage nanofluidic energy generator based on ion-concentration-gradients mimicking electric eels, Nano Energy. 43 (2018) 291–299. https://doi.org/https://doi.org/10.1016/j.nanoen.2017.11.054.
[39] A. Siricharoenpanich, S. Wiriyasart, P. Naphon, Study on the thermal dissipation performance of GPU cooling system with nanofluid as coolant, Case Stud. Therm. Eng. 25 (2021) 100904. https://doi.org/https://doi.org/10.1016/j.csite.2021.100904.
[40] S. Sarvar-Ardeh, R. Rafee, S. Rashidi, Hybrid nanofluids with temperature-dependent properties for use in double-layered microchannel heat sink; hydrothermal investigation, J. Taiwan Inst. Chem. Eng. (2021). https://doi.org/https://doi.org/10.1016/j.jtice.2021.05.007.
[41] T. Balaji, C. Selvam, D.M. Lal, S. Harish, Enhanced heat transport behavior of micro channel heat sink with graphene based nanofluids, Int. Commun. Heat Mass Transf. 117 (2020) 104716. https://doi.org/https://doi.org/10.1016/j.icheatmasstransfer.2020.104716.
[42] J. Mohammadpour, F. Salehi, M. Sheikholeslami, M. Masoudi, A. Lee, Optimization of nanofluid heat transfer in a microchannel heat sink with multiple synthetic jets based on CFD-DPM and MLA, Int. J. Therm. Sci. 167 (2021) 107008. https://doi.org/https://doi.org/10.1016/j.ijthermalsci.2021.107008.
[43] B. Bakthavatchalam, K. Habib, R. Saidur, S. Shahabuddin, B.B. Saha, Influence of solvents on the enhancement of thermophysical properties and stability of MWCNT nanofluid., Nanotechnology. 31 (2020) 235402. https://doi.org/10.1088/1361-6528/ab79ab.
[44] B. Kanargi, P.S. Lee, C. Yap, A numerical and experimental investigation of heat transfer and fluid flow characteristics of an air-cooled oblique-finned heat sink, Int. J. Heat Mass Transf. 116 (2018) 393–416. https://doi.org/https://doi.org/10.1016/j.ijheatmasstransfer.2017.09.013.
[45] I.S. Walker, M.H. Sherman, Energy implications of meeting ASHRAE Standard 62.2, ASHRAE Trans. 114 (2008) 505–516.
[46] R.J. de Dear, G.S. Brager, Thermal comfort in naturally ventilated buildings: revisions to ASHRAE Standard 55, Energy Build. 34 (2002) 549–561. https://doi.org/https://doi.org/10.1016/S0378-7788(02)00005-1.
[47] R.J. Moffat, Describing the uncertainties in experimental results, Exp. Therm. Fluid Sci. 1 (1988) 3–17. https://doi.org/https://doi.org/10.1016/0894-1777(88)90043-X.
[48] G. Tan, D. Zhao, Study of a thermoelectric space cooling system integrated with phase change material, Appl. Therm. Eng. 86 (2015) 187–198. https://doi.org/https://doi.org/10.1016/j.applthermaleng.2015.04.054.
[49] M. Emam, M. Ahmed, Performance analysis of a new concentrator photovoltaic system integrated with phase change material and water jacket, Sol. Energy. 173 (2018) 1158–1172. https://doi.org/https://doi.org/10.1016/j.solener.2018.08.069.
[50] L. Shen, F. Xiao, H. Chen, S. Wang, Investigation of a novel thermoelectric radiant air-conditioning system, Energy Build. 59 (2013) 123–132. https://doi.org/10.1016/j.enbuild.2012.12.041.
[51] G. Tan, D. Zhao, Study of a thermoelectric space cooling system integrated with phase change material, Appl. Therm. Eng. 86 (2015) 187–198. https://doi.org/10.1016/j.applthermaleng.2015.04.054.
[52] K. Irshad, K. Habib, N. Thirumalaiswamy, B.B. Saha, Performance analysis of a thermoelectric air duct system for energy-efficient buildings, Energy. 91 (2015) 1009–1017. https://doi.org/https://doi.org/10.1016/j.energy.2015.08.102.
[53] M. Ibañez-Puy, J. Bermejo-Busto, C. Martín-Gómez, M. Vidaurre-Arbizu, J.A. Sacristán-Fernández, Thermoelectric cooling heating unit performance under real conditions, Appl. Energy. 200 (2017) 303–314. https://doi.org/10.1016/j.apenergy.2017.05.020.
[54] A. Rincón-Casado, A. Martinez, M. Araiz, P. Pavón-Domínguez, D. Astrain, An experimental and computational approach to thermoelectric-based conditioned mattresses, Appl. Therm. Eng. 135 (2018) 472–482.

https://doi.org/10.1016/j.applthermaleng.2018.02.084.
[55] S.-Y. Cheon, H. Lim, J.-W. Jeong, Applicability of thermoelectric heat pump in a dedicated outdoor air system, Energy. 173 (2019) 244–262. https://doi.org/10.1016/j.energy.2019.02.012.
[56] C. Chen, L. Mao, T. Lin, T. Tu, L. Zhu, C. Wang, Performance testing and optimization of a thermoelectric elevator car air conditioner, Case Stud. Therm. Eng. 19 (2020) 100616. https://doi.org/10.1016/j.csite.2020.100616.
[57] K.K. Looi, A.T. Baheta, K. Habib, Investigation of photovoltaic thermoelectric air-conditioning system for room application under tropical climate, J. Mech. Sci. Technol. 34 (2020) 2199–2205. https://doi.org/10.1007/s12206-020-0441-8.
[58] T.H. Oh, S.C. Chua, Energy efficiency and carbon trading potential in Malaysia, Renew. Sustain. Energy Rev. 14 (2010) 2095–2103. https://doi.org/10.1016/j.rser.2010.03.029.
[59] S.M. Shafie, T.M.I. Mahlia, H.H. Masjuki, Life cycle assessment of rice straw co-firing with coal power generation in Malaysia, Energy. 57 (2013) 284–294. https://doi.org/10.1016/j.energy.2013.06.002.
[60] M. Akmaliyah, 済無No Title No Title, J. Chem. Inf. Model. 53 (2013) 1689–1699. https://phys.org/news/2016-04-malaysian-carbon-tax-pave-renewable.html.
[61] BANK NEGARA MALAYSIA, INTEREST RATES (CONVENTIONAL), Cent. BANK MALAYSIA. (2019). https://www.bnm.gov.my/interest-rates-volumes?p_p_id=bnm_market_rate_display_portlet&p_p_lifecycle=0&p_p_state=normal&p_p_mode=view&_bnm_market_rate_display_portlet_product=rro&_bnm_market_rate_display_portlet_monthStart=0&_bnm_market_rate_display_portlet.
[62] K. Irshad, K. Habib, S. Algarni, B.B. Saha, B. Jamil, Sizing and life-cycle assessment of building integrated thermoelectric air cooling and photovoltaic wall system, Appl. Therm. Eng. 154 (2019) 302–314. https://doi.org/10.1016/j.applthermaleng.2019.03.027.

Highlights

- Novel radiator coupled nanofluid based thermoelectric air conditioning (NTEAC) system was developed.
- Performance of the PV powered NTEAC system is analysed in a real time building of 25.6 m^3 size.
- NTEAC system reduced the temperature of the test room below 22°C with 6A current.
- Significant savings in power consumption and carbon emissions has been fortified.

Graphical abstract

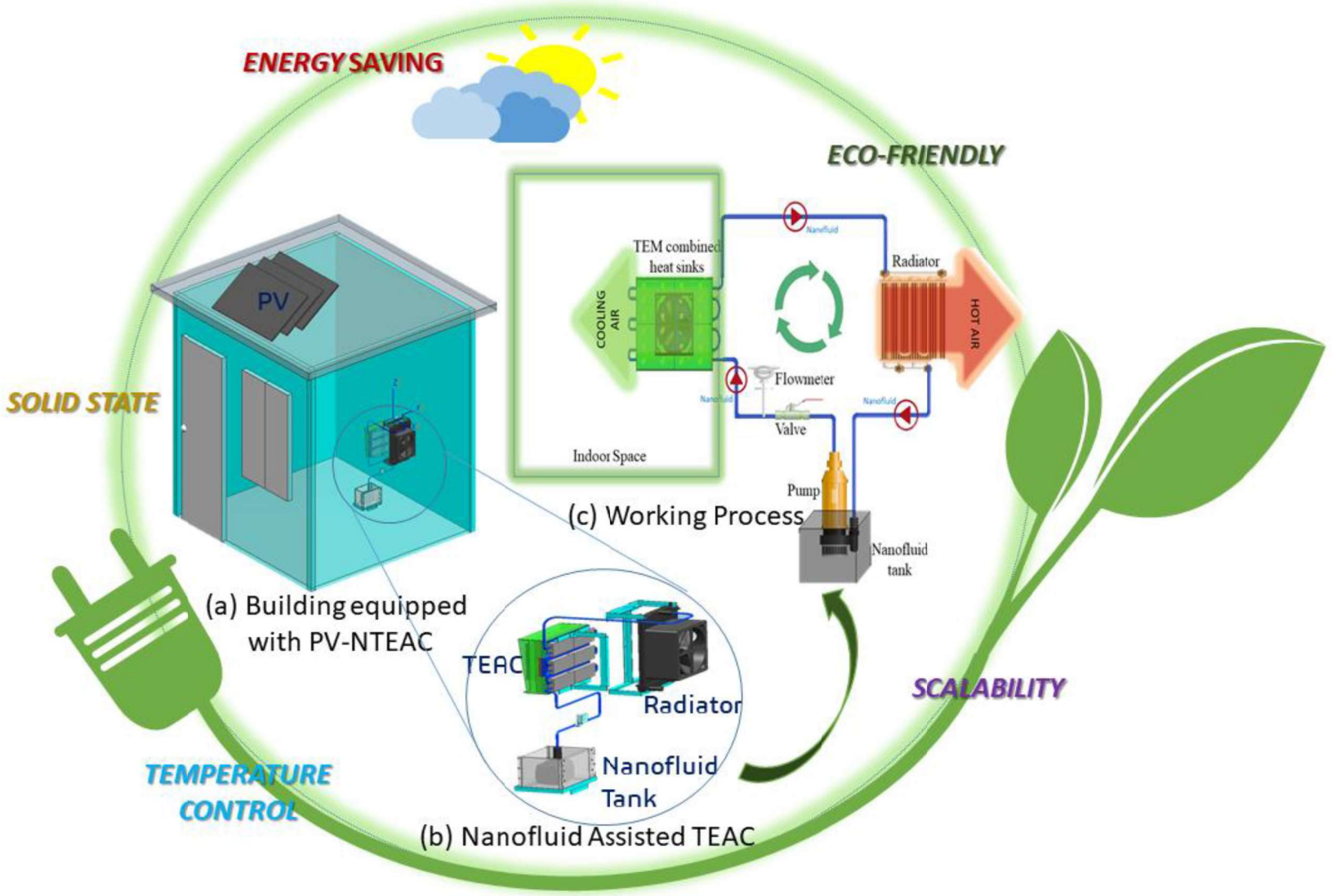

Conflict of Interest

Declaration of interests

☒ The authors declare that they have no known competing financial interests or personal relationships that could have appeared to influence the work reported in this paper.

☐The authors declare the following financial interests/personal relationships which may be considered as potential competing interests:

No conflicts of interest to declare

Cooling Performance Analysis of Nanofluid Assisted Novel Photovoltaic Thermoelectric Air Conditioner for Energy Efficient Buildings

Balaji Bakthavatchalam [a*], Khairul Habib [a], R. Saidur [b, c] and Bidyut Baran Saha [d]

[a] *Department of Mechanical Engineering, Universiti Teknologi PETRONAS, 32610 Bandar Seri Iskandar, Perak Darul Ridzuan, Malaysia*

[b] *Research Centre for Nano-Materials and Energy Technology (RCNMET), School of Engineering and Technology, Sunway University, Malaysia*

[c] *Department of Engineering, Lancaster University, LA1 4YW, United Kingdom*

[d] *International Institute for Carbon-Neutral Energy Research, Kyushu University, 744 Motooka Nishi-ku Fukuoka-shi, Fukuoka 819-0395, Japan*

Corresponding author, E-mail address: balaji_17004028@utp.edu.my

Tel: +60 11 36218966

ABSTRACT

Carbon emissions and excessive power usage are addressed by applying thermoelectric cooling, which benefits from its ability to be portable, economical, and reliable. However, a conventional thermoelectric air conditioner's coefficient of performance (COP) is much less due to the sustained heat generated on the thermoelectric module's hot side. This work presents a novel idea of utilizing a nanofluid cooled radiator as an external cooling jacket around the thermoelectric module's hot side to enhance the heat transfer rate of thermoelectric air conditioners. In this research, the performance of a newly designed thermoelectric air conditioner (TEAC) powered by photovoltaic systems (PV) installed in a residential building is analyzed using nanofluid as a coolant. Furthermore, by supplying different input currents (2-6A), the cooling characteristics and performance of the newly designed nanofluid assisted thermoelectric air conditioner (NTEAC) system were experimentally studied in a test room of 25.6 m^3 volume in Malaysia's tropical climate. The system's best performance was at 6A, with a maximum temperature drop of 4.9 °C, a cooling capacity of 571W, and a coefficient of performance of 1.27. In addition, the NTEAC system showed an energy saving of 67% and CO_2 emission mitigation of 76% when compared with a conventional split air conditioner. Thus, an alternative to the traditional air conditioning system was developed from this research, which is Freon free. This system is expected to consume less energy and emit less CO_2 for the tropical climatic conditions.

Keywords: Nanofluid assisted thermoelectric air conditioner (NTEAC); photovoltaic; nanofluid; Coefficient of performance; energy saving; CO_2 emission.

1. INTRODUCTION

Conventional air conditioning systems have become more efficient in recent years, but they also account for most electricity use and CO_2 emissions in most residential, commercial, and industrial buildings [1,2]. According to the International Energy Agency, air conditioners (ACs) in buildings will increase from 1.6 to 5.6 billion by 2050 [3]. In 30 years, each second, there will be ten new ACs purchased. Furthermore, the HVAC industry is dominated by vapour-compression systems. However, these systems employ harmful refrigerants that pollute the atmosphere. Thermoelectric cooling is seen as a valuable alternative to vapour compression, possessing several advantages compared to traditional vapour compression technologies, including smaller size and weight, excellent reliability, no moving parts, zero noise, and the possibility of using photovoltaic. Although the fundamental principles of thermoelectricity are widely understood, studies to comprehend the heat transfer process in small and medium-sized prototypes have been carried out throughout the years [4–6]. A thermoelectric module (TEM) or thermoelectric cooler (TEC) is a novel solid-state cooling system of thermocouples that rely on the Peltier effect to transfer heat from one side of a device to another. As shown in Figure 1, a thermocouple has a sequence of p-type and n-type semiconductors connected with top and bottom electrodes in series. The other components are thermally connected in parallel. Additionally, TECs may be directly connected to renewable energy systems to meet the urgent requirement for lowering building energy consumption [7].

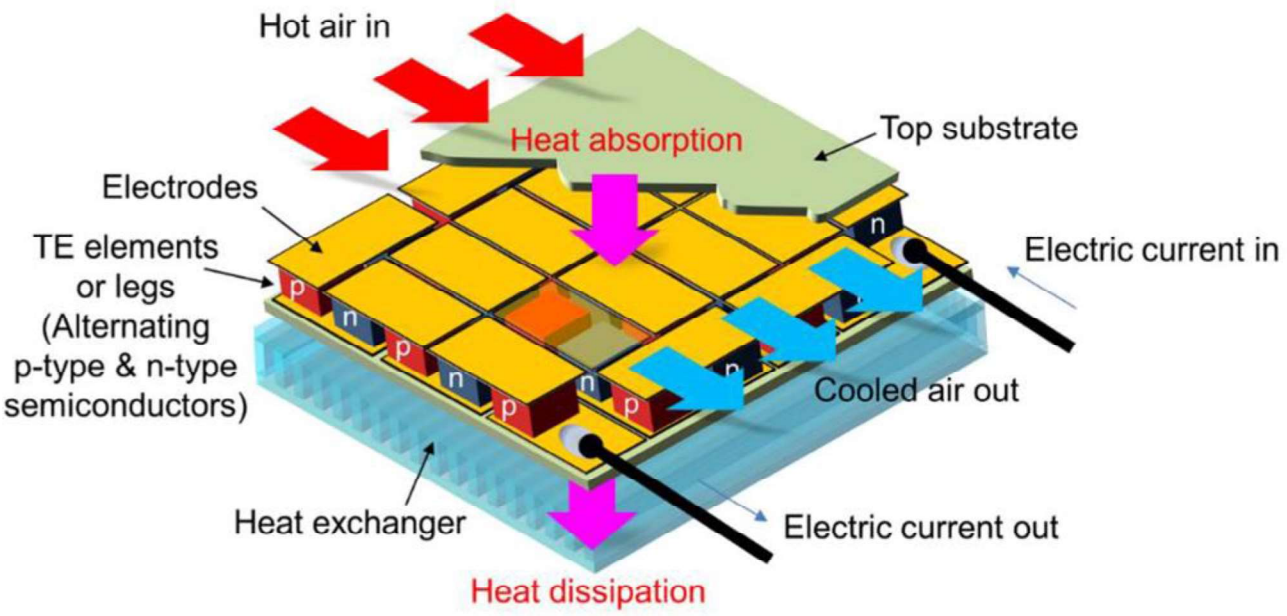

Figure 1: Thermoelectric module with semiconductor elements and heat exchangers [8]

Thermoelectric air conditioners (TEACs) are composed of multiple thermoelectric modules (TEMs) that are selected in accordance with the building's cooling load (for example, a 600W cooling load requires 12 TEMs of 50 W). When an electric current is provided to the TEMs in a TEAC, heat is transferred through the TEMs from the cold side to the hot side, making one junction colder and the other junction warmer. Then the cooled air from the cold junction is subjected to the building while the hot air is released into the atmosphere. The typical working principle of TEAC installed in a house is described in Figure 2. One of the significant problems with TEAC is poor COP (Coefficient of Performance), especially in high-performance applications. A high COP can be attained by improving heat transfer on the TEM's hot side and increasing the number of TEMs. A critical review on maintaining the cold side temperature of a TEM through different heat dissipation mechanisms was conducted by Sajid et al. [9]. Their study demonstrates that the performance of a thermoelectric device depends on effective thermal management of TEM's cold side and a hot side. On the other hand, Dizaji et al. [10] discovered that when the hot side of a thermoelectric module is cooled by a liquid such as water, the cold side may work as an excellent air conditioning system.

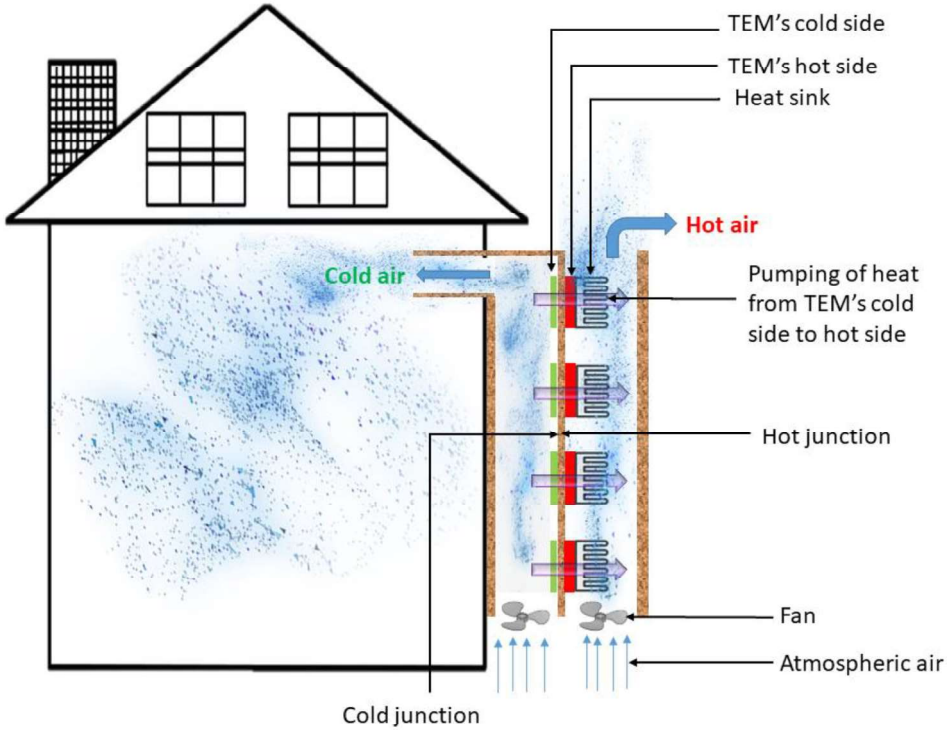

Figure 2: Schematic illustration of a building equipped with TEAC

Atta et al. [11] evaluated the performance of a TEAC system coupled with liquid-to-air heat exchangers. Within 90 minutes, the system could chill an enclosed space at a temperature of 14 °C below ambient and showed a maximum COP of 0.72. In another study, Sun et al. [12] employed a flat heat pipe to dissipate heat and saved ten minutes of the total thermal reaction time. Additionally, Zhao et al. [13] used the heat radiated by the TEM to heat the hot water by combining

it with a radiative sky cooler. This helps to minimize energy usage and save natural resources. Cheng et al. [14] reported that both the absorbed solar energy and the generated heat in the thermoelectric cooler might be evacuated via the cooling water, resulting in higher performance for the cooling module. Liu et al. [15] examined the performance of a solar thermoelectric air conditioner (STACHWS) with water as a heat transfer fluid (HTF). From their results, the water temperature has an enormous impact on the operation of the STACHWS system. The STACHWS system's COP reached a high of 4.51 and 2.74 with water temperatures of 20 °C and 42 °C, respectively. Putra et al. [16] investigated the use of nanofluids in conjunction with thermoelectric cooling to cool a computer's CPU using a heat pipe liquid block system. With the nanofluids, their cooling system can lower the CPU temperature by an immense value than the other typical cooling systems. Thermoelectric coolers are still employed for refrigeration and electrical equipment, despite their intriguing features for buildings.

Recently, new ideas for using TECs in buildings have been explored. For instance, Manikandan et al. [17] improved a thermoelectric cooler's COP and cooling performance using modified pulse operation for building space cooling. Compared with the thermoelectric cooler's regular operating mode, the modified pulse operation increased the cooling power and COP by 23.3% and 2.12%, respectively. Tian et al. [18] developed a novel air cooler composed of thermoelectric modules arranged in a tube-bundle shape. According to the author, a tubular thermoelectric system that includes a tubular component is more efficient and functional because it does not require channels to divide the hot and cold sides. Su et al. [19] proposed a novel building envelope with TEC and a radiative sky cooler (RSC) to avoid heat gains and deliver cooling. The TEC-RSC exhibited a cooling capability of 25.49 W/m^2 under global solar radiation of 1000 W/m^2, with an outdoor temperature of 35°C and relative humidity of 60%. Han et al. [20] studied a unique split-type liquid circulation thermoelectric cooling performance under various parameters. Their findings demonstrate that as the outdoor temperature is reduced from its expected value, the device cooling power and COP increase. Kang et al. [21] conducted trials in active and passive modes to examine the performance of a PCM integrated radiant cooling panel. Their proposed system had an active cooling capacity of about 58 W/m^2 and a passive cooling capacity of about 54 W/m^2 when the mean radiant temperature (MRT) was 26 °C. He et al. [22] developed a solar-driven thermoelectric cooling system for a model room of 0.125 m^3. The authors reported a maximum COP of 0.45 and a minimum temperature of 17 °C. In a recent study, Khalvati et al. [23] analyzed the effects of air temperature attenuation, working interval time, and the number of modules on the performance of a thermoelectric cooling system. Operating the thermoelectric air-cooling system during a short period reduces energy consumption while using it for a longer time might raise it. Also, TEAC with

more than twenty TEMs will increase the energy consumption, attributed to less COP. In 2021, Garayo et al. [24] optimized the COP of a thermoelectric cooling system with double flux mechanical ventilation in a house of 80 m^2 area. The authors emphasized the significance of airflows, voltage supply, and temperature gaps attributed to a maximum cooling capacity and COP of 375W and 2.5. Gillott et al. [25] used eight TEMs in a small-scale building to generate a cooling capacity and COP of 220W and 0.46. Their results reveal that TEMs' cooling capacity relies on the temperature (hot and cold side) and quantity of the TEMs. Therefore, minimizing the temperature difference between the hot and cold sides is critical for optimal heat transfer via the thermoelectric cooling module.

Accordingly, the reviewed literature affirms a direct correlation between the TEAC's COP and hot/cold side temperature difference, which may be enhanced with more effective thermal management techniques. Since the heat flow on the hot side is enormous, the thermoelectric cooling system's hot side thermal management is more complicated than the cold side. Reduced hot/cold side temperature difference generally results in better cooling [26]. Higher-efficient heat sinks or high thermal conductivity heat transfer fluids can reduce the hot side temperature. Nanofluid is considered one of the best heat transfer fluids suitable for low-temperature and high-temperature applications. For instance, nanoparticle-based working fluids were investigated in cooling systems where the authors reported a maximum COP of 4.7 [27]. Furthermore, Akkaya et al. [28] enhanced the performance of a refrigeration system with TiO_2 and polyol ester oil, resulting in a COP improvement of 39%. Likewise, Akkaya and Yurtdaş [29] experimentally investigated the COP of a heat pump using deionized water and CuO/ZnO hybrid nanofluids. The COP of the heat pump ranged from 4.23 to 4.44 for deionized water and CuO/ZnO nanofluid, respectively. Recently, Çiftçi et al. [30,31] used binary hybrid nanofluids to develop an efficient heat pipe for air to air heat exchangers and thermosiphon. Most prior methods have revolved around using nanofluid on heat exchangers [32–36], electronic devices [37–39] and heat sinks [40–42]. None of the previous studies was conducted on a system that integrated a nanofluid, a radiator coupled heat sink, and a thermoelectric air conditioner utilizing solar photovoltaic systems in real-time buildings. The novelty of this paper is that it studies the use of nanofluid cooled radiators as an alternative to conventional methods (air-cooled heat sinks) in thermoelectric air conditioners. The newly proposed nanofluid cooled radiator can cool the hot side junction of the TEAC. This can provide a cheap and straightforward retrofit solution that can contribute to increasing the performance of TEACs in residential buildings. Against this background, this study proposed a novel thermoelectric air conditioner coupled with a radiator integrated with nanofluids (NTEAC) consisting of air and liquid (nanofluid) cooled heat sinks for space conditioning. Heat is removed

from the thermoelectric cooling system's hot side junction via nanofluid. The radiator unit transfers the heat from the nanofluid inside to the outside atmospheric air, cooling the nanofluid turn cools the TEM's hot side. Therefore, this research aims to design, build, and evaluate the performance of a novel NTEAC system for a building located in the tropical climate of Malaysia.

2. EXPERIMENTAL APPARATUS AND METHODOLOGY

This section intends to illustrate the experimental research involved in field measurements in Tronoh, Perak, Malaysia's realistic climatic environments, utilizing a test room fitted with PV and NTEAC. The experimental test room or building configuration is outlined in section 2.1. The preparation of MWCNT/Water nanofluid is explained in section 2.2. The fabrication, description, evaluation of NTEAC components and NTEAC system are discussed in sections 2.3 and 2.4. Furthermore, the design and arrangement of the test room equipped with the NTEAC system are presented in section 2.5. Ultimately, the methodology for data acquisition and uncertainty analysis is depicted in sections 2.6 and 2.7.

2.1. Building description

In a test room at Universiti Teknologi Petronas in Tronoh, Perak, Malaysia (4° 23' 2.292" N and 100° 58' 16.824" E), the studied NTEAC system was installed. The schematic image of the test room or building is depicted in Figure 3(a). The test room is installed with photovoltaic panels and a weather link station. Figure 3(b) illustrates the dimensions of the test room, which are as follows: 3200 mm (length), 3200 mm (width) and 2500 mm (height). The external walls are three-layered, with a 200 mm thick stone centre layer, while all side walls are cemented. The inside layer of cement is 13 mm thick, while the exterior layer is 18 mm thick. Clay roof tiles were used for the roof cover, and the ceiling (1800 × 1200 × 6.3 mm) is made of a Gypsum board. The wall window is 304 mm high, 1200 mm wide, and 22 mm thick plywood. In addition, the test room has a single steel door measuring 2000 mm in height, 850 mm in width, and 450 mm in thickness on the northwest wall. Table 1 summarises the thermophysical parameters of the materials utilized in the test room.

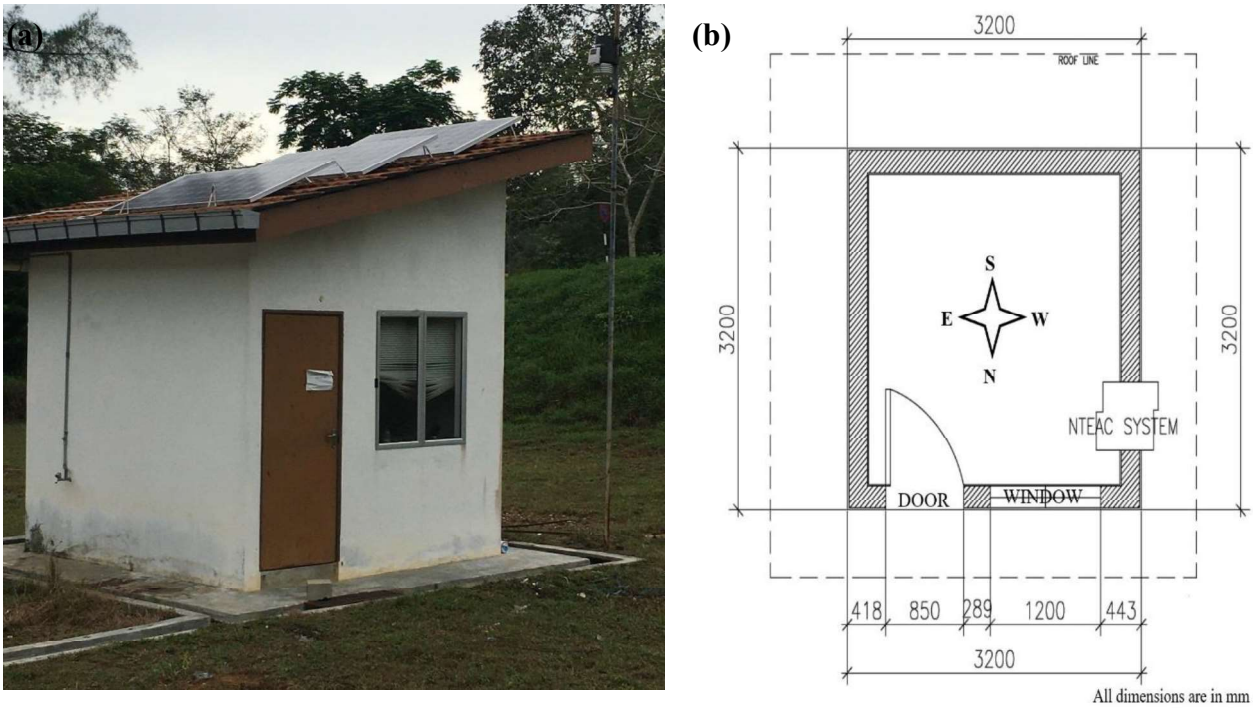

Figure 3: (a) Original image and (b) floor plan of the studied building

172

173 Table 1: Significant parameters of the building materials

Materials	**Thermal conductivity (W/m. K)**	**Density (kg/m^3)**	**Specific heat capacity (kJ/kg.K)**
Limestone tile	1.8	2420	0.84
Sand grave	1.740	2240	0.84
Brick tile	0.798	1892	0.88
Mud brick	0.75	1731	0.88
Soil	0.518	1620	0.88
Cement mortar	0.716	1647	0.92
Cement plaster	0.719	1761	0.84
Roof tile	0.632	2531	1.42
GI sheet	61.06	7520	0.50

174

175 **2.2. Nanofluid preparation**

176 The Multiwalled Carbon Nanotubes (MWCNTs) with 10nm diameter purity 98% was bought from
177 Sigma Aldrich, USA. Distilled water-based MWCNT nanofluid was prepared using the two-step
178 method. MWCNT nanoparticles are dispersed in distilled water with SDBS surfactant to create a
179 highly effective and stable heat transfer fluid. A mixture of MWCNTs and SDBS at 0.5wt%
180 concentration is swirled together using a magnetic stirrer for 30 minutes at 800 RPM without
181 increasing the temperature to ensure uniformity in MWCNT/SDBS mixture distribution. Our

previous literature can provide more detailed information on the studied nanoparticle, base fluid, and nanofluid [43]. The schematic image of the nanofluid preparation is depicted in Figure 4.

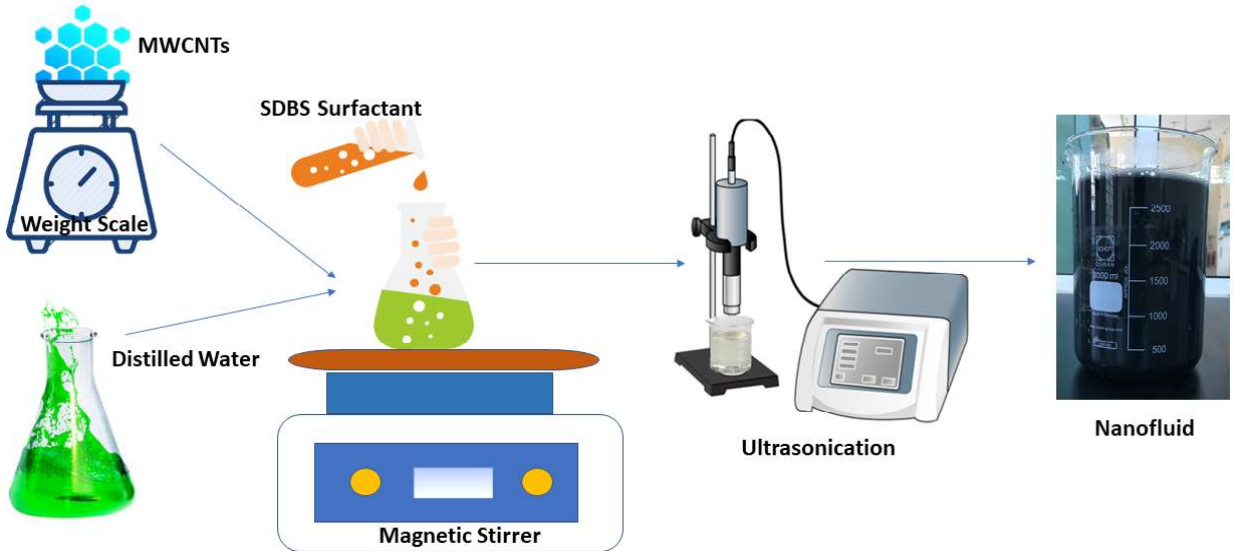

Figure 4: Schematic presentation of nanofluid preparation

2.3. Description of heat sinks, radiators, TEMs and PV panels

2.3.1 Air-cooled heat sinks

A heat sink may effectively absorb or disperse heat from thermal systems to atmospheric air with extended surfaces such as fins and spines. When effective heat dissipation is necessary, heat sinks are utilized in a broad range of applications; notable examples include refrigeration, heat engines, and electronic equipment that need to be cooled. Most heat sinks are made of metal with a cluster of cooling fins, called a fin array. The heat sink's performance can be increased by increasing the surface area, thermal conductivity, or heat transfer coefficient. Longitudinal fins are available in various shapes, including rectangular, triangular, and parabolic fins. The rectangular design is the most fundamental and extensively utilized when it comes to multiple fin arrays. In this study, a multiple-fin array with forced convection is herein preferred for the rectangular profile. The proposed finned heat sink was fabricated based on the conventional heat sink designs [44]. Figure 5 indicates the schematic view of the multi finned heat sink and its dimensions. This heat sink has a channel height of 20 mm, a channel width of 4 mm, a fin width of 2 mm, a total length and breadth of 55 mm, and a base height of 3 mm.

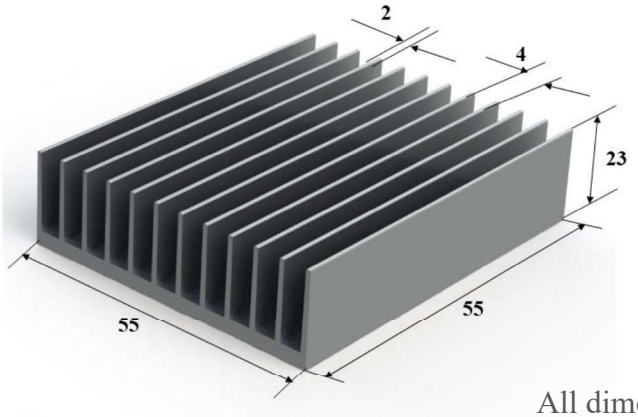

All dimensions are in mm

Figure 5: Schematic diagram of the air-cooled heat sink

199

200 2.3.2 Nanofluid cooled heat sinks

201 Increasing the thermal performance of heat sinks employing traditional heat transfer fluids (HTF)
202 has become ubiquitous in the last decade. The improved thermophysical characteristics of
203 nanofluids compared to conventional HTF allowed them to operate as highly efficient HTF to solve
204 various heat transfer challenges. In this study, MWCNT/Water nanofluid is used as a coolant. A
205 schematic view of the proposed heat sink with a circular channel is presented in Figure 6. The heat
206 sink used for cooling the hot side of the TEMs has a total length of 196 mm, width of 72 mm and
207 height of 23 mm. The diameter of each channel is 2.8 mm, and each channel is surrounded by solid
208 material. The heat generated due to the current flow in TEMs is removed by circulating
209 MWCNT/Water coolant through a channelled heat sink. The heat transfer is carried by conduction
210 in the solid material and the coolant by convection. The nanofluid enters the heat sink in the axial
211 direction with controlled speed and temperature.

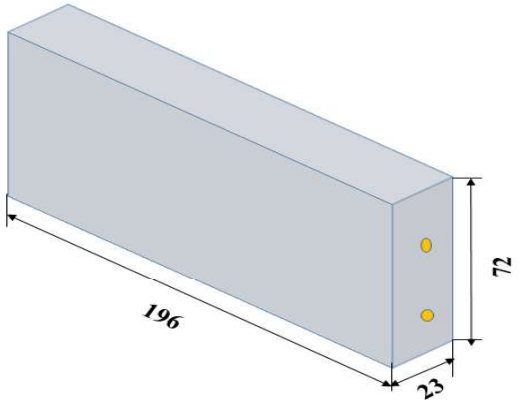

All dimensions are in mm

Figure 6: Schematic diagram of the nanofluid cooled heat sink

212

2.3.3 Electrical connections of TEMs

The amount of heat absorbed at the cold junction is associated with the Peltier cooling, the half of Joule heating, and the thermal conduction. Figure 7 depicts a basic electrical circuit for the studied thermoelectric cooler. Three rows of twelve thermoelectric modules (55 × 26 × 15 cm) were placed in four columns. The positive wires of each series of TEMs were linked to the negative cables of the following sequence of TEMs. Furthermore, the positive cables are connected to a bus bar (positive side) at the end of each row, and the negative cables are attached to a separate bus bar (negative side) at the end. The positive bar was then attached to the positive power supply terminal, and the negative bar was connected to the negative power supply terminal.

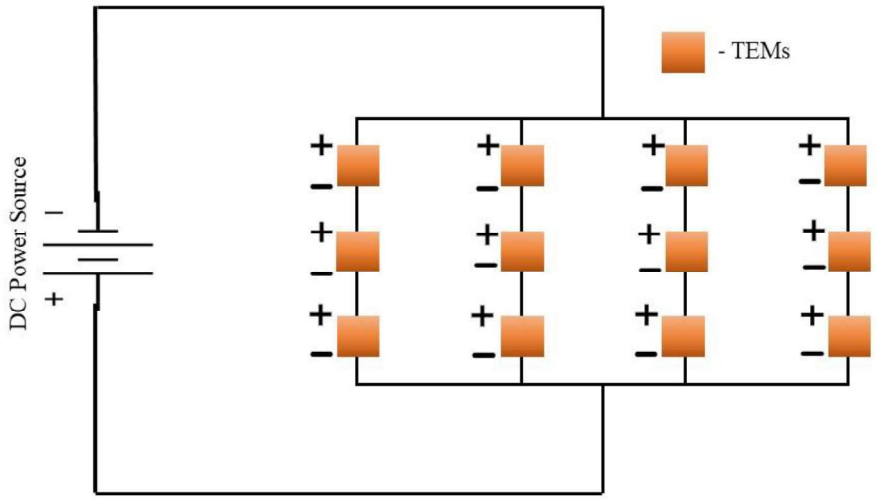

Figure 7: Electrical connection of TEMs

As shown in Figure 7, the internal connection between columns was in series, while connections to other columns were in parallel, and all the columns (with TEMs) were installed in plastic nylon. The configuration of the studied thermoelectric modules is listed in Table 2. The dimension of the plastic nylon layer is 303 × 294 × 25 mm. The nylon layer is extruded to the TEM size, and small ways are paved for wire connections.

Table 2: Specification of the selected TEMs

Company	**Model**	**Current (A)**	**Max. Voltage (V)**	**Max. Cooling Power (W)**	**Max. Temperature Difference (°C)**	**No. of p-n couples**
Ferrotec	9500/391/ 085B	8.5	53.8	248	72	391

2.3.4 Arrangement of heat sinks and thermoelectric modules

On the hot side of the TEMs, waste heat is dissipated into the environment (outdoor space) using nanofluid cooled heat sinks coupled with a radiator. Also, on the cold side of the TEMs, the cooling capacity is enhanced by using air-cooled heat sinks and blower fans, as illustrated in Figure 8. The first aspect of this project is that six nanofluid-cooled heat sinks are connected to the hot side of the twelve TEMs, where each heat sink is connected to two TEMs using thermally conductive grease. Secondly, each TEM's cold side is fixed to separate finned heat sinks, supported by a nylon layer. Consequently, twelve TEMs are connected to twelve heat sinks to stimulate the sustained cooling favoured by the TEMs' cold sides. Furthermore, the cooling obtained by the finned heat sink is fanned out to the test room through the twelve small axial flow fans and a single large fan. The specifications of a single small fan (80 × 80 × 25 mm) are 0.96 W, 2050 RPM, 33.5 CFM, 21.5 Pa, 22 dB and 95 g. Meanwhile, the big fan (200 × 200 × 50 mm) has a configuration of 78 W, 285 CFM, 1800 RPM, 285 CFM, 50 dB, and 400 g. All the layers are tightly enclosed via nuts and bolts to prevent leakage. The NTEAC dimensions were in line with the ASHRAE standard [45].

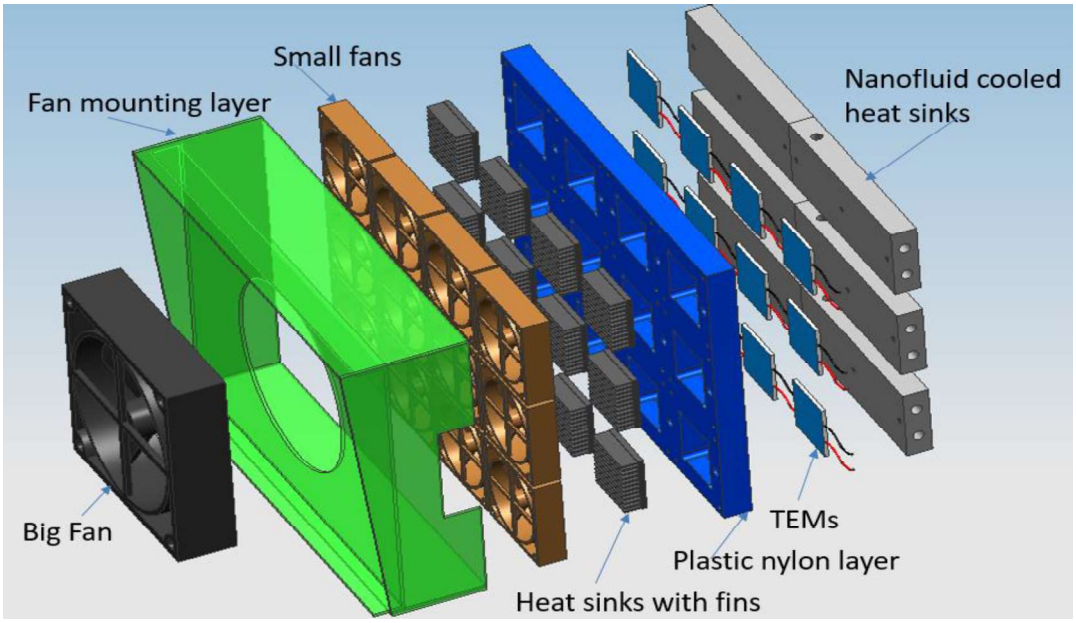

Figure 8: Arrangement of thermoelectric modules and heat sinks (Part B)

2.3.5 Radiator

In the NTEAC system, a Proton automobile radiator made of aluminium material with a louvre fin type is used. On both sides of the tubes, louvred fins are connected. When air enters the radiator's system, it blows in a transverse direction to the arrangement of tubes. Steel is used for both the tube and the louvred fins. Radiators consist of three main parts: heat pipes, an aluminium substrate, and flat fins. Steel is a common material used in radiators since it has a strong anti-corrosion property. It is built to handle heat flow from the hot nanofluid coolant, which passes through it and transfer to

the outside air. Figure 9 depicts the schematic design of the radiator. There are 46 aluminium fins with a dimension of 430 mm × 350 mm × 38 mm. The heat transfer performance of the nanofluid coolant directly affects the running state of the NTEAC system. The MWCNT/water coolant carries the waste heat generated by the TEM incorporated heat sinks (Part B) to the radiator for cooling.

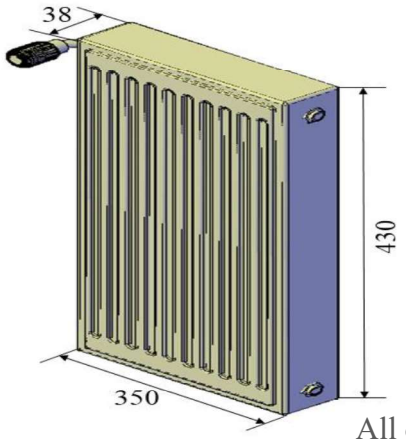

All dimensions are in mm

Figure 9: Schematic diagram of the studied radiator

2.3.6 Photovoltaic panels

Malaysia's energy sector strongly depends on non-renewable fuels as a source of energy, such as natural gas or fossil fuels. The government of Malaysia has made various efforts to promote investment in solar photovoltaic projects. Solar energy has fewer potential environmental consequences than other energy sources, such as fossil fuels, often generated with adverse side effects. A solar PV system comprises several PV modules, also known as solar panels. A module consists of tiny solar cells, each generating 1 to 2 watts of electricity. A PV module with a surface area of one square metre will produce 150 W of electricity. At an angle of 15°, the PV panels are installed on the test room's east-facing roof. Figure 3(a) in the earlier section shows the installed PV on the test room roof. In the current research, three pieces of polycrystalline photovoltaic panels of 325 Wp each generate the PV-NTEAC system's electricity. Table 3 lists the configurations of the PV panels.

Table 3: Specifications of the PV panel

Parameters	**Specifications**
Mechanical properties:	
Type of element used	Polycrystalline silicon
Size (Length × Breadth × Height)	1.99 × 1× 0.035 m
Weight	24 kg
Cells used	72

Type of output node	Amphenol H4
Gauge of output cable wire	12 AWG
Length of the output cable	1.2 m
Electrical properties:	
Maximum efficiency	16.3%
Tolerance limit of power	±3%
Maximum current	8.8A
Maximum voltage	36V
Current of the short circuit (I_{sc})	9.4A
Voltage of the open circuit (V_{oc})	46.4V
Nominal operating cell temperature	45°C
Coefficient of temperature for I_{sc}	0.05 %/K
Coefficient of temperature for V_{oc}	-0.134V/K
Coefficient of temperature of the power	-0.4%/K
Fuse rating of series connection	15A
Maximum voltage of the system	1000V

2.4. Novel proposed NTEAC system description

Evaporative air conditioners and refrigerative air conditioners are the two types of air conditioners typically used in houses. These systems, which use compressors to disperse heat, are called "air-cooled systems" and operate similarly to a car radiator. Since this cooling system absorbs moisture as it cools, it dehumidifies the air. The system absorbs water from the air within the cooled region and distributes it as hot air to the outside air. The proposed NTEAC system also follows the same principle, and it is illustrated in Figure 10, combining a nanofluid tank (Part A), TEMs incorporated heat sinks (Part B), and a radiator (Part C). The basic principle of the NTEAC system is the transfer of heat from the indoor air to the atmospheric air using forced convection. The components used in this system are a submersible pump, a small tank, an adjustable valve, a liquid-cooled heat sink, TEMs, air-cooled heat sinks, nylon layer, connecting pipes, and a radiator. The major part of the NTEAC system is Part B, where the thermoelectric modules are installed. It consists of six layers: a big fan; a fan mounting layer; small fans; air-cooled heat sinks; nylon layer; TEMs; and nanofluid-cooled heat sinks. Hot and humid weather conditions in Malaysia's Perak state were considered while designing the manufactured system.

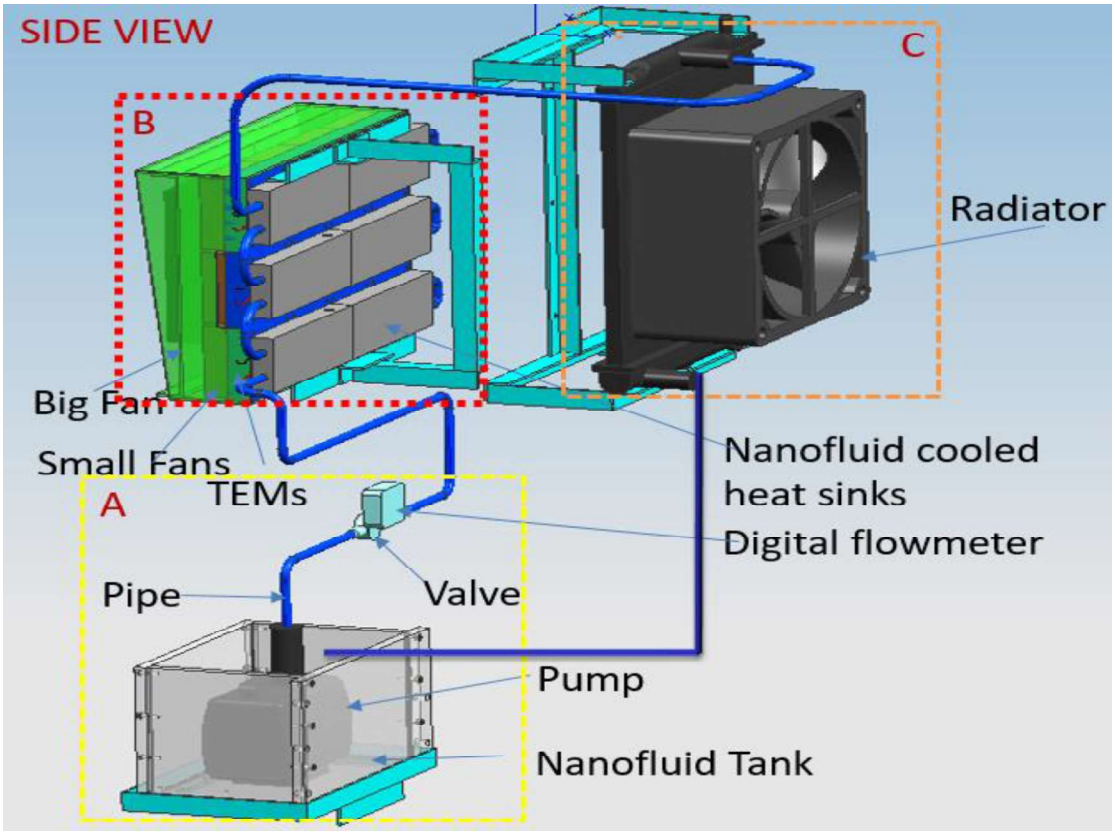

Figure 10: Schematics of the Nanofluid Assisted Thermoelectric Air Conditioner

The proposed NTEAC system has two main units: an indoor unit (pump and TEM combined heat sinks) and an outdoor unit (radiator). An adjustable valve and a digital flowmeter control the nanofluid flow and measure the flow rate. The sequential operations in the NTEAC system are demonstrated as follows. (i) MWCNT/Water nanofluid is pumped to the TEM combined heat sinks with a 13.50 LPM flow rate and 1012.6 kPa pressure. (ii) Heat from the hot side of the thermoelectric module is absorbed by the circulated nanofluid, while the cooling side of the TEM is subjected to indoor air via air-cooled heat sinks and fans resulting in a reduction in test room temperature. (iii) Then, the heated nanofluid flows to the radiator, where the heat is transferred to the atmosphere and enters the pump (with tank) to repeat the cycle. The schematic diagram of the processes in the NTEAC system is illustrated in Figure 11. The design details of the NTEAC components are listed in Table 4.

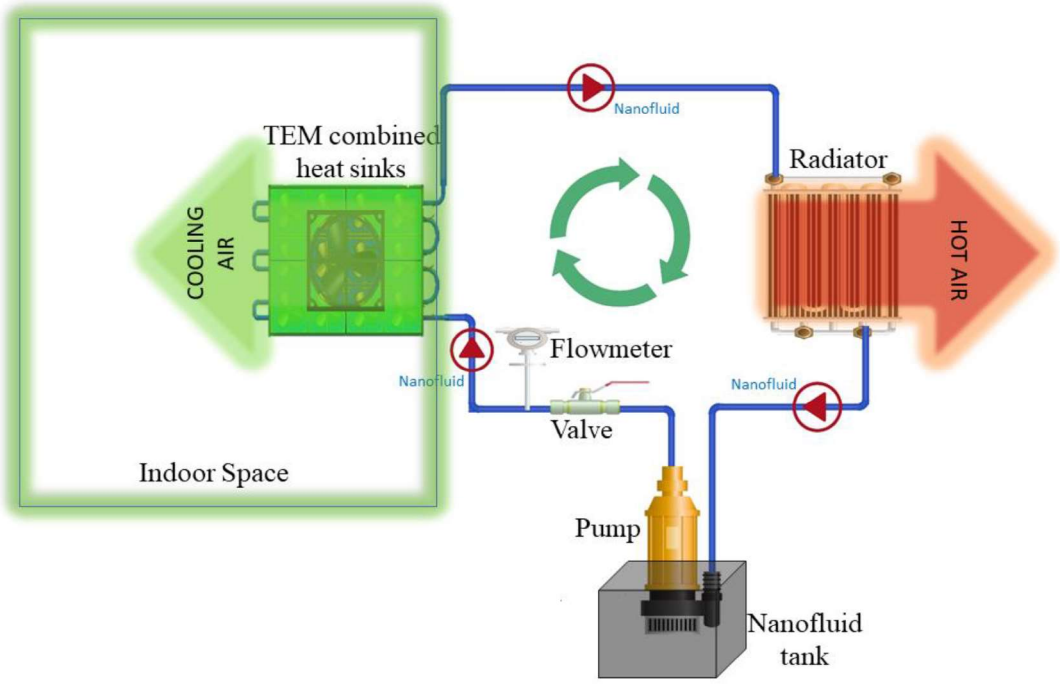

Figure 11: Schematic diagram of the processes in the NTEAC system

295

296 Table 4: Technical details of the NTEAC components

Sl. No.	Components	Parameters	Unit	Quantity
1.	Submersible Pump	220 V, 50 Hz, 85 W, 4000 L/H, 4m	-	1 No.
2.	Nanofluid tank	250 × 155 × 155	mm	1 No.
3.	TEM	I_{max} = 8.5 A V_{max} = 53.8 V	-	12 Nos.
4.	Air-cooled heat sinks	55 × 55 × 23 (20 fins)	mm	12 Nos.
5.	Small fan	24 V, 0.04 A, 33.5 CFM	-	12 Nos.
6.	Big fan	12 V, 6.5 A 200 × 200 × 50	mm	1 No.
7.	Nanofluid cooled heat sink	196 × 72 × 25	mm	6 No.
8.	Brass valve	½	inch	1 No.
9.	MWCNT/Water nanofluid	k = 0.71	W/m.K	5 Litres

10.	Radiator	430×350×38, 0.09 (fin thickness), 0.3 (Radiator tube)	mm	1 No.
11.	Digital flowmeter	0.3 – 15	LPM	1 No.

297

298 **2.5. Building equipped with NTEAC system**

299 The actual NTEAC system installed in a building consists of three main parts, namely a tank filled
300 with nanofluids (Part A), TEMs incorporated with heat sinks (Part B), and a radiator (Part C).
301 Figure 12 illustrates the studied PV-NTEAC device installed in the test room. From 1st September
302 to 30th September 2020, the experiment was conducted in a test room situated at the Universiti
303 Teknologi PETRONAS, Malaysia. Before the installation of the NTEAC system, the test room's
304 estimated peak cooling demand was 590 W. Each TEM produced a cooling power of 50 W at an
305 applied voltage of 10 V and 5 A. Since the required cooling load for the test room is 590W, the
306 NTEAC system uses twelve 50W (600 W) thermoelectric modules, which are slightly more (10 W)
307 than the required cooling load. Once the DC power supply was turned on, the current flowed
308 through the TEMs, creating a temperature difference between the module's cold and hot sides. With
309 an exhaust fan (78 W), the ambient air was scattered inside the test room through the NTEAC
310 device (Part B) mounted on the test room's inside wall. There were twenty-four fins in each heat
311 sink linked to the cold side of the TEMs, which absorbed the heat sustained in the test room's
312 ambient air. The heat sinks were also cooled using 0.96 W (12 Nos) power exhaust fans by forced
313 convection.

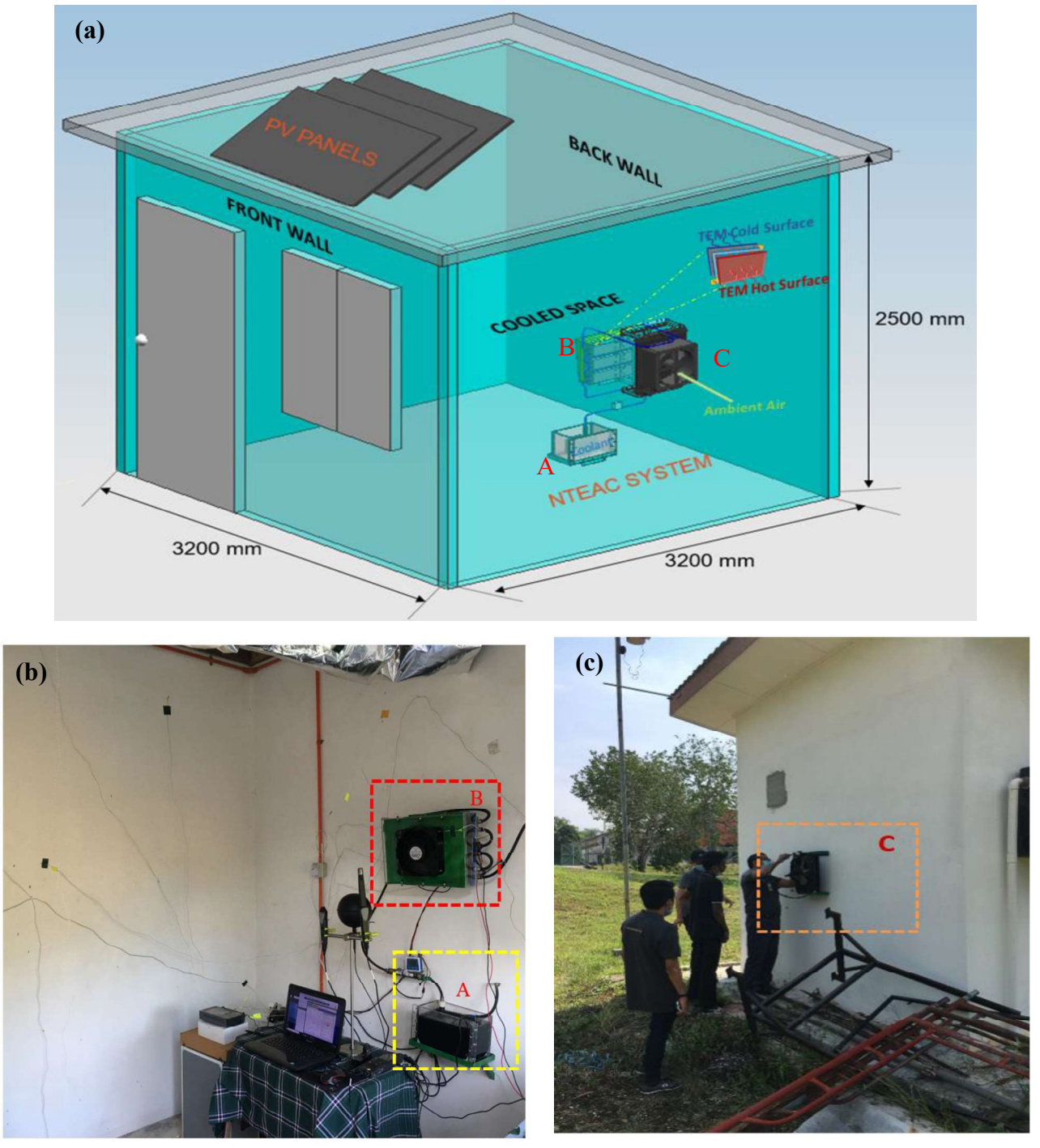

Figure 12: Building equipped with PV-NTEAC(a) Schematic diagram (b) Indoor unit with Part A and Part B (c) Outdoor unit with Part C

2.6. Experimental procedure

As mentioned earlier, the experiment was conducted in September 2020. The CLTD (Cooling Load Temperature Difference) calculation showed that the test room needed 590 watts of cooling capacity to compensate for the thermal acceptability criteria without considering the influx of heat through the floor. As shown in Figure 13, the electricity generated from photovoltaic panels was

stored in batteries (RA-12-40 Batteries) through a solar charge controller (Beta 2.0). This research explores the PV-NTEAC system's performance at current levels, ranging from 2 A to 6 A.

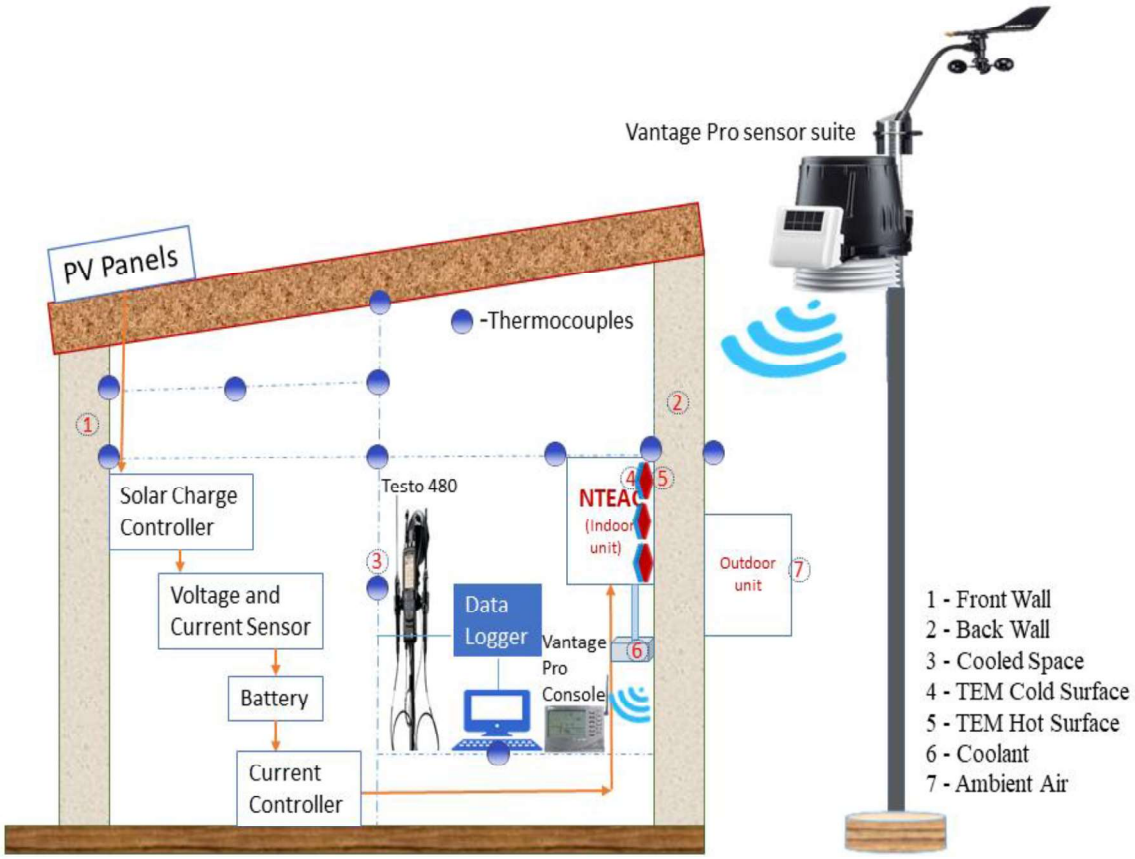

Figure 13: Schematic diagram of the experimental setup

It also uses an adjustable current controller (DPS 5015) to control the current supply into the PV-NTEAC system. Moreover, different temperatures, such as inlet temperature (T_{in}), hot junction temperature ($T_{hot,out}$), cold junction temperature (T_c) and cold outlet temperature ($T_{c,out}$), were measured at various positions in the test room using 10 K-type thermocouples. Based on the ASHRAE standard 55 [46], the methodology for measuring the test room's indoor thermal condition was chosen. The Class II field research protocol [47] was followed to render the data collection method. To obtain the indoor air quality (IAQ) such as room temperature (T_{room}), room humidity (RH), air pressure (P_{room})and air velocity (Vroom), TESTO 480 was placed at 1000 mm above the ground and near the occupant region. Data were gathered during the solar hours of 8 AM to 8 PM with an interval of 5 minutes for 30 days. Figure 14 shows the original image of the experimental setup used in the study. The details of various electrical instruments used in the NTEAC system are listed in Table 5.

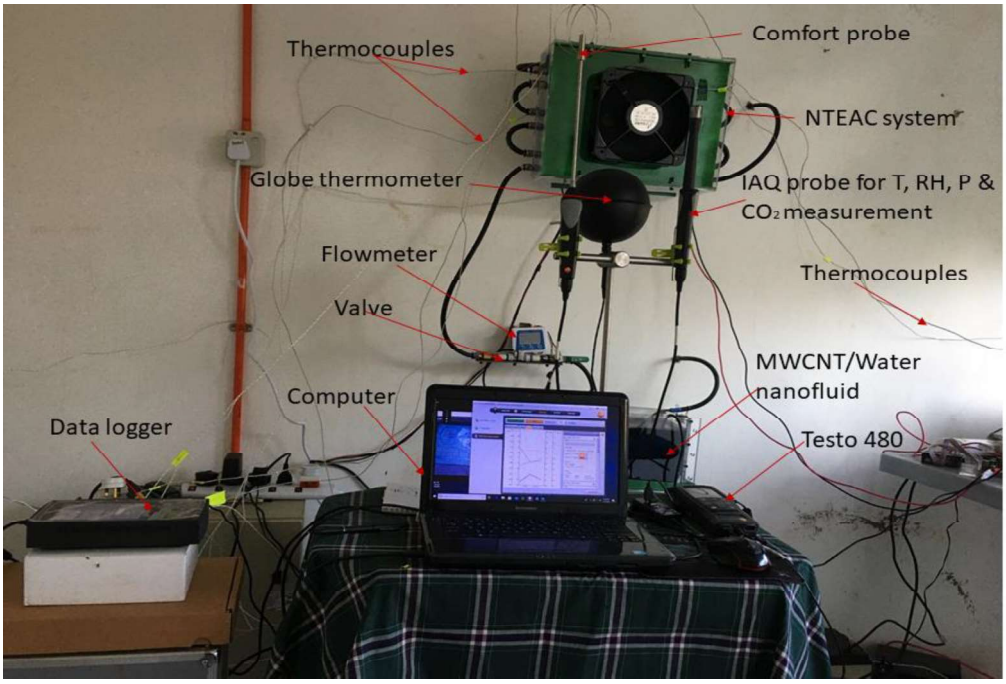

Figure 14: Original image of the experimental setup

336

337 Table 5: Specification of electrical devices

Descriptions	**Values**
Current Controller (Model: DPS 5015)	
Voltage output accuracy	0.01V (0.5%)
Voltage input accuracy	6-60V
Maximum Voltage output	50V
Maximum power output	1000W
Maximum output current	20A
Current output accuracy	0.5%
Charge Controller (Model: Solar Beta 2)	
Length × Breadth × Height	0.159 × 0.81 × 0.47 m
Operating voltage of the system	12-24V
Input PV voltage (Max.)	50V
Maximum Charge Current	15A
Terminal voltage of the battery (Max.)	34V
Maximum current supply (Battery)	20A
Voltage drop of the circuit (Charge)	≤0.28V
Voltage drop of the circuit (Discharge)	≤0.20V
Battery Bank (Model: MSB RA 12-40)	

Length × Breadth × Height	0.19 × 0.16 × 0.17 m
Unit voltage	12V
Battery Capacity	40Ah@10hr-rate
Discharge current (Max.)	400 (5) A/sec
Internal resistance	8 mΩ
Temperature range for discharge	-20 to 60
Temperature range for charge	0 - 50°C
Operating temperature during current storage	-20 to 60°C
Operating temperature during normal condition	25±5°C
Maximum charging current	12A
Submersible Pump (Venus Aqua V4800)	
Voltage	220 – 240V
Frequency	50/60 Hz
Power	85 W
Maximum flow rate	4000 L/hr
Maximum flow height	4m

Besides, the Davis Vantage Pro 2 weather station is fixed outside the test room at the height of 3000 mm. All the measured data is displayed on a console placed inside the test room through a low power radio (wireless). The Davis vantage pro 2 can determine the inside temperature, outside temperature, inside humidity, outside humidity, pressure, heat index, wind speed, solar radiation, dew point, UV index, etc. This study measured ambient temperature, humidity, and wind speed at a 5-minute interval via the Davis vantage pro 2 weather station. Table 6 presents the technical specifications of the Davis vantage Pro 2 sensors.

Table 6: Specification of sensors in Davis Vantage Pro 2

Variable	Descriptions	Values
Humidity	Range	1 – 100%
	Resolution	1%
	Accuracy	±2%
Pressure	Range	410 – 820 mmHg
	Resolution	0.1 mmHg
	Accuracy	±0.8 mmHg
Temperature	Range	0 – 60 °C
	Resolution	0.1 °C

	Accuracy	±0.3 °C
Solar radiation	Range	0 – 1800 W/m^2
	Resolution	1 W/m^2
	Accuracy	±5%
Dew point	Range	-76 °C to +54 °C
	Resolution	1 °C
	Accuracy	±1 °C

348

349 **2.7. Data reduction and uncertainty analysis of the PV-NTEAC system**

350 2.7.1 Data reduction

351 The cooling capacity (*Qc*) of the NTEAC system is calculated using Eq. 1. [26]

$$Q_C = SIT_c - 0.5I^2R - K\Delta T \quad (1)$$

352 Where *S*, *I*, *R*, *K* and ΔT represent the Seebeck coefficient, input current, electrical resistance,
353 thermal conductivity, and temperature gradient of the thermoelectric module. T_c and T_h denote the
354 temperature of the hot and cold sides of the TEM, respectively.

355

356 The Coefficient of Performance (COP) of the studied PV-NTEAC is estimated using Eq. 2. [20]

$$COP = \frac{Q_c}{P_{TEM} + W} \quad (2)$$

$$P_{TEM} = I^2R + SI\Delta T \quad (3)$$

$$W = P_{small\ fan} + P_{big\ fan} + P_{pump} + P_{radiator} \quad (4)$$

357 Where P_{TEM} reflects the input power provided by TEM, *W* illustrates the input power given to other
358 components (fan, pump, radiator) of the NTEAC system.

359

360 The thermoelectric cooling module's input power is determined using Eq. 5.

$$P = VI \quad (5)$$

361 *I* is the input current, and *V* is the input voltage supplied to the TEM.

362

363

2.7.2 Uncertainty analysis

Due to calibration and data recording, systematic errors can emerge during the experiment. Therefore, measuring probes such as thermocouples are adjusted to increase the precision of data collection. Therefore, measurement probes such as thermocouples are calibrated with a bi-metallic thermometer immersed in water under different temperatures to enhance their data collection precision. As shown in Table 7, systematic errors are also considered in the uncertainty analysis to get a complete picture of the measurement's accuracy. The root-sum-squares (RSS) technique has been used to do the total uncertainty analysis. Moffat [47] pioneered this method, which defines the uncertainty of a function, δF, as follows:

$$\delta F = \left[\sum_{i=1}^{n} \left(\frac{\partial F}{\partial X_i}\delta X_i\right)^2\right]^{\frac{1}{2}} \quad (6)$$

Where X_i indicates the uncertainty sensitivity coefficient, fore, using the above equation (Eq. 6), the estimated uncertainty of COP (δCOP) is determined with a 98% certainty, and the computed value was less than 0.1%, as far as significant components are concerned.

Table 7: Uncertainty analysis of the obtained experimental data

Variable	**Typical Value (X)**	**Uncertainty (∂X)**	**Relative Uncertainty** $(\frac{\partial X}{X})\%$
T_{in} (°C)	30-35	0.51	1.7
$T_{c,out}$ (°C)	22-25	0.54	2.4
$T_{h,out}$ (°C)	21-23	0.21	1
T_{amb} (°C)	25-28	0.24	0.9
T_{room} (°C)	27-30	0.3	1.1
RH_{in} (%)	85-100	0.6	0.7
RH_{out} (%)	90-94	0.64	0.71
Current (A)	1-6	0.01	0.16
Voltage (V)	5	0.05	1.66
Nanofluid flow rate (LPM)	13 - 15	0.12	1
Solar radiation (W/m^2)	100 - 1000	1.5	1.5

3. RESULTS AND DISCUSSION

In this section, the results of the performed experiments are discussed to observe the PV-NTEAC system's performance with MWCNT/water nanofluids. First, the detailed experimental results of the test room acquitted with the PV-NTEAC system are reported. Then, the effect of changing input current supply on the COP and cooling power of the PV-NTEAC system is discussed in detail. Following that, the test room's indoor thermal conditions during optimal operating conditions are measured and compared to the initial test room to determine the system's suitability for building cooling in Malaysia's climate.

3.1. Thermal environments

3.1.1 Air temperature and Relative humidity

Tronoh, located at latitude 4° 23' 2.292" N and longitude 100° 58' 16.824" E, is a tropical city in Malaysia's hot and humid area. Since the performance of the PV-assisted NTEAC system is dependent on the outside climatic conditions, such as outside temperature, relative humidity (RH), and solar radiation intensity, it is no surprise that the PV-assisted NTEAC system's performance varies widely based on the climate at the installation site. In this study, the ambient air temperature, relative humidity, and UV index were evaluated by Davis Vantage Pro for 30 days (720 hours) in September 2020, as shown in Figure 15. The annual mean temperature ranges between 25 and 27°C, and the monthly mean temperature and humidity in September are 26.5°C and 82%. Moreover, the minimum and maximum temperatures recorded during the September month were 23.6 and 30.1 °C, with an average UV index of 6. The lowest RH ranged between 46 and 55.73% during daylight, while the highest RH ranged from 79.3 to 99% at night.

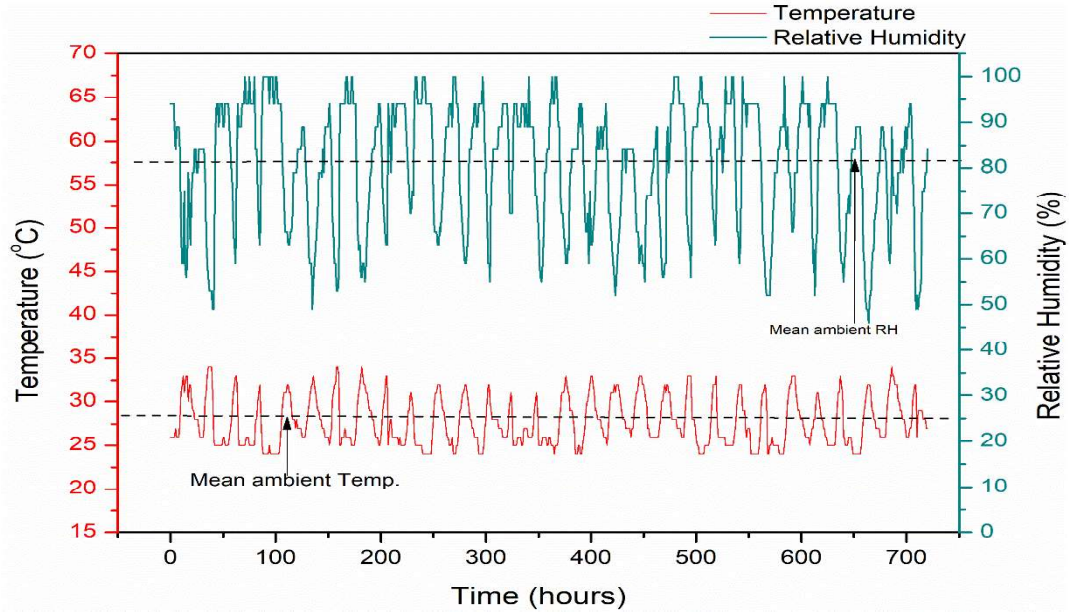

Figure 15: Hourly changes of ambient air temperature and relative humidity for September 2020

3.1.2 Solar irradiance and PV power

Assessment of the solar irradiance of a region is just as critical as evaluating the humidity and temperature data collection for a given time in deciding the viability of a solar-powered project. The variation of solar irradiance and the PV panel power output from 1st to 30th September 2020 is displayed in Figure 16. Underlying darkness and cloudiness lead to reduced electrical power production. An average solar irradiance of 661.42 W/m^2 was observed during the experiment. The maximum solar irradiance was 1045.81 W/m^2 on 18th September 2020, and a minimum solar irradiance of 126.03 W/m^2 was detected on 19th September 2020. The photovoltaic (PV) panel delivered a maximum of 595.81 W and 1.12 kWh of daily power output. Also, three PV panels were used to provide sufficient power to the PV-NTEAC device via batteries. Two solar charge controllers controlled the power supplied by three PV panels and stored directly in the batteries. The impact of input current on the PV-NTEAC device's output was investigated using this as a source of input control.

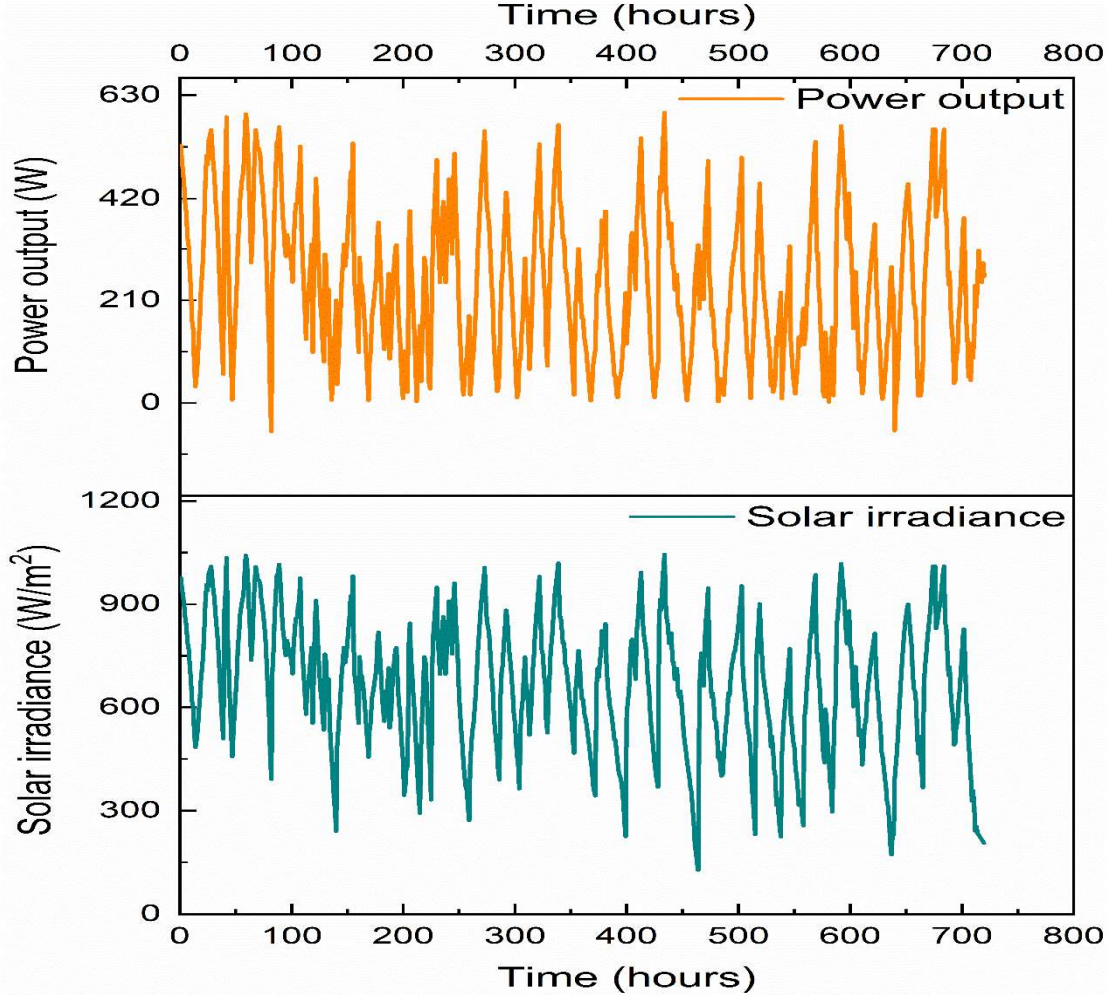

Figure 16: Hourly changes in solar irradiance and PV power output for September 2020

3.1.3 Mean radiant temperature and air velocity

The daily changes of mean radiant temperature (MRT) and air velocity from 1st to 30th September 2020 are depicted in Figure 17. Air temperature, velocity, and globe temperature were used to determine mean radiant temperature (MRT) according to ISO 7726 standards [48]. The average ambient air velocity was 1.16 m/s, with a minimum and maximum air velocity of 0.67 m/s and 2.02 m/s observed on September 16th and 20th. Therefore, the daily change of MRT is similar to that of the air temperature. Many of the MRT values recorded in the analysed building were much higher than the air temperature (about 1°C), indicating a significant radiant impact that needed to be accounted for.

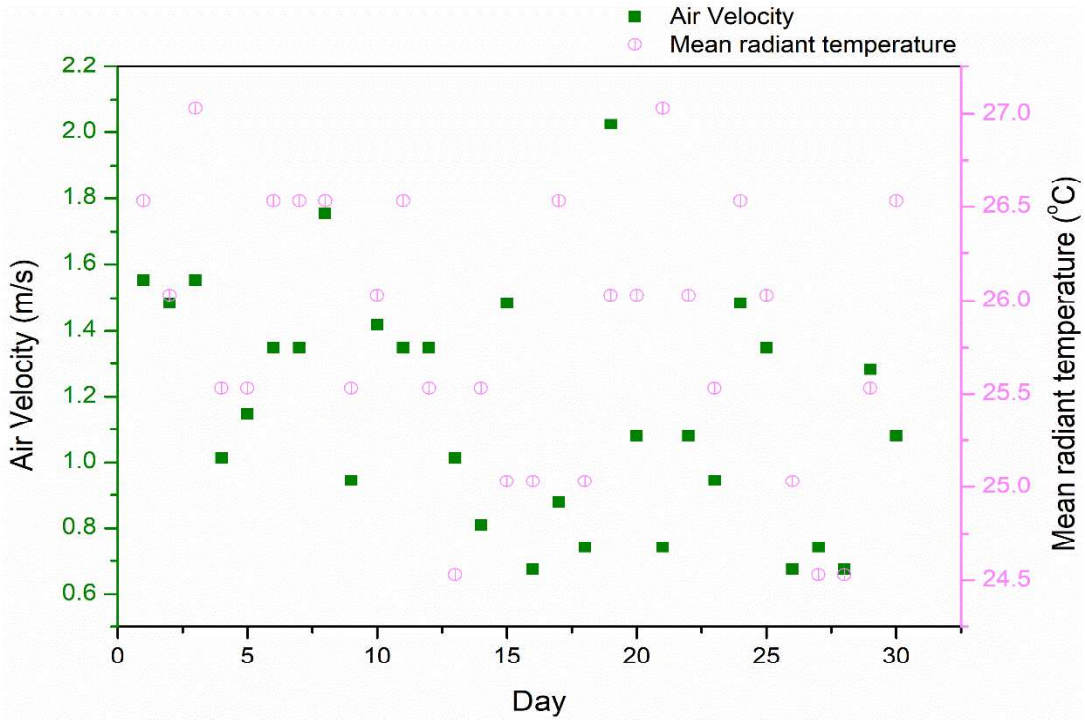

Figure 17: Daily changes of mean radiant temperature and air velocity for September 2020

The ambient data from 7th to 11th September (8 hours to 20 hours each day) is considered the most identical to ensure the results are comparable under natural weather conditions. The ambient weather conditions are presented in Table 8.

Table 8: Summary of ambient weather conditions of the test room

Parameters	Description	7/9/2020	8/9/2020	9/9/2020	10/9/2020	11/9/2020
Outdoor Temperature (°C)	Minimum	24.9	26.02	25.11	26.3	25.4
	Maximum	34.23	31.4	33.2	32.1	33.6
	Mean	27.7	27.41	28.33	29.2	30.1

	Standard Deviation	2.70	2.60	4.10	3.50	3.80
Indoor Temperature (°C)	Minimum	24.01	25.8	25.25	24.92	25.02
	Maximum	33.12	31.78	32.67	32.30	32.9
	Mean	27.26	25.49	27.66	27.31	26.40
	Standard Deviation	2.45	2.80	2.020	2.50	2.90
Radiant Temperature (°C)	Minimum	25	24.90	22.80	23.71	24.50
	Maximum	27.42	27.03	26.89	26.84	26.50
	Mean	27.51	27.26	25.64	26.57	26.8
	Standard Deviation	2.70	2.40	2.90	2.60	2.30
Outdoor Relative Humidity (%)	Maximum	97	96	89	91	93
	Minimum	57	55	49	53	57
	Mean	79	75	82	84	81
	Standard Deviation	5.40	4.80	4.20	6.20	5.10
Indoor Relative Humidity (%)	Maximum	80	83	91	85	79
	Minimum	61	72	59	64	55
	Mean	77	79	84	75	78
	Standard Deviation	3.40	4.20	5.50	5.30	3.80
Velocity of air (m/s)	Maximum	3.20	2.50	2.10	1.80	2.20
	Minimum	0.8	1.20	0.70	1.20	1.00
	Mean	1.60	1.80	1.40	1.30	1.50
	Standard Deviation	0.68	0.30	0.20	0.70	0.50

3.2. Thermal performance of the NTEAC system

Figure 18 presents the time-dependent temperature measurements conducted on a hot, humid day in September 2020 for the internal front wall, internal rear wall, the hot surface of TEM, cold surface of TEM, cooled space, ambient air, and coolant (MWCNT/water nanofluid) of the NTEAC system installed in the test room. While the cold side temperature of the TEM ranged between 29.3 and

69.4°C, this value ranged between 47.1 and 147.7 °C for the TEM's hot side. An improvement of 17% was obtained in the cooling system using 0.5wt% MWCNT/Water nanofluid with respect to pure distilled water when the initial and final state temperature differences were compared. As the temperature of the surrounding environment rises, the temperature difference (ΔT) of the test room is cooled using the studied nanofluid-based TEAC. The obtained data also shows that MWCNT/water nanofluids give the most impressive improvements in heat transfer performance. Furthermore, it is observed that the rate of enhancement depends on various factors, including thermal conductivity, agglomeration, viscosity, density, and the specific heat capacity of the heat transfer fluid. These aspects were briefly explored in our previous literature [43]. In principle, the thermal conductivity of nanofluids has the most significant effect on heat transfer characteristics, which is also supported by the results of ΔT, which shows a similar trend to that seen in the prior research [49]. As a whole, it can be said that the thermal performance of the PV-NTEAC system is highly dependent on solar irradiation and ambient temperature. The PV-NTEAC system, on the other hand, may function differently depending on the climate.

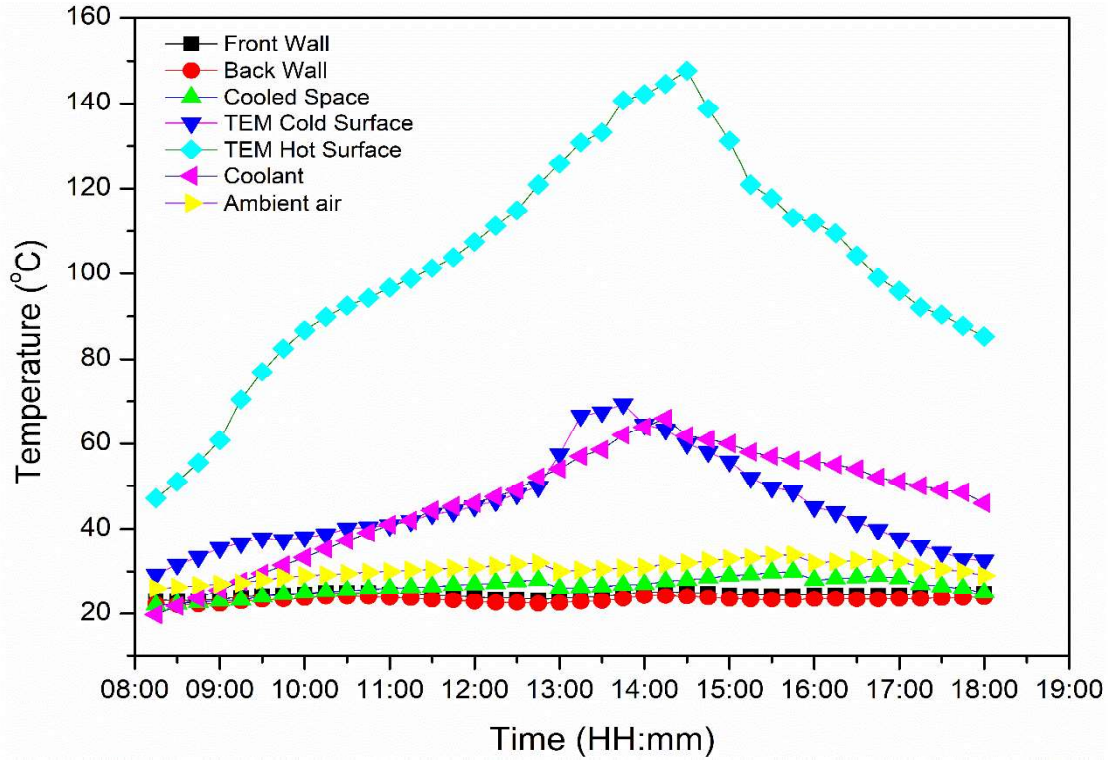

Figure 18: Thermal performance of NTEAC device for 0.5wt% MWCNT/Water nanofluid

3.3. Coefficient of performance and Cooling Capacity of the NTEAC system

The coefficient of performance (COP) was assessed by calculating the cooling energy dissipated inside the test room and the thermoelectric modules' electrical energy input. As aforementioned, the COP of the photovoltaic powered nanofluid assisted thermoelectric air conditioner (PV-NTEAC)

can be improved by reducing the hot side temperature of the thermoelectric modules. This can be done by removing heat more efficiently from the hot side of the TEMs through the nanofluid cooled heat sink unified to a radiator. Nanofluids are ideal coolants for radiators because of their excellent thermal properties, contributing to high heat transfer. To analyze the cooling effect of the enhanced thermophysical properties of working fluid (nanofluid), more tests were performed on the PV-NTEAC system by varying the input current supply (2-6.5A). Figure 19 shows the COP variation of the PV-NTEAC system implemented in the test room. As seen in the above figure, the COP of the PV-NTEAC system increased to its maximum at first and then decreased gradually when the current supply increased to 6.5A. The maximum obtained COP is 1.27 when the applied current is 6A, and the cold side temperature is 22.7 °C. The results show that the PV-NTEAC system requires less electrical energy and works more efficiently with an optimum input current supply of 6A. On the other hand, the COP decreased from 1.27 to 1.19 when the current supply increased from 6A to 6.5A. When the system was operating at current levels greater than 6.5A, it was discovered that a significant quantity of heat was being transmitted to the cold side of the TEMs, thus negating the total cooling capacity of the system.

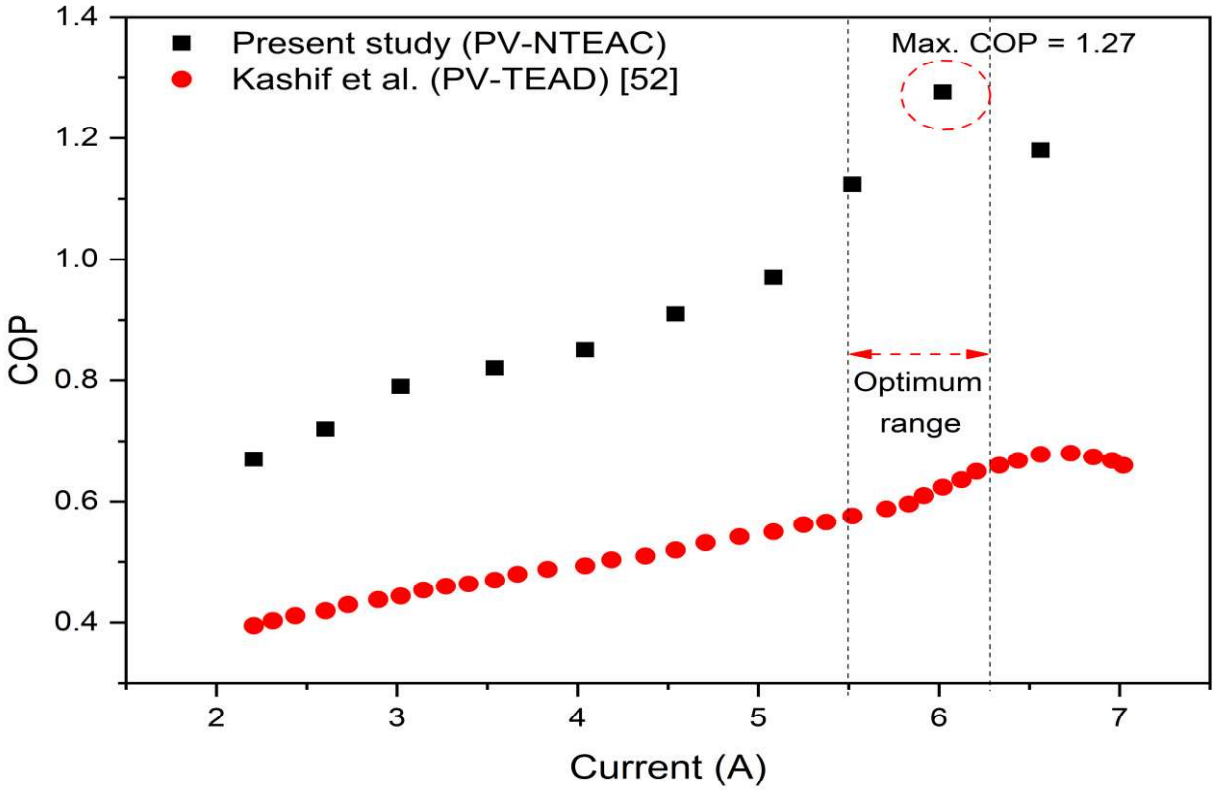

Figure 19: Effect of current on the COP of the PV-NTEAC system

By circulating nanofluids on the heat sink (hot side of TEMs), the temperature difference between the hot and cold sides of the TEMs can be maintained, allowing for constant cooling of the heat

sink (hot side of TEMs). As MWCNT/water nanofluid possesses fascinating heat transfer characteristics, this method effectively calms buildings with a minimum number of TEMs in TEACs. Furthermore, the obtained results are compared with earlier thermoelectric cooling studies, shown in Table 9.

Table 9: Comparison with previous studies on thermoelectric cooling

References	**Number of TEMs & Model No.**	**Operation current(A)/ Voltage(V)**	**Maximum COP**	**Maximum Cooling capacity (W)**	**Application**
Shen et al. 2013, [50]	1 TEM (TEC1-12706)	1.2A	1.77	6.38	Small office space
Tan et al. 2015, [51]	42 TEMs (RC12-8)	5A	0.78	1534	Office room (33.6 m^3)
Kashif et al. 2015, [52]	24 TEMs (TEC1-12730)	2 – 7A	0.679	499	Test room (18.9 m^3)
Puy et al. 2017, [53]	16 TEMs (RC12-8)	12 V	0.78	600	Residential building (0.27 m^3)
Rincon et al. 2018, [54]	12 TEMs (RC12-6L)	120 V	0.77	480	Climatic chamber
Cheon et al. 2019, [55]	9 TEMs (HMN 6040)	1 – 3.2A	0.73	504	Office building (3000 m^3)
Chen et al. 2020, [56]	9 TEMs	1.5 – 9.9A	1.24	324	Simulation box (0.42 m^3)
Looi et al. 2020, [57]	9 TEMs (Ferrotec 9500/391/085B)	5A	1.67	181	Test chamber (3.6 m^3)
Present work	12 TEMs (Ferrotec 9500/391/085B)	2 – 6A	1.27	571	Test room (25.6 m^3)

In order to ensure continuous operation and appropriate performance, the hot sides must efficiently disperse heat into the ambient air. Cooling performance is affected by both the convection heat transfer coefficient and the heat dissipation regions on the hot side TEM. The high heat transfer coefficient of MWCNT/water nanofluid is attributed to the high heat dissipation rate, resulting in cooling capacity enhancement. Figure 20 shows the PV-NTEAC system's cooling capacity (Q_c) with various current supplies. Increasing the input current first allows the cooling capacity to achieve its maximum value. Following that, the Q_c falls in accordance with the rise in electrical current flow. Using a current supply of 6A, the maximum possible Q_c of 571W was obtained. As long as the input current is sufficient, the Peltier cooling rises in proportion to an increase in electrical current, eventually taking over and reducing Q_c ultimately. This is attributed to the rise of Q_c with the rise of electrical current. Apart from that, Q_c declines after reaching its maximum value since Joule heat rises faster than Peltier cooling does. These results are in good agreement with Irshad et al. [52], in which the COP and Q_c increased (3-5A) first and decreased (> 5A) at greater current supply. Furthermore, the COP and Q_c increase when the hot side temperature of the TEMs are lowered. In a nutshell, the maximum COP is 1.27, and the corresponding Q_c is 571W.

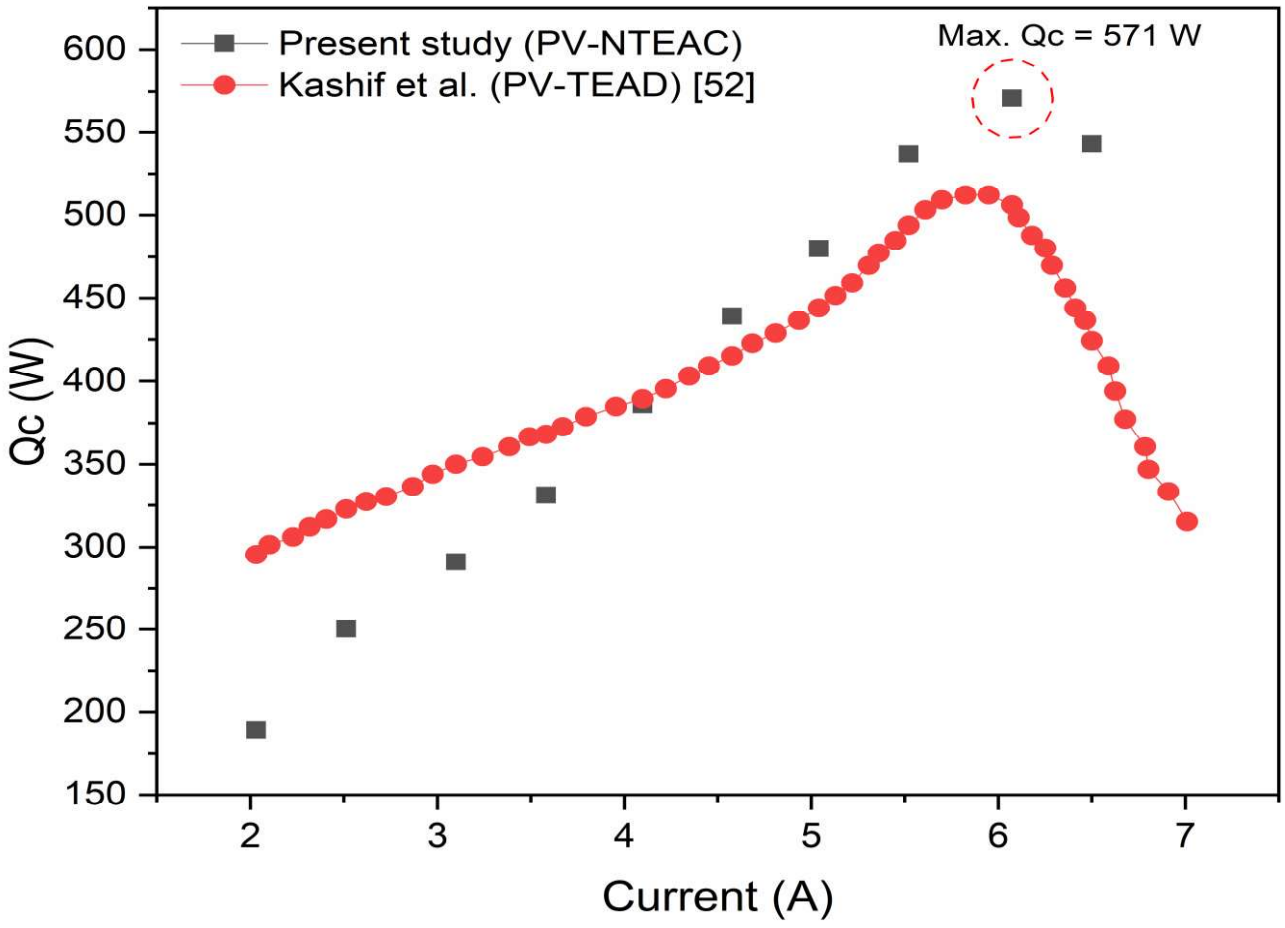

Figure 20: Effect of current on the cooling capacity of the PV-NTEAC system

3.4. Performance of the test room equipped with NTEAC system

This section will present and discuss TEM's cold side and hot side temperatures, indoor temperature, and relative humidity under different input currents to analyze the PV-NTEAC system's performance. The temperature variations seen at the outlet areas of the hot and cold junctions occur due to the Peltier effect when the PV-NTEAC system is turned on at 8 AM. The decrease in the incoming air temperature was due to heat absorption on the cold side of the TEMs, and the absorbed heat was discharged via forced convection, which transferred the heat to the hot side of the system. The airflow rates to the cold junction and the hot junction are monitored to ensure no change for all current supplies. Regarding the experimental findings shown in Figure 21, different outcomes were found for the hot and cold sides' temperatures, depending on the nanofluids' temperature. The results show that both the nanofluid temperature and the hot side temperature rise in tandem, whereas the cold side temperature rises slower. This increases the difference between the hot and cold sides' temperatures, thus making the temperature gradient wider.

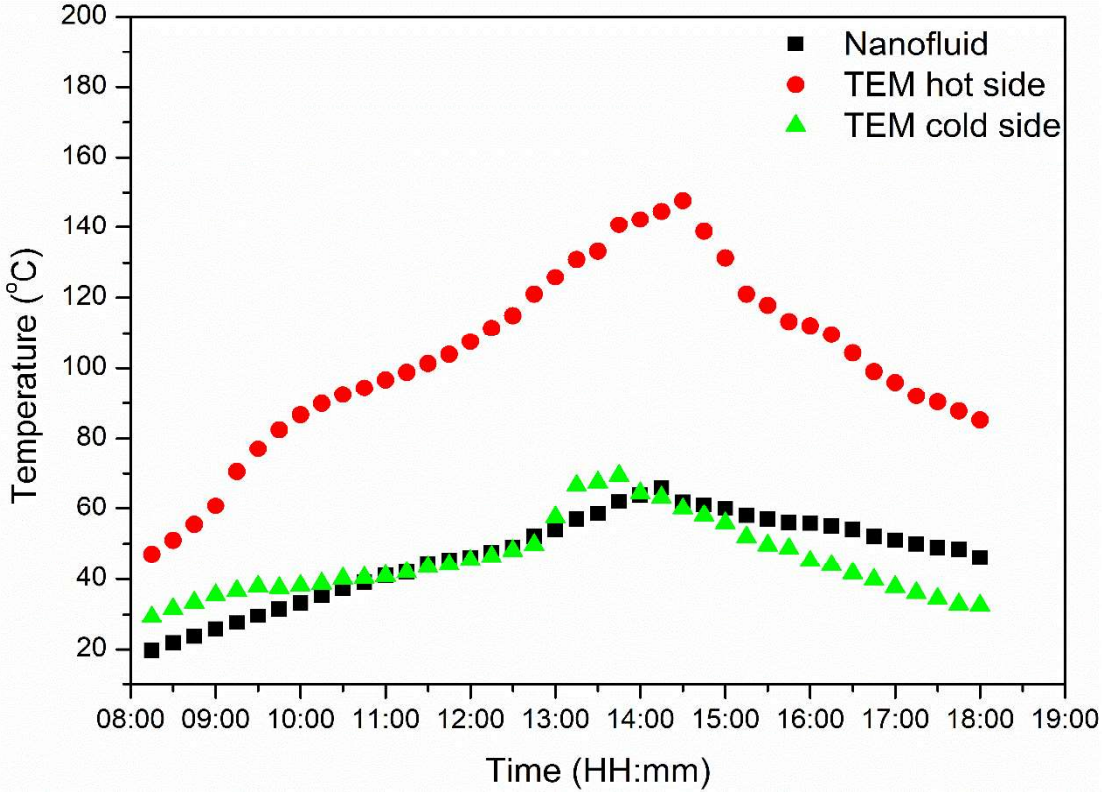

Figure 21: Temperature of TEM and nanofluid at different timings

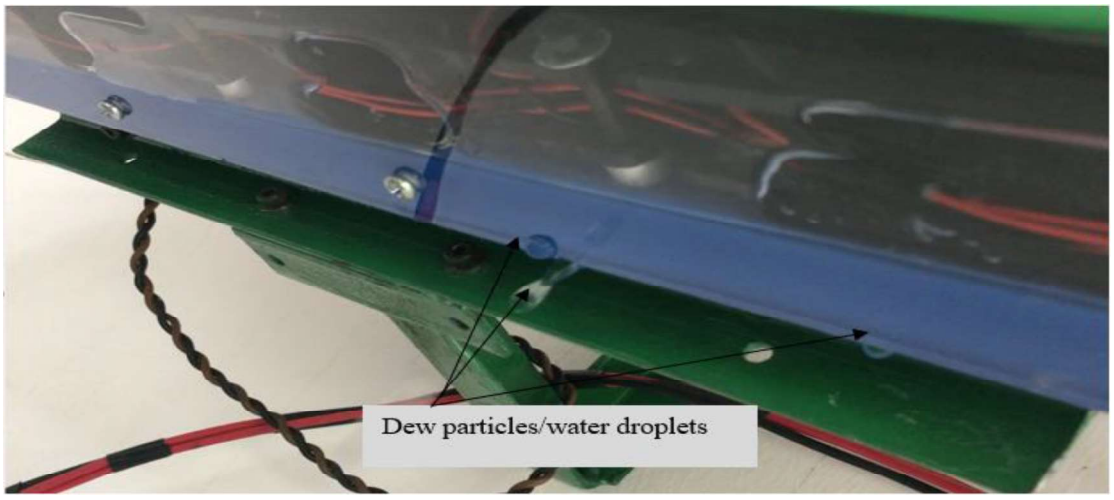

Figure 22: Deposits of dew particles and water drops in the PV-NTEAC

508

509 As the temperature of an object drops below the dew point, water vapour condenses on the
510 comparatively cool surface of the object to create water droplets and dew particles. The formation
511 of water droplets and dew particles is shown in Figure 22. At constant pressure and continuous
512 water vapour, moisture in moist air is cooled to achieve the dew point temperature. Due to the fact
513 that the dew point temperature is a measure of humidity, it functions as a comfort index. Usually,
514 the dew point temperature should be lower than the wet-bulb temperature to attain optimum human
515 comfort. Figure 23 illustrates the dry bulb and dew point temperature fluctuation of the processed
516 air at 6A current. Results showed that the dew point and the dry bulb temperature differed slightly,
517 which expedited moisture removal. The maximum dew point and dry bulb temperature were 24.77
518 °C and 26.14 °C, respectively, which occurred around 13.30 hours.

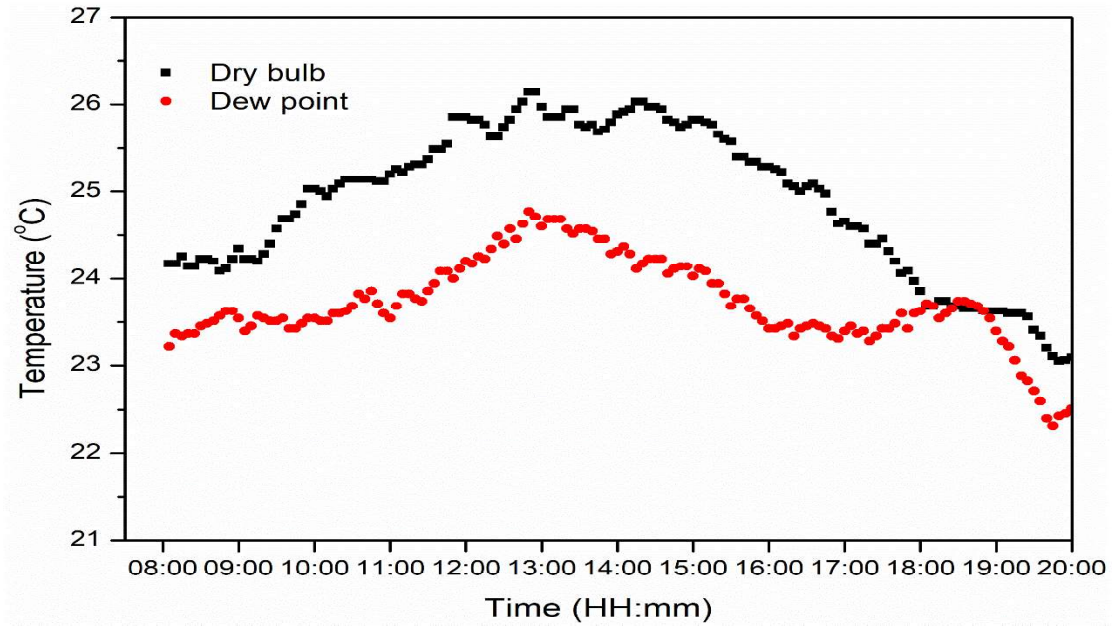

Figure 23: Variation of dry bulb and dew point temperature with time at 6A

The impact of the PV-NTEAC system on the test room's indoor temperature by supplying different input currents from 2-6A to TEMs is shown in Figure 24. The data for five cloudless days (7^{th} – 11^{th} Sept 2020) is presented in Table 8. The results obtained for the operation period between 8 and 20 hours were compared with normal test room conditions (See Table 8). With 2A of input current from the PV and DC power systems to the NTEAC system, the average indoor temperature was 25.26°C, 2°C lower than the normal test room temperature. It was apparent from the figure that the interior temperature of the test room was lower during the morning session (from 8 to 11 hours). Then, during the peak hour session (from 11 to 17 hours), the interior temperature increases and then decreases during the last session of the trial (from 17 to 20 hours). When PV and DC power system current is increased to 3 A, the NTEAC's cooling capacity increases, and the test room temperature is reduced by 2.4 °C, resulting in a final temperature of 23.09 °C. When the current input of the NTEAC system was increased to 4A, the temperature decrease in the test room was 3.2°C less than the typical test room temperature. Additional improvements were made to the test room by increasing the supply current of the NTEAC system from a PV and DC power source that delivered 5A. The temperature within the building was reduced to a maximum of 23.31°C, resulting in a 4°C drop below the room temperature. With an increase in the input current supply of NTEAC to 6A, the system now provided a 4.9°C decrease in indoor room temperature, attributable to an optimum temperature of 21.5°C. So, with 6A of input current, the optimal performance of the PV-NTEAC system was achieved.

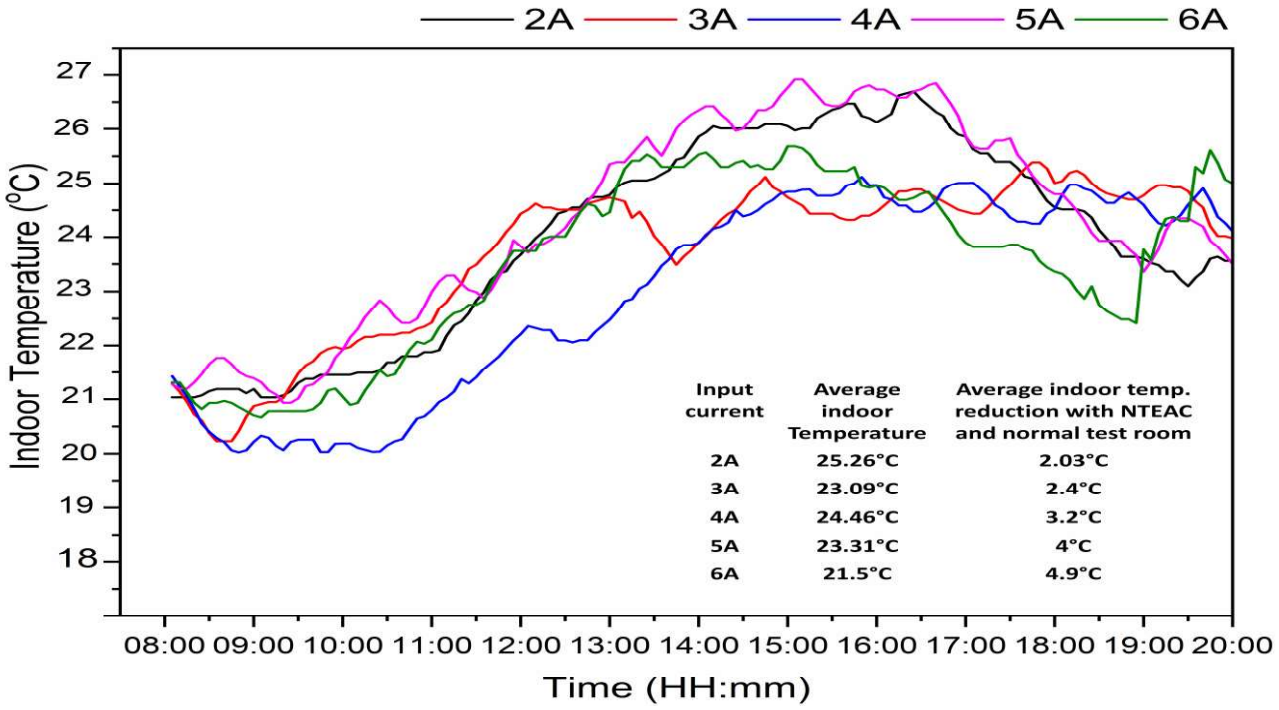

Figure 24: Variation of the indoor temperature of the test room equipped with PV-NTEAC system operated at 2-6A (7^{th} – 11^{th} September 2020)

An acceptable range for specific physical properties of relative humidity is 50 to 60%, according to the Malaysian Industry Code of Practice on Indoor Air Quality (IAQ). Figure 25 illustrates the variation of the relative humidity of the PV-NTEAC system at different input current levels (2-6A) in the test room. The mean ambient outdoor relative humidity ranged from 75 to 84% during September 2020. At the 2A current level, the average relative humidity reduction was 9-15%. Furthermore, when the current supply was increased to 3A, the average relative humidity reduction ranged from 17-23%. Consequently, the current supply to the NTEAC system was raised to 4A and 5A, where the average relative humidity reduction ranged between 23-27% and 30-35%, respectively. To further enhance the indoor relative humidity in the test room, the input current supply of the NTEAC system was increased to 6A using the PV and DC power systems. It showed a maximum average indoor relative humidity decrease of 35 to 41% at this current supply.

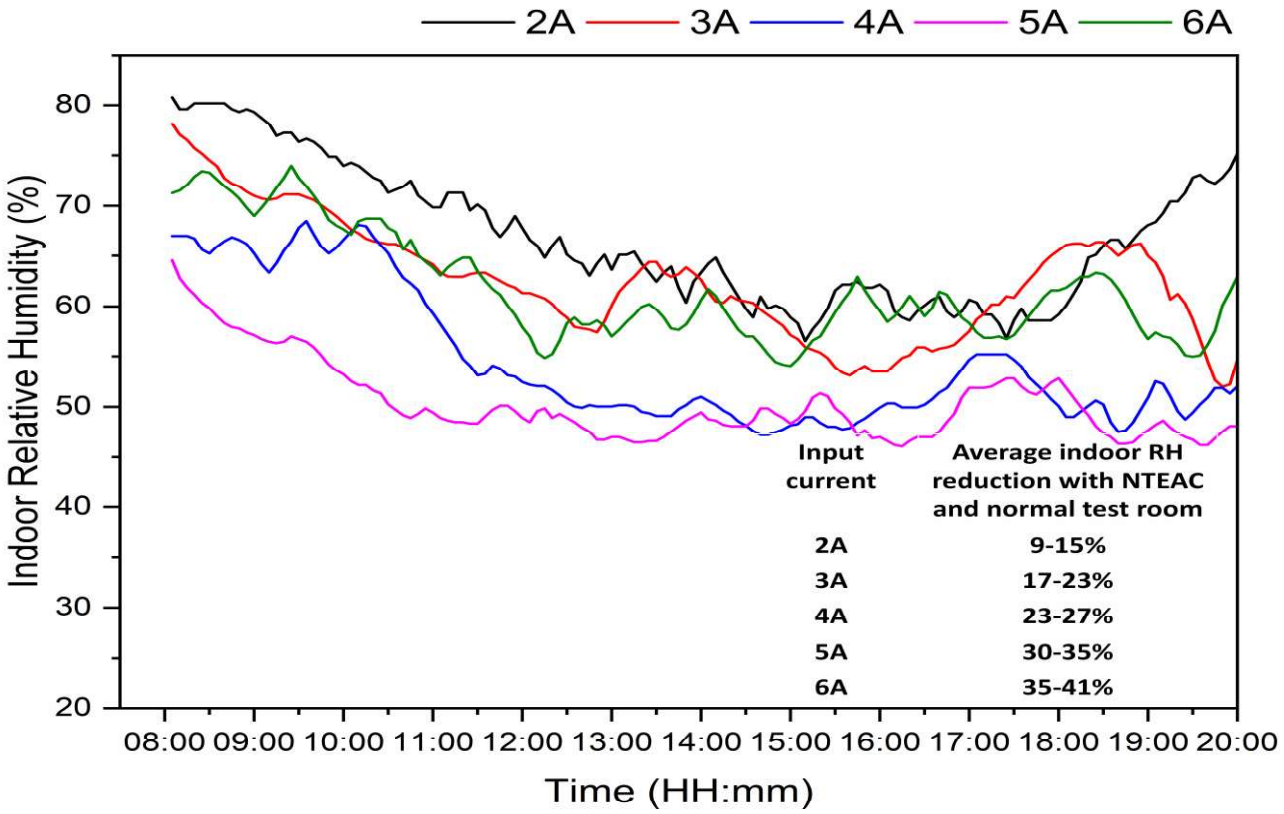

Figure 25: Variation of the indoor relative humidity of the test room equipped with PV-NTEAC system operated at 2-6A (7^{th} – 11^{th} September 2020)

3.5. Carbon credit potential and CO_2 mitigation

Energy is critical for the survival and development of contemporary civilization since it is the main factor that stimulates economic growth and development. A significant amount of energy has been used over the last several decades due to the continuous development of the global economy.

Carbon dioxide emissions have resulted in global climate change, which has now emerged as one of the most significant factors influencing sustainable socio-economic growth throughout the globe. Climate change is becoming an unassailable reality as global CO_2 emissions continue to grow alarming, increasing the unabated global average temperature. Thus, fossil fuel energy use is the most significant contributor to carbon dioxide emissions. Therefore, limiting fossil fuel CO_2 emissions is critical to mitigating global warming. Carbon mitigation should be a significant component of strategies to reduce greenhouse gas emissions. One approach to introduce relevant energy policies is to manage market behaviour, introduce regulation of producers and consumers, and so steer the economy toward a low-carbon country. According to estimates, Malaysia's six major CO_2-emitting industries are power production, transportation, industrial, residential, commercial, and agriculture. Essentially, air conditioners in residential sectors consume many fossil fuels to provide thermal comfort, resulting in a large quantity of CO_2 emissions. In Malaysia, gross CO_2 emissions rose considerably by the end of the 1990s and were more than 160 million metric tons (MMt) by 2003, increasing to 328 MMT by 2020 [58]. The PV-NTEAC device is a highly efficient and environmentally sustainable clean energy solution to minimize CO_2 emissions. The total CO_2 pollution mitigated by the investigated PV-NTEAC system was quantified numerically compared to conventional air conditioning systems. Eq. 7 was used to calculate the cumulative emission of CO_2 pollution from current PV-NTEAC devices and traditional air conditioning systems over 25 years. In general, CO_2 pollution emitted from power plants totalled 2.02 kg/kWh per unit of electricity produced annually [59].

$$Emission\ of\ CO_2\left(\frac{kg}{life}\right) = 2.02\left(\frac{kg}{kWh}\right) \times E\left(\frac{kWh}{year}\right) \times n(years) \tag{7}$$

Where E denotes the annual electrical energy units consumed by the device over a 12-hour cycle and is calculated using Eq. 8:

$$E\left(\frac{kWh}{year}\right) = Daily\ electrical\ load\ \left(\frac{kWh}{day}\right) \times Operation\ days/year \tag{8}$$

The carbon credit allocation is set at 33 US$ per tonne, which is predicted in the article "Malaysia carbon tax could pave the way for potential clean energy" [60], so the value of the carbon credit earned by the system can be calculated by Eq. 9.

$$Carbon\ credit\ earned, C_c = 33\ US\$/ton \times CO_2(\frac{ton}{life}) \tag{9}$$

Due to solar energy and carbon credit potential, the electricity cost is saved, attributed to the initial cost subjugation of the studied PV-NTEAC system. Furthermore, the payback period is evaluated using a line cash flow diagram with the following assumptions:

- The PV-NTEAC system is projected to have a 25-year life span.
- Based on Bank Negara Malaysia (BNM), the payback period of the PV-NTEAC was estimated at a 3% interest rate [61].
- The operational cost of a conventional air conditioner is 197 US$ per annum [62].

The studied PV-NTEAC systems have an operating temperature range of 22.33 to 29 °C with a 6A current supply. The system uses 3.39 kWh of electricity daily when operating in the testing room for 12 hours. The PV-NTEAC system saves 6.89 kWh of electrical energy compared to a 1-ton split air conditioner. The comparison between the test room's electrical energy savings with the PV-NTEAC system and a split air conditioner with a 1-ton capacity is presented in Table 10. Furthermore, this PV-NTEAC system can mitigate 71.54 tonnes of CO_2 emissions from buildings for 25 years.

Table 10: Comparative analysis of PV-NTEAC system with split air conditioner

Parameters	Split air conditioner (1-ton)	PV-NTEAC system
Electrical energy consumption (kWh/year)	3752.2	1237.35
Electrical energy saving (kWh/year)	0	2514.85
CO_2 emission (ton/life)	93.54	22
CO_2 reduction (ton/life)	0	71.54
Carbon credit earned (US$)	0	2360
Operating temperature (°C)	18-40	22.3-29
Weight (kg)	9 (indoor), 10 (outdoor)	7 (indoor), 2.5 (outdoor)
Life span (years)	~15	~25

4. CONCLUSIONS

The research investigated a novel photovoltaic powered nanofluid assisted thermoelectric air conditioner (PV-NTEAC) system for building cooling applications in Malaysia's tropical climate. Feasible heat sinks were designed to integrate nanofluids with thermoelectric air conditioners to

enhance TEM's hot side heat conduction. System performance was examined by evaluating cooling capacity, COP, energy, cost benefits, and CO_2 emission mitigation. Significant conclusions were discussed as follows:

- The use of nanofluids in conjunction with the radiator and TEAC resulted in a significant increase in thermal performance. This is because nanoparticles can compress the fluid's transverse temperature gradient, mainly caused by the enhanced mobility of liquid atoms in the presence of nanoparticles.
- Analysis of NTEAC's cooling performance indicates that raising the input current from 2A to 6A significantly impacted the cooling performance. However, increasing the input current supply further deteriorated the system's performance.
- With an input current of 6A, the test room's optimum temperature difference (indoor and outdoor) reached 4.9 °C, resulting in a COP of 1.27 and a cooling capacity of 571 W.
- The CO_2 emission mitigation resulted in around 71.54 tonnes when compared with a conventional split air conditioner that contributed to a carbon credit allowance of 2360 US$.

Furthermore, to achieve even greater system performance, consider lowering the thermal resistance on the hot side of the thermoelectric modules. Even though the PV-NTEAC system has a lower COP than the traditional split air conditioner, it may be used for space conditioning in rural areas with abundant solar energy. Integration of nanofluids with the PV-NTEAC system reduces the temperature difference between the cold and hot sides of the TEMs, leading to an enhanced cooling performance in thermoelectric air conditioners. As a result, the innovative PV-NTEAC system, in conjunction with the MWCNT/Water nanofluids, offers a freon-free, fossil fuel independent, energy-efficient, and low CO_2 emission approach for space conditioning.

NOMENCLATURE

A	Area (m^2)	*Greek symbols*	
Cp	Specific heat capacity (kj/kg.K)	α	Seebeck coefficient ($V.K^{-1}$)
G	Solar irradiance (W/m^2)	Δ	Delta/difference
i	interest rate (%)	η	Efficiency
I	Current (A)	ω	Specific humidity
K	Thermal conductivity (W/m. K)	σ	Resistivity (Ω cm)
N	Number of thermoelectric couples	χ	Range of measured value
n	Time in years	*Subscripts*	
P	Power (W)	c	cold

PV	Photovoltaic	h	hot
Q	Rate of heat transfer (W)	in	inlet
RH	Relative humidity (%)	out	outlet
t	Time (s)	max	maximum
T	Temperature (°C)	*Abbreviations*	
ΔT	Temperature difference between the hot side and cold side TEM (°C)	NTEAC	Nanofluid Assisted Thermoelectric Air Conditioner
Wt.	Weight fraction (%)	MWCNT	Multiwalled Carbon Nanotubes
wh	Watt-hour	TEM	Thermoelectric module
ZT	Figure of merit	Water	Distilled water

ACKNOWLEDGEMENTS

The authors are grateful to Universiti Teknologi PETRONAS for their facilities for conducting the research. We want to acknowledge the financial support offered through the YUTP grant (YUTP FRG 015LC0-118).

CONFLICTS OF INTEREST

The authors declare no conflicts of interest.

REFERENCES

[1] D.D. Kim, H.S. Suh, Heating and cooling energy consumption prediction model for high-rise apartment buildings considering design parameters, Energy Sustain. Dev. 61 (2021) 1–14. https://doi.org/https://doi.org/10.1016/j.esd.2021.01.001.

[2] B. Bakthavatchalam, K. Habib, Thermoelectric Air Conditioners for Tropical Countries, in: S.A. Sulaiman (Ed.), Clean Energy Oppor. Trop. Ctries., Springer Singapore, Singapore, 2021: pp. 289–307. https://doi.org/10.1007/978-981-15-9140-2_14.

[3] International Energy Agency, The Future of Cooling, IEA, Paris. (2018). https://www.iea.org/reports/the-future-of-cooling (accessed March 23, 2022).

[4] L. Lou, D. Shou, H. Park, D. Zhao, Y.S. Wu, X. Hui, R. Yang, E.C. Kan, J. Fan, Thermoelectric air conditioning undergarment for personal thermal management and HVAC energy saving, Energy Build. 226 (2020) 110374. https://doi.org/https://doi.org/10.1016/j.enbuild.2020.110374.

[5] Y. Lyu, A.R.M. Siddique, S.A. Gadsden, S. Mahmud, Experimental investigation of thermoelectric cooling for a new battery pack design in a copper holder, Results Eng. 10 (2021) 100214. https://doi.org/https://doi.org/10.1016/j.rineng.2021.100214.

[6] M. Di Capua H, W. Jahn, Performance assessment of thermoelectric self-cooling systems for electronic devices, Appl. Therm. Eng. 193 (2021) 117020.

https://doi.org/https://doi.org/10.1016/j.applthermaleng.2021.117020.
[7] M. Duan, H. Sun, B. Lin, Y. Wu, Evaluation on the applicability of thermoelectric air cooling systems for buildings with thermoelectric material optimization, Energy. 221 (2021) 119723. https://doi.org/https://doi.org/10.1016/j.energy.2020.119723.
[8] A. Saini, S.J. Watzman, J.-H. Bahk, Cost-Performance Trade-off in thermoelectric air conditioning system with graded and constant material properties, Energy Build. 240 (2021) 110931. https://doi.org/https://doi.org/10.1016/j.enbuild.2021.110931.
[9] M. Sajid, I. Hassan, A. Rahman, An overview of cooling of thermoelectric devices, Renew. Sustain. Energy Rev. 78 (2017) 15–22. https://doi.org/https://doi.org/10.1016/j.rser.2017.04.098.
[10] H. Sadighi Dizaji, S. Jafarmadar, S. Khalilarya, A. Moosavi, An exhaustive experimental study of a novel air-water based thermoelectric cooling unit, Appl. Energy. 181 (2016) 357–366. https://doi.org/https://doi.org/10.1016/j.apenergy.2016.08.074.
[11] R.M. Atta, Solar thermoelectric cooling using closed loop heat exchangers with macro channels, Heat Mass Transf. 53 (2017) 2241–2254. https://doi.org/10.1007/s00231-017-1965-z.
[12] H. Sun, B. Lin, Z. Lin, Y. Zhu, H. Li, X. Wu, Research on a radiant heating terminal integrated with a thermoelectric unit and flat heat pipe, Energy Build. 172 (2018) 209–220. https://doi.org/https://doi.org/10.1016/j.enbuild.2018.04.054.
[13] D. Zhao, X. Yin, J. Xu, G. Tan, R. Yang, Radiative sky cooling-assisted thermoelectric cooling system for building applications, Energy. 190 (2020) 116322. https://doi.org/https://doi.org/10.1016/j.energy.2019.116322.
[14] T.-C. Cheng, C.-H. Cheng, Z.-Z. Huang, G.-C. Liao, Development of an energy-saving module via combination of solar cells and thermoelectric coolers for green building applications, Energy. 36 (2011) 133–140. https://doi.org/https://doi.org/10.1016/j.energy.2010.10.061.
[15] Z.B. Liu, L. Zhang, G. Gong, Y. Luo, F. Meng, Experimental study and performance analysis of a solar thermoelectric air conditioner with hot water supply, Energy Build. 86 (2015) 619–625. https://doi.org/https://doi.org/10.1016/j.enbuild.2014.10.053.
[16] N. Putra, Yanuar, F.N. Iskandar, Application of nanofluids to a heat pipe liquid-block and the thermoelectric cooling of electronic equipment, Exp. Therm. Fluid Sci. 35 (2011) 1274–1281. https://doi.org/https://doi.org/10.1016/j.expthermflusci.2011.04.015.
[17] S. Manikandan, S.C. Kaushik, R. Yang, Modified pulse operation of thermoelectric coolers for building cooling applications, Energy Convers. Manag. 140 (2017) 145–156. https://doi.org/https://doi.org/10.1016/j.enconman.2017.03.003.
[18] X.-X. Tian, S. Asaadi, H. Moria, A. Kaood, S. Pourhedayat, K. Jermsittiparsert, Proposing tube-bundle arrangement of tubular thermoelectric module as a novel air cooler, Energy. 208 (2020) 118428. https://doi.org/https://doi.org/10.1016/j.energy.2020.118428.
[19] X. Su, L. Zhang, Z. Liu, Y. Luo, D. Chen, W. Li, Performance evaluation of a novel building envelope integrated with thermoelectric cooler and radiative sky cooler, Renew. Energy. 171 (2021) 1061–1078. https://doi.org/https://doi.org/10.1016/j.renene.2021.02.164.
[20] X. Han, Y. Wang, Experimental investigation of the thermal performance of a novel split-type liquid-circulation thermoelectric cooling device, Appl. Therm. Eng. 194 (2021) 117090. https://doi.org/https://doi.org/10.1016/j.applthermaleng.2021.117090.
[21] Y.-K. Kang, H. Lim, S.-Y. Cheon, J.-W. Jeong, Phase-change material-integrated thermoelectric radiant panel: Experimental performance analysis and system design, Appl. Therm. Eng. 194 (2021) 117082. https://doi.org/https://doi.org/10.1016/j.applthermaleng.2021.117082.
[22] W. He, J. Zhou, J. Hou, C. Chen, J. Ji, Theoretical and experimental investigation on a thermoelectric cooling and heating system driven by solar, Appl. Energy. 107 (2013) 89–97. https://doi.org/https://doi.org/10.1016/j.apenergy.2013.01.055.

[23] F. Khalvati, A. Omidvar, F. Hadianfard, Study on summer thermal performance of a solar ventilated window integrated with thermoelectric air-cooling system, Int. J. Energy Environ. Eng. (2021). https://doi.org/10.1007/s40095-020-00376-8.
[24] S. Diaz de Garayo, A. Martínez, P. Aranguren, D. Astrain, Prototype of an air to air thermoelectric heat pump integrated with a double flux mechanical ventilation system for passive houses, Appl. Therm. Eng. 190 (2021) 116801. https://doi.org/https://doi.org/10.1016/j.applthermaleng.2021.116801.
[25] M. Gillott, L. Jiang, S. Riffat, An investigation of thermoelectric cooling devices for small-scale space conditioning applications in buildings, Int. J. Energy Res. 34 (2010) 776–786. https://doi.org/10.1002/er.1591.
[26] M.-W. Tian, F. Aldawi, A.E. Anqi, H. Moria, H.S. Dizaji, M. Wae-hayee, Cost-effective and performance analysis of thermoelectricity as a building cooling system; experimental case study based on a single TEC-12706 commercial module, Case Stud. Therm. Eng. 27 (2021) 101366. https://doi.org/https://doi.org/10.1016/j.csite.2021.101366.
[27] M. Akkaya, T. Menlik, A. Sözen, M. Gürü, EXPERIMENTAL INVESTIGATION OF NANOLUBRICANT USAGE IN A COOLING SYSTEM AT DIFFERENT NANOPARTICLE CONCENTRATIONS, Heat Transf. Res. 51 (2020) 949–965. https://doi.org/10.1615/HeatTransRes.2020033812.
[28] M. Akkaya, T. Menlik, A. Sözen, M. Gürü, The Effects of Triton X-100 and Tween 80 Surfactants on the Thermal Performance of a Nano-Lubricant: An Experimental Study, Int. J. Precis. Eng. Manuf. Technol. 8 (2021) 955–967. https://doi.org/10.1007/s40684-020-00280-w.
[29] M. Akkaya, S. Yurtdaş, ENERGY EFFICIENCY IMPROVEMENT OF THE HEAT PUMP BY EMPLOYING SYNTHESIZED CuO/ZnO HYBRID NANOFLUID, Heat Transf. Res. 53 (2022) 47–60. https://doi.org/10.1615/HeatTransRes.2021040242.
[30] E. Çiftçi, K. Martin, A. Sözen, ENHANCEMENT OF THERMAL PERFORMANCE OF THE AIR-TO-AIR HEAT PIPE HEAT EXCHANGER (AAHX) WITH ALUMINATE SPINEL-BASED BINARY HYBRID NANOFLUIDS, Heat Transf. Res. 52 (2021) 81–97. https://doi.org/10.1615/HeatTransRes.2021039920.
[31] E. Çiftçi, Distilled Water-Based AlN + ZnO Binary Hybrid Nanofluid Utilization in a Heat Pipe and Investigation of Its Effects on Performance, Int. J. Thermophys. 42 (2021) 38. https://doi.org/10.1007/s10765-021-02792-2.
[32] H.M. Maghrabie, K. Elsaid, E.T. Sayed, M.A. Abdelkareem, T. Wilberforce, M. Ramadan, A.G. Olabi, Intensification of heat exchanger performance utilizing nanofluids, Int. J. Thermofluids. 10 (2021) 100071. https://doi.org/https://doi.org/10.1016/j.ijft.2021.100071.
[33] O. Mahian, A. Kianifar, S.Z. Heris, D. Wen, A.Z. Sahin, S. Wongwises, Nanofluids effects on the evaporation rate in a solar still equipped with a heat exchanger, Nano Energy. 36 (2017) 134–155. https://doi.org/https://doi.org/10.1016/j.nanoen.2017.04.025.
[34] A. Sözen, Ç. Filiz, İ. Aytaç, K. Martin, H.M. Ali, K. Boran, Y. Yetişken, Upgrading of the Performance of an Air-to-Air Heat Exchanger Using Graphene/Water Nanofluid, Int. J. Thermophys. 42 (2021) 35. https://doi.org/10.1007/s10765-020-02790-w.
[35] D.Y. Aydın, E. Çiftçi, M. Gürü, A. Sözen, The Impacts of Nanoparticle Concentration and Surfactant Type on Thermal Performance of A Thermosyphon Heat Pipe Working With Bauxite Nanofluid, Energy Sources, Part A Recover. Util. Environ. Eff. 43 (2021) 1524–1548. https://doi.org/10.1080/15567036.2020.1800141.
[36] R.A.A. Babat, K. Martin, E. Çiftçi, A. Sözen, Experimental study on the utilization of magnetic nanofluids in an air-to-air heat pipe heat exchanger, Chem. Eng. Commun. 0 (2021) 1–11. https://doi.org/10.1080/00986445.2021.1977634.
[37] G. Colangelo, E. Favale, M. Milanese, A. de Risi, D. Laforgia, Cooling of electronic devices: Nanofluids contribution, Appl. Therm. Eng. 127 (2017) 421–435. https://doi.org/https://doi.org/10.1016/j.applthermaleng.2017.08.042.

[38] C. Wang, E. Choi, J. Park, High-voltage nanofluidic energy generator based on ion-concentration-gradients mimicking electric eels, Nano Energy. 43 (2018) 291–299. https://doi.org/https://doi.org/10.1016/j.nanoen.2017.11.054.
[39] A. Siricharoenpanich, S. Wiriyasart, P. Naphon, Study on the thermal dissipation performance of GPU cooling system with nanofluid as coolant, Case Stud. Therm. Eng. 25 (2021) 100904. https://doi.org/https://doi.org/10.1016/j.csite.2021.100904.
[40] S. Sarvar-Ardeh, R. Rafee, S. Rashidi, Hybrid nanofluids with temperature-dependent properties for use in double-layered microchannel heat sink; hydrothermal investigation, J. Taiwan Inst. Chem. Eng. (2021). https://doi.org/https://doi.org/10.1016/j.jtice.2021.05.007.
[41] T. Balaji, C. Selvam, D.M. Lal, S. Harish, Enhanced heat transport behavior of micro channel heat sink with graphene based nanofluids, Int. Commun. Heat Mass Transf. 117 (2020) 104716. https://doi.org/https://doi.org/10.1016/j.icheatmasstransfer.2020.104716.
[42] J. Mohammadpour, F. Salehi, M. Sheikholeslami, M. Masoudi, A. Lee, Optimization of nanofluid heat transfer in a microchannel heat sink with multiple synthetic jets based on CFD-DPM and MLA, Int. J. Therm. Sci. 167 (2021) 107008. https://doi.org/https://doi.org/10.1016/j.ijthermalsci.2021.107008.
[43] B. Bakthavatchalam, K. Habib, R. Saidur, S. Shahabuddin, B.B. Saha, Influence of solvents on the enhancement of thermophysical properties and stability of MWCNT nanofluid., Nanotechnology. 31 (2020) 235402. https://doi.org/10.1088/1361-6528/ab79ab.
[44] B. Kanargi, P.S. Lee, C. Yap, A numerical and experimental investigation of heat transfer and fluid flow characteristics of an air-cooled oblique-finned heat sink, Int. J. Heat Mass Transf. 116 (2018) 393–416. https://doi.org/https://doi.org/10.1016/j.ijheatmasstransfer.2017.09.013.
[45] I.S. Walker, M.H. Sherman, Energy implications of meeting ASHRAE Standard 62.2, ASHRAE Trans. 114 (2008) 505–516.
[46] R.J. de Dear, G.S. Brager, Thermal comfort in naturally ventilated buildings: revisions to ASHRAE Standard 55, Energy Build. 34 (2002) 549–561. https://doi.org/https://doi.org/10.1016/S0378-7788(02)00005-1.
[47] R.J. Moffat, Describing the uncertainties in experimental results, Exp. Therm. Fluid Sci. 1 (1988) 3–17. https://doi.org/https://doi.org/10.1016/0894-1777(88)90043-X.
[48] G. Tan, D. Zhao, Study of a thermoelectric space cooling system integrated with phase change material, Appl. Therm. Eng. 86 (2015) 187–198. https://doi.org/https://doi.org/10.1016/j.applthermaleng.2015.04.054.
[49] M. Emam, M. Ahmed, Performance analysis of a new concentrator photovoltaic system integrated with phase change material and water jacket, Sol. Energy. 173 (2018) 1158–1172. https://doi.org/https://doi.org/10.1016/j.solener.2018.08.069.
[50] L. Shen, F. Xiao, H. Chen, S. Wang, Investigation of a novel thermoelectric radiant air-conditioning system, Energy Build. 59 (2013) 123–132. https://doi.org/10.1016/j.enbuild.2012.12.041.
[51] G. Tan, D. Zhao, Study of a thermoelectric space cooling system integrated with phase change material, Appl. Therm. Eng. 86 (2015) 187–198. https://doi.org/10.1016/j.applthermaleng.2015.04.054.
[52] K. Irshad, K. Habib, N. Thirumalaiswamy, B.B. Saha, Performance analysis of a thermoelectric air duct system for energy-efficient buildings, Energy. 91 (2015) 1009–1017. https://doi.org/https://doi.org/10.1016/j.energy.2015.08.102.
[53] M. Ibañez-Puy, J. Bermejo-Busto, C. Martín-Gómez, M. Vidaurre-Arbizu, J.A. Sacristán-Fernández, Thermoelectric cooling heating unit performance under real conditions, Appl. Energy. 200 (2017) 303–314. https://doi.org/10.1016/j.apenergy.2017.05.020.
[54] A. Rincón-Casado, A. Martinez, M. Araiz, P. Pavón-Domínguez, D. Astrain, An experimental and computational approach to thermoelectric-based conditioned mattresses, Appl. Therm. Eng. 135 (2018) 472–482.

https://doi.org/10.1016/j.applthermaleng.2018.02.084.
[55] S.-Y. Cheon, H. Lim, J.-W. Jeong, Applicability of thermoelectric heat pump in a dedicated outdoor air system, Energy. 173 (2019) 244–262. https://doi.org/10.1016/j.energy.2019.02.012.
[56] C. Chen, L. Mao, T. Lin, T. Tu, L. Zhu, C. Wang, Performance testing and optimization of a thermoelectric elevator car air conditioner, Case Stud. Therm. Eng. 19 (2020) 100616. https://doi.org/10.1016/j.csite.2020.100616.
[57] K.K. Looi, A.T. Baheta, K. Habib, Investigation of photovoltaic thermoelectric air-conditioning system for room application under tropical climate, J. Mech. Sci. Technol. 34 (2020) 2199–2205. https://doi.org/10.1007/s12206-020-0441-8.
[58] T.H. Oh, S.C. Chua, Energy efficiency and carbon trading potential in Malaysia, Renew. Sustain. Energy Rev. 14 (2010) 2095–2103. https://doi.org/10.1016/j.rser.2010.03.029.
[59] S.M. Shafie, T.M.I. Mahlia, H.H. Masjuki, Life cycle assessment of rice straw co-firing with coal power generation in Malaysia, Energy. 57 (2013) 284–294. https://doi.org/10.1016/j.energy.2013.06.002.
[60] M. Akmaliyah, 済無No Title No Title, J. Chem. Inf. Model. 53 (2013) 1689–1699. https://phys.org/news/2016-04-malaysian-carbon-tax-pave-renewable.html.
[61] BANK NEGARA MALAYSIA, INTEREST RATES (CONVENTIONAL), Cent. BANK MALAYSIA. (2019). https://www.bnm.gov.my/interest-rates-volumes?p_p_id=bnm_market_rate_display_portlet&p_p_lifecycle=0&p_p_state=normal&p_p_mode=view&_bnm_market_rate_display_portlet_product=rro&_bnm_market_rate_display_portlet_monthStart=0&_bnm_market_rate_display_portlet.
[62] K. Irshad, K. Habib, S. Algarni, B.B. Saha, B. Jamil, Sizing and life-cycle assessment of building integrated thermoelectric air cooling and photovoltaic wall system, Appl. Therm. Eng. 154 (2019) 302–314. https://doi.org/10.1016/j.applthermaleng.2019.03.027.